Non-Smooth Dynamics in the Stommel Model of the Thermohaline Circulation

by

Cody Griffith

B.Sc., Metropolitan State University of Denver, 2016

A THESIS SUBMITTED IN PARTIAL FULFILLMENT OF
THE REQUIREMENTS FOR THE DEGREE OF

MASTER OF SCIENCE

in

The Faculty of Graduate and Postdoctoral Studies

(Mathematics)

THE UNIVERSITY OF BRITISH COLUMBIA

(Vancouver)

August 2018

The following individuals certify that they have read, and recommend to the Faculty of Graduate and Postdoctoral Studies for acceptance, a thesis entitled:

Non-Smooth Dynamics in the Stommel Model of the Thermohaline Circulation

submitted by **Cody Griffith** in partial fulfillment of the requirements of the degree of **Master of Science** in **Applied Mathematics**.

Examining Committee:

Rachel Kuske, Professor of Mathematics
Supervisor

Brian Wetton, Professor of Mathematics
Supervisory Committee Member

Abstract

We analyzed the non-smooth dynamics for the Stommel model for thermohaline circulation with additional mechanisms like slowly varying bifurcation parameters and high frequency oscillatory forcing. Our goal was to find an analytic approximation to the tipping point and forced bifurcation induced by the new features in the model. We first analyze a simpler one component model that has similar structure to the Stommel model and gradually build in more complexity into the one component problem and study the effects on the tipping point. In this context, we compare the relative strengths of the non-smooth effects on the tipping point to the smooth effects which has been previously studied. With the one component model understood, we then apply similar methods to the Stommel model and study the effects on the non-smooth tipping points and forced bifurcations. With these results we have the ability to fully describe the hysteresis found in the Stommel model.

Lay Summary

We study the behavior of the thermohaline circulation. This circulation is responsible for moving water from around the globe and thus a model was created to understand how it functions. Work has previously been done on certain components of this model, but the analysis we provide is done around the less studied pieces known as the non-smooth dynamics. We ultimately provide a solution to the non-smooth dynamics and even incorporate more mechanisms in the original model to account for a larger class of observable behavior. This allows for a better understanding of the thermohaline circulation and could help predict and prepare for sudden abrupt changes to the ocean currents that drive our climate.

Preface

This thesis is original, unpublished, independent work by the author, C. Griffith.

Table of Contents

Appendices

List of Figures

Acknowledgments

I would like to thank my supervisor Rachel Kuske for the project idea and guidance as well as my committee member Brian Wetton for helping me professionally through graduate school.

Special thanks are given to my peers Tim Jaschek and Matthias Klöckner for their aide in writing and support throughout the entire degree. Couldn't have done it without you both!

Chapter 1

Introduction

Dynamical systems is the study of the possible states an observable solution may experience and is important in most engineering, biological or even chemical systems to name a few. This approach allows conditions to be given for when a solution can be found or when there is stable behavior. Often we find that parameters inherent in the model play huge roles in the dynamical behavior and they can be the difference between a system having an equilibrium or not. When we find a parameter that has this effect, we call it a bifurcation parameter since there is some value that changes the qualitative behavior of the system.

For example, the Hodgkin-Huxley model for neurons contains a parameter for injected current I which turns out to be a bifurcation parameter with a Hopf bifurcation. This bifurcation is responsible for the actual firing of a neuron in the brain. In epidemiological modeling, the basic SIR model with an additional transition function between the infected and recovered population causes the reproduction number R_0 to become a bifurcation parameter with a backward bifurcation. This causes a temporary equilibrium to form in the infected population that usually would never see an equilibrium. Even in activation potentials of neural networks, using a hyperbolic tangent function causes a bifurcation to occur in the synaptic feedback parameter w which results in a pitchfork bifurcation. This causes wildly different equilibria for learned parameters in a machine learning setting. The canonical example is the *saddle-node* bifurcation and was the first to be found within a complex system studied from a dynamical perspective. The saddle-node bifurcation has the locally topological equivalent form

$$\dot{x} = a - x^2, \tag{1.1}$$

where by locally topological equivalence we mean the behavior near the bifurcation may be represented in this form. This property is critical to reducing most complex problems and models to simpler local problems that can be studied individually.

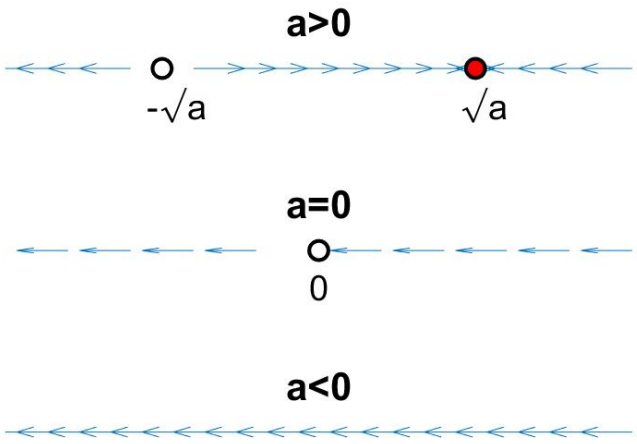

Figure 1.1: Vector field of a saddle-node bifurcation $a = 0$.

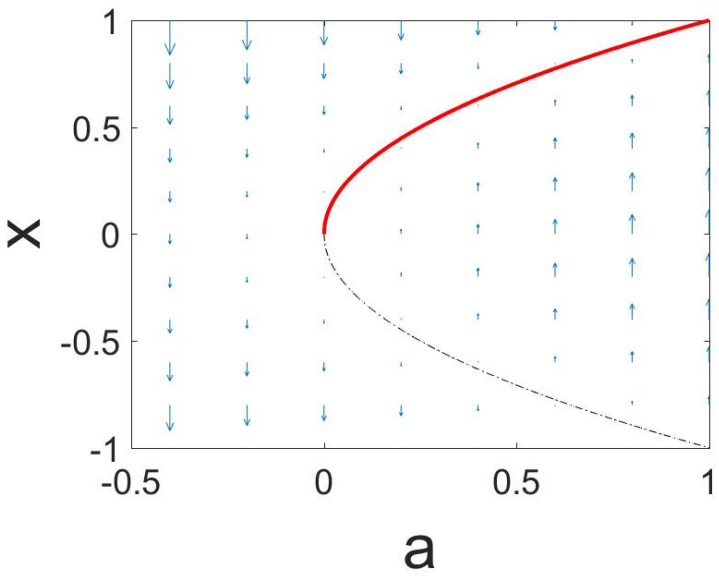

Figure 1.2: Bifurcation diagram of saddle-node bifurcation $a = 0$.

In figure 1.1 we show the vector field of the system that contains a saddle-node bifurcation. The equilibria of this system is $x = \pm\sqrt{a}$ for any $a \geq 0$ where stable equilibrium points are marked with red filled points and unstable with unfilled points. Notice that at $a = 0$ we are no longer able to find a stable equilibrium and when $a < 0$ there are no equilibria at all. Thus $a = 0$ is a simple example of a bifurcation where two equilibria annihilate. This

behavior is why the bifurcation is often referred to as a *fold* bifurcation, although we refer to this as a saddle-node bifurcation in this thesis. In figure 1.2 we plot the same system against the parameter a, which we call the bifurcation diagram. Here we see the region with two equilibrium $a > 0$, the bifurcation $a = 0$ and the region of no stability $a < 0$. For more on the saddle-node bifurcation see [12].

There are many types of bifurcations that appear in different systems that each have their own key properties. Studying these properties leads to a deeper understanding of the system on both a global and a local scale. Work has been done on systems that have smooth bifurcations due to how commonly these appear, but non-smooth dynamics still are present in the physical world.

Non-smooth bifurcations are a topic that arise in special systems and for how frequent they appear, they have not been studied nearly as much as their smooth counter parts. This thesis discusses the role of the non-smooth saddle-node bifurcation in a simplified one component system in chapter 2 as well as in the classic Stommel model for thermohaline circulation dynamics in chapter 3. Many interesting ocean and weather mechanisms may be incorporated into the Stommel model to provide more realistic predictions for weather patterns. We choose to study slowly varying bifurcation parameters and their effect on the stability of a system while contrasting this with non-autonomous oscillatory forcing. The interaction of these features causes complex dynamics around the standard bifurcations and can lead to an advanced bifurcation or delayed tipping. For the one component system, a detailed analysis of these features is done on the smooth bifurcation in [24].

Tipping in a Slowly Varying System

A system with a parameter known to cause a bifurcation will no longer admit a bifurcation in the standard sense when the parameter slowly varies. Instead, these conditions give rise to a smooth but rapid change in the system's equilibria. The point in which this behavior occurs is then called a *tipping point*.

More formally, a tipping point is a point that causes an abrupt smooth transition in dynamical behavior as the system moves into a qualitatively different state. This is usually caused by some exterior control system that pushes change towards a different state once a critical point has been passed, for example with biological systems seen in [2]. These are known to be caused by changes in one or more parameters in the system. An analysis that lays the theoretical backing of slowly varying parameters with algebraic bifurcations is found in [7].

Tipping points have been discovered to occur in a wide variety of systems and have become a big staple in the study of areas like catastrophe theory and dynamical systems. They aid in predicting the future of a system and even could be a warning for irreversible change like in the case of the Stommel model. A tipping point thus shares similar characteristics to a bifurcation and typically occurs close to the static bifurcation location.

In this thesis we use the results from [24] where the system

$$\begin{aligned} \dot{x} =& Da + k_0 + k_1 x + k_2 x^2, \\ \dot{a} =& -\epsilon, \end{aligned} \tag{1.2}$$

where $\epsilon \ll 1$ was studied. This model is a slowly varying quadratic differential equation containing a smooth saddle-node bifurcation and appears in many physical models, for example [6]. A key result from [24] is that the solution and tipping point for (1.2) have the form

$$x \sim \frac{1}{|k_2|}\left(\frac{k_1}{2} + \left(\frac{D|k_2|}{\epsilon}\right)^{1/3}\right)\frac{Ai'\left([D|k_2|\epsilon]^{-2/3}\left(\frac{k_1^2}{4} + k_0|k_2| + D|k_2|a\right)\right)}{Ai\left([D|k_2|\epsilon]^{-2/3}\left(\frac{k_1^2}{4} + k_0|k_2| + D|k_2|a\right)\right)} \tag{1.3}$$

$$a_{\text{tip}} = (D|k_2|)^{-1/3}a_{\text{Airy}} - \frac{a_s}{D} \quad \text{for} \quad a_s = k_0 + \frac{k_1^2}{4|k_2|}, \tag{1.4}$$

with $Ai(\cdot)$ being the Airy function and $a_{\text{Airy}} = \epsilon^{2/3} \cdot (-2.33810\ldots)$ corresponding to the first zero of the Airy function. The singularity found in (1.4) is a recurring tool for the work presented in this thesis, even though we deal with a version of (1.2) that has a non-smooth bifurcation.

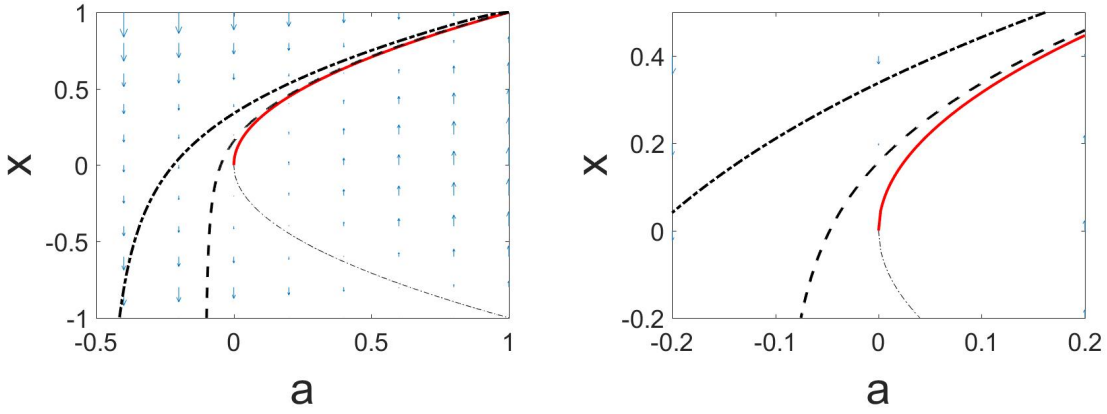

(a) (b)

Figure 1.3: The saddle-node bifurcation. In (a) an example of tipping occurring around the bifurcation for two sizes of slow variation, $\epsilon = \{.01, .1\}$. In (b) a zoom in closer to the bifurcation. The dashed ($\epsilon = .01$) and dash-dotted ($\epsilon = .1$) black lines are the numerical solutions, we overlay the bifurcation diagram for reference.

In figure 1.3 we show a numerical solution to the simple saddle-node system with tipping (1.2). Here we have $D = 1$, $k_0 = k_1 = 0$ and $k_2 = -1$ which is the model from (1.1). The solution follows closely to the stable branch even after the bifurcation for the static model, which is an example of this delayed behavior. From here on we refer to the numerical tipping point to be when the numerical solution has passed a threshold away from the equilibrium such that it is reasonable to say the solution is transitioning to a new state. We call this threshold the tipping criterion and it is specified whenever we compare our estimates to the numerical solution.

The task of finding where tipping points occur depends on the situation, but in general the approach is to search for when a solution to a model fails or becomes large. Examples

could be when the solution fails to be real or when an exponential term grows large, both of which are seen throughout this thesis.

The Stommel Model

Global circulation models have primarily focused on three different categories:

- Atmospheric components - the effect greenhouse gases have on the atmosphere,
- Oceanic components - the effect of tides and interaction of temperature with salinity in the oceans,
- Sea ice and land surface components.

These categories all contribute significantly to the overall prediction of weather and climate for the planet, which has importance to just about every industry and economy. Failure to adhere to and prepare for sudden changes in the climate has led to drastic situations like severe droughts or ocean acidification. Atmospheric models have been vastly studied but far less work has been done on the contribution from the ocean and the dynamics that drive the tides and currents.

A key feature of oceanic models is when patterns form around regions of bi-stability of temperature and salinity. An example of this is the thermohaline circulation (THC) which has abrupt qualitative changes at certain points, see [1, 14, 17, 18]. Just earlier this year evidence was found of weakening occurring around these abrupt changes in a system of ocean patterns known as the Atlantic meridional overturning circulation (AMOC) [4]. This is the first evidence of ocean dynamics responding to temperature change on the surface and can help further predict the future of the system. It is imperative that appropriate action is taken to prepare for the future of these type of systems as they are outside our realm of control.

To study these phenomena we create parametric models to replicate the dynamics we observe. Initially, Henry Stommel proposed the two box model in 1961 to understand the physics of the THC, shown in figure 1.4. In [23], it is suggested that there are actually two different stability regimes which even overlap in the system that is proposed and concluded that oceanic dynamics behave very similarly about these equilibria. These type of systems have since been a heavily studied area for both climatology due to the wide ranging applications and dynamical systems for its generalization into bi-stability.

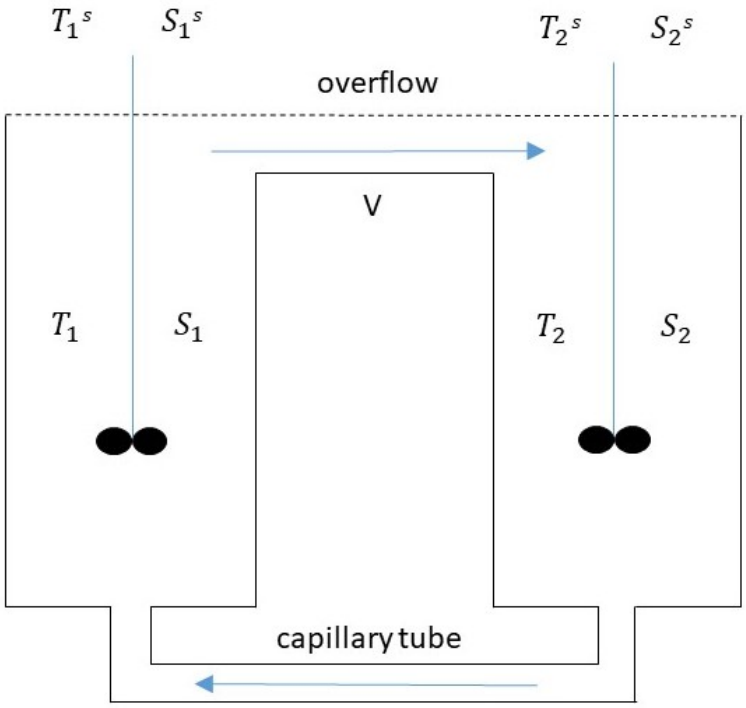

Figure 1.4: The Stommel Two Box Model: Differing volume boxes with a temperature and salinity, T_i and S_i. The boxes are connected by an overflow and capillary tube that has a circulation rate V. There is also a surface temperature and salinity for each box, $T_i{}^s$ and $S_i{}^s$. We assume that there is some stirring to give a well mixed structure.

With emphasis on mathematics, the focus of this thesis is on developing an effective approach to models with bi-stability and additional mechanisms. Thus the physical quantities are brushed aside in favor of their non-dimensional alternatives, see Appendix A for the derivation. The non-dimensionalized Stommel model is represented with the system

$$\begin{aligned} \dot{T} &= \eta_1 - T(1 + |T - S|), \\ \dot{S} &= \eta_2 - S(\eta_3 + |T - S|). \end{aligned} \tag{1.5}$$

The variables T and S are the temperature and salinity respectively where the non-smoothness is seen directly from the $|T - S|$ term. The parameters η_1, η_2, and η_3 are all dimensionless quantities that each have physical interpretation to the relaxation times and volumes of the box. Here η_1 is thought of as the thermal variation, η_2 as the saline variation otherwise known as the freshwater flux, and η_3 as the ratio of relaxation times of temperature and salinity. It also is a physical restriction for both η_1 and η_3 to be positive quantities that take any value. The parameter η_3 has the additional property to determine the orientation of the equilibria. We denote a standard orientation to be when $\eta_3 < 1$, reverse orientation for $\eta_3 > 1$, and $\eta_3 = 1$ a special case. The different orientations are shown in figure 1.6. Recall that η_3 is the ratio of relaxation rates and when $\eta_3 = 1$ the relaxation rates for both the thermal and salinity variables are the same. Under these conditions we lose bi-stability and instead see a single stable equilibrium.

The parameter η_2 is the most interesting as different values cause major qualitative and quantitative changes in the dynamics of the system. Bifurcations have been discovered at two different points in the system, each being called either a smooth or a non-smooth saddle-node bifurcation. In the Stommel model, it is convenient to view the system in terms of the circulation rate $V = T - S$, see Appendix A for the derivation. This leads to the system

$$\begin{aligned} \dot{T} &= \eta_1 - T(1 + |V|), \\ \dot{V} &= (\eta_1 - \eta_2) - V|V| - T + \eta_3(T - V). \end{aligned} \tag{1.6}$$

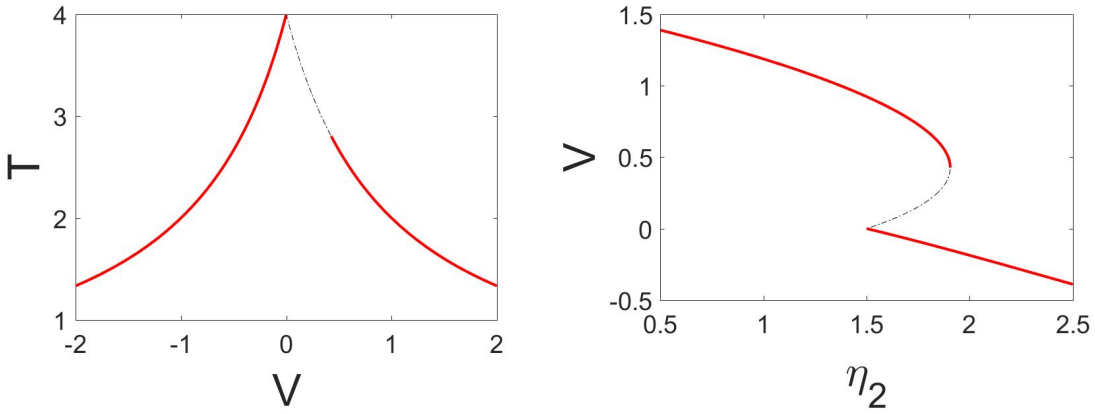

(a) V vs. T (b) η_2 vs. V

Figure 1.5: The equilibria of the non-dimensionalized system (1.6). Parameters values are $\eta_1 = 4$ and $\eta_3 = .375$. The above plots are two-dimensional projections of the full 3-dimensional system in (η_2,V,T). We see non-smooth behavior happening in both plots when $V = 0$. The red line indicates a stable branch where the dashed dotted line is for an unstable branch.

As shown in figure 1.5, the equilibrium curves reveal much about the dynamics. In (a) the graph of the equilibria for V vs. T shows non-smooth behavior occurring at $V = 0$ and in (b) the two types of bifurcation appear clearly in the graph of equilibria for η_2 vs. V. In this plot, both the upper and lower branches of the equilibrium are stable with the middle branch being unstable. The stable branches relate to which variable is dominant. For the lower branch, we call this the saline branch, and the upper branch the thermal branch. The location of the non-smooth bifurcation is found analytically, $(\eta_{2_{\text{ns}}}, V_{\text{ns}}, T_{\text{ns}}) = (\eta_1\eta_3, 0, \eta_1)$, and the smooth bifurcation, $(\eta_{2_{\text{smooth}}}, V_{\text{smooth}}, T_{\text{smooth}})$, is the only real solution to a cubic polynomial. The smoothness of each bifurcation is apparent and arises from the absolute value term in the defining dynamics of (1.6), which is non-smooth only at $V = 0$.

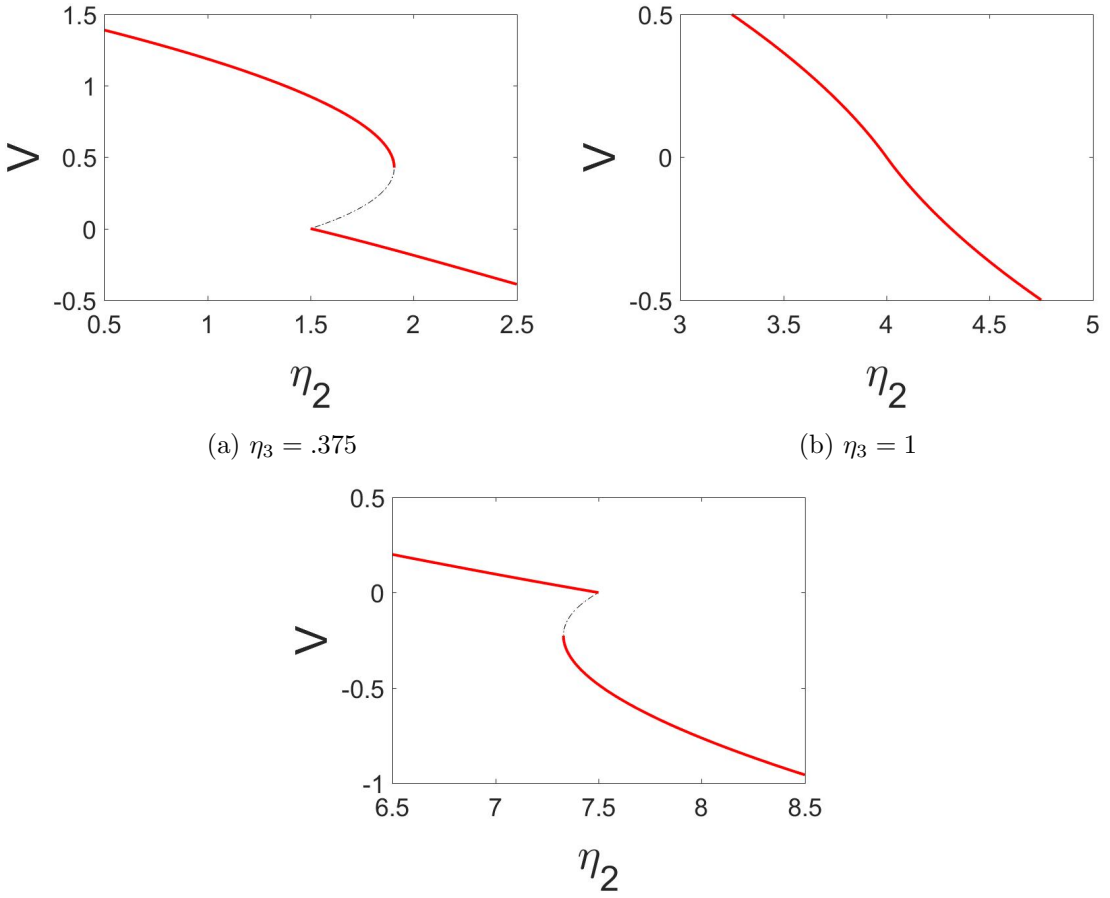

(a) $\eta_3 = .375$

(b) $\eta_3 = 1$

(c) $\eta_3 = 1.875$

Figure 1.6: The choice in η_3 dictates the orientation of the problem, in each plot we have fixed $\eta_1 = 4$. The case for $\eta_3 = 1$ is special due to the two bifurcations overlapping and the unstable equilibrium vanishing.

Much is known about the Stommel model in the case where η_2 is fixed but realistically this is not the case. In [17], this parameter is described as the influx of freshwater into the Atlantic and the changing nature of η_2 is justified by a positive feedback loop for salinity that drives the THC to move high-salinity water towards deep oceans. This loop causes the abrupt smooth bifurcation but then afterwards, a salinity deficit causes the parameter to decrease back towards the non-smooth bifurcation.

This type of behavior is known as hysteresis, where there is some bi-stability region that the solution cycles through and observes both states of the equilibria. A similar analysis to the Stommel model's hysteresis can be found in [19]. The phenomena of hysteresis appears in many physical systems, for example [11, 8, 10]. The smooth component of the hysteresis curve has been studied in a reduced one component model, see [24]. In this thesis we complement these results with an analysis of the non-smooth component.

Numerical Methods

To obtain numerical solutions to the ordinary differential equations studied in this thesis, we choose to use both 2nd order and 4th order Runge-Kutta methods. The 2nd order method are used for the one component model and the 4th order method for the two component model. The choice in these methods comes from using the simplest scheme since numerical sensitivity is not present in our problem. We use the numerical solutions to compare our approximations to the observed state transition.

Chapter 2

One Component Model

We consider a simpler system to give insight into the more complex two component Stommel model. Here we use a toy system to build the analysis on and the spatial variables may not have a physical interpretation. This system is the following one component model in terms of the variables x and μ

$$\begin{aligned} \dot{x} &= -\mu + 2|x| - x|x| + A\sin(\Omega t), \\ \dot{\mu} &= -\epsilon, \end{aligned} \tag{2.1}$$

$$x(0) = x^0, \quad \mu(0) = \mu^0,$$

where the fixed parameters are the slow variation rate of $\epsilon \ll 1$, the amplitude of oscillation A and the frequency of oscillation Ω. We also assume the initial conditions to be $x^0 = 1 - \sqrt{1+\mu^0}$ and $\mu^0 > \mu_{\text{ns}}$ which focuses our calculations on the lower equilibrium branch where $x < 0$ and study nearby behavior. The value μ_{ns} refers to the non-smooth bifurcation which is discussed below in section 2.1.

The system (2.1) is generalized from a basic model that contains both a smooth and non-smooth saddle-node bifurcation. This structure is similar to the Stommel model and hence a good model to test features like slow variation or oscillatory forcing. The slow variation is clear, but we use oscillatory forcing here in preparation for the two component model of the next chapter. In each case, emphasis is put on the non-smooth component of the model to study the non-smooth bifurcation and the role it plays in the hysteresis curve we anticipate in the Stommel model.

2.1 Static Bifurcations

The foundation to our understanding comes from the simplest structure lying within the canonical system (2.1) which is the bifurcation structure. This means finding the general form for the equilibria in (2.1) with $A = 0$ and $\epsilon = 0$, which is our basic model with a static μ and no forcing. As we have a fixed parameter value, we search for a point or set of points that the solution relaxes to as $t \to \infty$. We call these points the equilibrium points and they are either stable or unstable. Since we are considering all possible μ, we want all of the equilibrium points for each μ and thus we call these the equilibrium branches.

To find all equilibrium branches, we search for when the solution has come to a rest, which is equivalent to setting the derivative of x to zero. Thus we set (2.1) to zero with

$$0 = -\mu + 2|x| - x|x|. \tag{2.2}$$

Solving (2.2) results in 3 solutions where the stability of each is characterized by small perturbations to the equilibrium either linearly growing or decaying. We denote the stable

equilibria as x_l and x_u for the lower and upper branches respectively, and a single unstable middle branch, x_m. These are given by

$$x_l = 1 - \sqrt{1+\mu}, \quad x_u = 1 + \sqrt{1-\mu}, \quad x_m = 1 - \sqrt{1-\mu}.$$

We note that x_l is valid for $\mu \geq 0$ and both x_u and x_m for $\mu \leq 1$. Thus this system has a stable equilibrium for each value of the parameter and has a region of bi-stability for $0 \leq \mu \leq 1$. The boundaries of this region are $(\mu_{\text{ns}}, x_{\text{ns}}) = (0,0)$ and $(\mu_{\text{smooth}}, x_{\text{smooth}}) = (1,1)$ which are the non-smooth and smooth saddle-node bifurcations respectively. Both are saddle-node due to pairs of equilibria annihilating at these locations which is shown in figure 2.1.

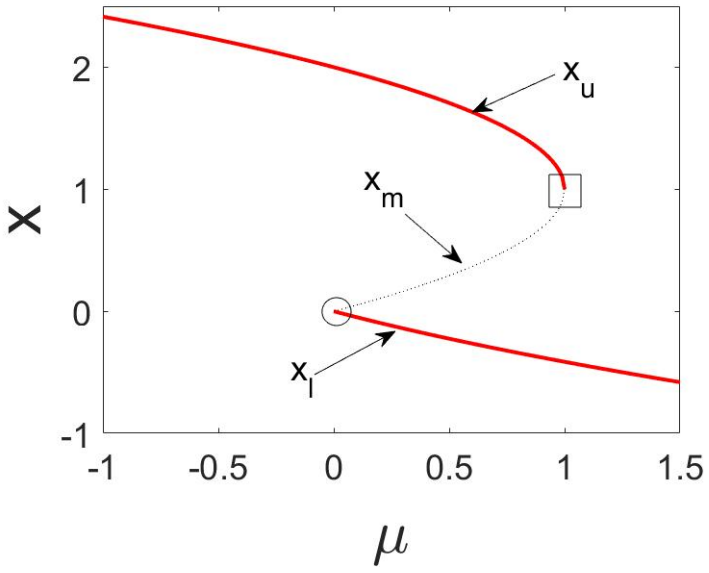

Figure 2.1: The one component bifurcation diagram with the upper and lower equilibrium branches as well as the unstable middle branch. The non-smooth bifurcation occurs at (0,0) denoted by the circle and the smooth bifurcation occurs at (1,1) by the box.

2.2 Slowly Varying Bifurcation Parameter

To develop a method for the slowly varying Stommel model, we consider (2.1) with $\epsilon \ll 1$ and $A = 0$. Under these conditions, $\mu(t)$ is a function of time and thus a bifurcation no longer occurs. Instead, it is expected that a tipping point occurs nearby the static bifurcation points as long as ϵ is small. Also, due to $\mu(t)$ being a function of time, we will find equilibria that are also functions in time, which we call pseudo-equilibira. The smooth case is well understood, see [24], so we consider the behavior of the non-smooth bifurcation with $x < 0$. From [7] as well as the smooth model [24], it is common practice to rescale time in a model with slow variation to put the dynamics on the same order and allow for algebraic solutions to be found. Here the parameter $\mu(t)$ is slowly varying in time so it

makes sense to rescale using this as our slow time, $\tau = \epsilon t$. Applying both $x < 0$ and this slow time approach to the system (2.1) then gives

$$\begin{aligned} \epsilon x_\tau &= -\mu(\tau) - 2x + x^2, \\ \mu_\tau &= -1. \end{aligned} \tag{2.3}$$

A standard approach to extracting information out of complicated models is to find reduced equations by separating the behavior at each order of the slow time. This approach is known as using an asymptotic expansion and further details can be found in Murray's *Asymptotic Analysis* [15]. With ϵ being the small quantity that dictates our slow time, we choose to use an asymptotic expansion of x with

$$x(\tau) \sim x_0(\tau) + \epsilon x_1(\tau) + \epsilon^2 x_2(\tau) + O(\epsilon^3). \tag{2.4}$$

This approach captures the slowly varying behavior of the solution in terms of this small quantity ϵ and aims to relate the slow variation to the solution. We substitute the expansion (2.4) into the scaled system (2.3) to get

$$\epsilon x_{0\tau} + \epsilon^2 x_{1\tau} + \ldots = -\mu(\tau) - 2x_0 + x_0^2 + \epsilon(-2x_1 + 2x_1 x_0) + \epsilon^2(-2x_1 + 2x_2 x_0 + x_1^2) + \ldots$$

Once we separate the equations at each order of ϵ, we find the following system of equations

$$O(1): \quad 0 = -\mu(\tau) - 2x_0 + x_0^2, \tag{2.5}$$

$$O(\epsilon): \quad 0 = -x_{0\tau} - 2x_1 + 2x_1 x_0, \tag{2.6}$$

$$O(\epsilon^2): \quad 0 = -x_{1\tau} - 2x_2 + 2x_2 x_0 + x_1^2. \tag{2.7}$$

Each of the equations (2.5)-(2.7) gives the respective order's pseudo-equilibrium. Thus we solve each equation progressively to find the terms of our asymptotic expansion (2.4) as

$$x(t) \sim 1 - \sqrt{1 + \mu(t)} + \frac{\epsilon}{4(1 + \mu(t))} - \frac{3\epsilon^2}{32(1 + \mu(t))^{5/2}} + O(\epsilon^3). \tag{2.8}$$

We call (2.8) the outer solution as it approximates the solution well for values of $x(t)$ away from the bifurcation value μ_{ns}. Since the dynamics of the system (2.1) change at $x = 0$ due to the non-smooth bifurcation of the underlying static system, this solution is valid only for $x < 0$ and $\mu > 0$.

It is a key assumption of an asymptotic expansion that the terms are clearly separated by order of ϵ. We search for a scaling of μ and x for which (2.8) is no longer valid under this assumption of order separation. This assumption fails when $x_0 \sim \epsilon x_1$ which occurs here for $\mu \sim O(\epsilon)$. To confirm, we conduct a simple scale analysis to determine the appropriate scaling for the local analysis about $x = 0$. Hence we consider the general scales

$$x = \epsilon^\alpha y, \quad \mu = \epsilon^\beta m,$$

with $\alpha > 0$ and $\beta > 0$ for an inner scaling. We apply these local variables in (2.1) to get the system

$$\begin{aligned} \epsilon^{\alpha}\dot{y} &= -\epsilon^{\beta}m + \epsilon^{\alpha}2|y| - \epsilon^{2\alpha}y|y|, \\ \epsilon^{\beta}\dot{m} &= -\epsilon. \end{aligned} \tag{2.9}$$

We balance the leading order terms $\epsilon^{\alpha}\dot{y}$ with $\epsilon^{\beta}m$ to find $\alpha = \beta$. Here the equation for m calls for $\beta = 1$, thus we have the scaling for the local analysis

$$x = \epsilon y, \quad \mu = \epsilon m. \tag{2.10}$$

We have found that the scalings in (2.10) apply to all x and thus we consider the region of $x > 0$. Substituting the local variables (2.10) into the original model (2.1) we find the following inner system for the region of $x > 0$

$$\begin{aligned} \dot{y} &= -m(t) + 2y - \epsilon y^2, \\ \dot{m} &= -1. \end{aligned} \tag{2.11}$$

We recall that we are searching for a link between y and m, and from [7] we use that it is then convenient to change the differentiation on y to be with respect to the slowly varying parameter m. This incorporates the behavior of $m(t)$ directly into the equation we solve and gives us a direct method for finding the tipping point. Then the leading order equation is

$$y_m = m - 2y. \tag{2.12}$$

The leading order solution to (2.12) is found explicitly as follows

$$y(m) = Ce^{-2m} + \frac{m}{2} - \frac{1}{4} + O(\epsilon).$$

With the inner solution found in terms of the parameter m, we write this in terms of the original variables with

$$x(t) \sim Ce^{-2\mu(t)/\epsilon} + \frac{\mu(t)}{2} + O(\epsilon). \tag{2.13}$$

We call the solution (2.13) the inner solution as it approximated the solution well near the bifurcation value μ_{ns}. Since the inner solution behaves exponentially, the tipping point, μ_{slow}, occurs when the exponential term begins to grow rapidly. Here we consider tipping to occur when the solution becomes $O(1/\epsilon)$. Then we find the tipping point μ_{slow} to take the form

$$\mu_{\text{slow}} = \frac{1}{2}\epsilon\log(\epsilon). \tag{2.14}$$

Thus we have the tipping point for the slowly varying model. Notice that for small values of ϵ, $\mu_{\text{slow}} < \mu_{\text{ns}}$ and this is consistent with considering the inner equation (2.11) for the region $x > 0$ as we found in the analysis. Hence we find that a slowly varying bifurcation parameter causes a delay in the rapid transition to the upper branch and we expect the

solution to remain near the lower branch for longer than in the static problem. In terms of hysteresis, then slow variation allows for a longer period before the states switch from the lower to the upper branch.

In figure 2.2 (a,b), two examples of this tipping is shown for different sizes of ϵ along with the standard bifurcation diagram where (c) demonstrates the tipping approximation across a range of ϵ. The concavities match as well as agreement in the estimation of the tipping point as ϵ goes to 0.

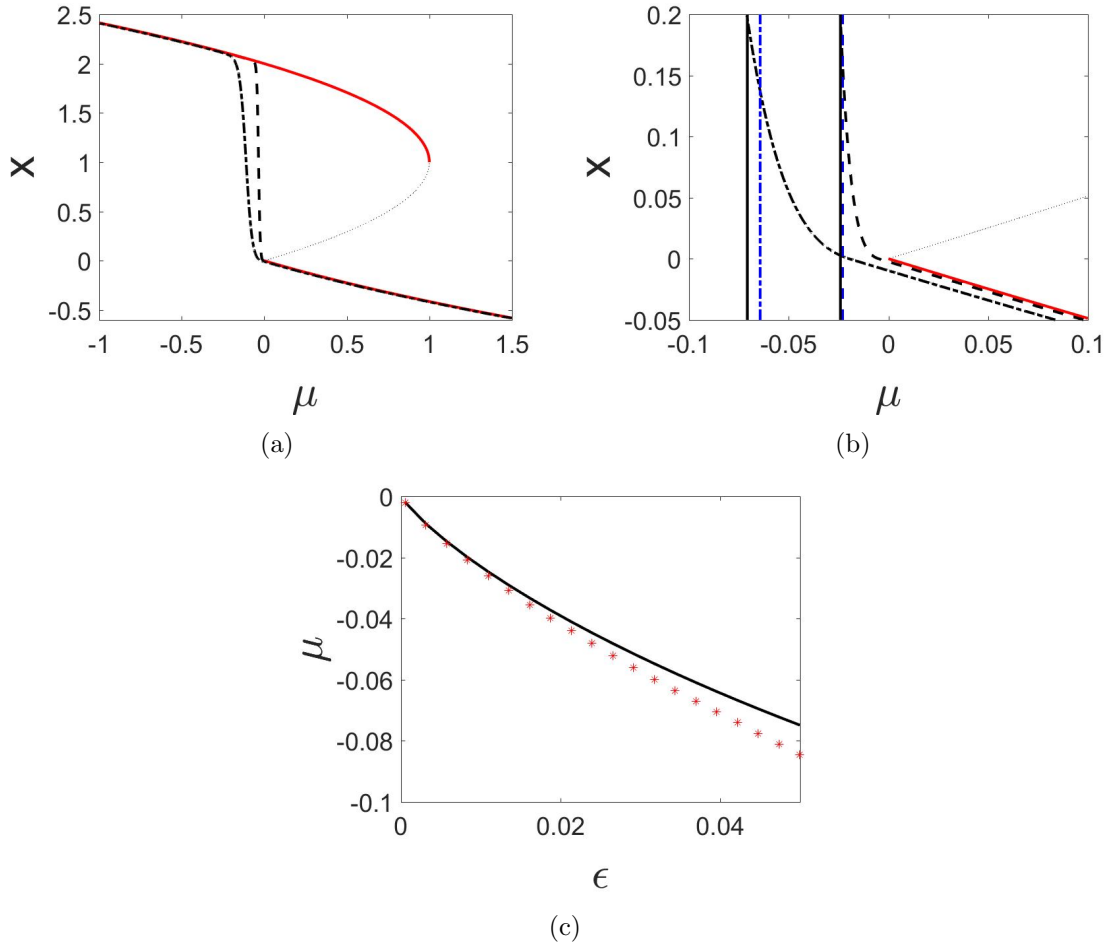

Figure 2.2: In (a) the numerical solutions (black dashed and dash-dotted lines) to (2.1) are given with $A = 0$ and $\epsilon = \{.01, .04\}$ respectively. The bifurcation plot is overlayed for convenience. In (b) a zoom in of what happens near the non-smooth bifurcation. The solid vertical lines (black) are tipping points where we use the tipping criterion $x > .5$ on the numerical solution. The dashed and dash-dotted vertical lines (blue) are the tipping estimates. In (c) a range of ϵ and their corresponding tipping (red stars) are compared to our estimate (solid black line) from (2.14).

2.2.1 Stability

From the static model we know our outer solution (2.8) to be stable, but to verify that the inner solution (2.13) is stable we use a simple linear stability analysis on the inner system. Typically to do this, an analysis would be performed about an equilibrium to see if perturbations would grow or decay. Although, in this model there is a parameter that is allowed to vary and hence we must be careful to note the analysis is about the pseudo-equilibrium instead. In the first region of interest, $m(t) \geq 0$, the following inner equation and pseudo-equilibrium, $z^0(t)$, hold below the axis

$$\dot{y} = -m(t) - 2y = f(t, y), \quad z^0(t) = -\frac{m(t)}{2}. \tag{2.15}$$

We then consider simple perturbations of the pseudo-equilibrium, u, in (2.15) with

$$y(t) = z^0(t) + u(t), \quad \|u(t)\| \ll 1.$$

Normally, a Taylor expansion would result in expressing the perturbations with their own equation that we could use to determine stability. Since $z^0(t)$ is not fixed, we must consider its contribution to the derivative in this region of the parameter space with $m(t) \geq 0$. Thus we find

$$\begin{aligned} \dot{y} &= \dot{z}^0 + \dot{u}, \\ \dot{z}^0 &= \begin{cases} -\frac{1}{2}\dot{m} = \frac{1}{2} & m(t) > 0, \\ 0 & m(t) = 0. \end{cases} \end{aligned} \tag{2.16}$$

Now we apply the standard Taylor expansion to see the behavior of these perturbations and with the contributions in (2.16), the inner equation (2.15) becomes

$$\begin{aligned} \dot{y} &= f(t, z^0) + f_y(t, z^0)(y - z^0) = f_y(t, z^0)u, \\ \dot{u} &= \begin{cases} -\frac{1}{2} - 2u, & m(t) > 0, \\ -2u, & m(t) = 0. \end{cases} \end{aligned} \tag{2.17}$$

If this were the static parameter problem, we would always have the second case in (2.17), which is always stable due to the sign. Since we allow for a varying parameter, we learn that the solution is attracted to just below the pseudo-equilibrium $z^0(t)$. As this system always experiences the critical point $m = 0$ due to the continuous decrease in $m(t)$, the slowly varying parameter eventually acts like the static parameter in section 2.1. Hence we have that for $x < 0$, the pseudo-equilibrium is hyperbolic and asymptotically stable. Here there is a critical point at $(\mu_{\text{ns}}, x_{\text{ns}}) = (0, 0)$ which corresponds to a non-hyperbolic equilibrium point. Generally, non-hyperbolic behavior signals equilibrium structures to change. Here, this signals a transition in behavior for $x > 0$ and helps identify that the tipping occurs in this region.

For the second region of interest, $m(t) < 0$, we found a solution that had the following inner equation which has the pseudo-equilibrium above the axis with

$$\dot{y} = -m(t) + 2y, \quad z^0(t) = \frac{m(t)}{2}. \tag{2.18}$$

In (2.18) we find a contradiction, here $m(t) < 0$ yet the solution of this region is above the axis $x = 0$. Thus we may conclude that this inner equation has no equilibrium in this region and further verifies that the critical point $(\mu_{\text{ns}}, x_{\text{ns}})$ was non-hyperbolic and tipping occurs for $m(t) < 0$.

2.3 High Frequency Oscillatory Forcing

To understand the oscillatory forcing in the Stommel model, consider the canonical system (2.1) with $A \sim O(1)$, $\Omega \gg 1$ and $\epsilon = 0$, which gives high frequency oscillatory forcing in the system. Under these conditions, we have a static parameter and for each parameter value there is oscillatory forcing with solutions characterized by oscillations about a fixed point. Thus we should expect to find a bifurcation influenced by oscillations occurring under these conditions. Here we develop a method to find oscillatory solutions to determine what the effect of oscillatory forcing has on the bifurcation of (2.1). In section 2.2, we focused only on the slowly varying dynamics but here we have both a slow time scale t and a fast time scale $T = \Omega t$. This naturally suggests a multiple scales approach where we search for a solution that is dependent on both of these scales, $x(t) = x(t, T)$. This method is commonly used in problems that have behavior observable on multiple scales, and we use it here to find a way to accurately analyze each scale and effectively combine their behavior into a single unifying solution. Further discussion on this method can be found in [20].

Recall that our focus is on the non-smooth behavior and hence we restrict the solution to follow along the lower stable equilibrium branch where $x < 0$. Using this multiple scales approach, our canonical system (2.1) has the following form

$$x_T + \Omega^{-1} x_t = \Omega^{-1} \left(-\mu - 2x + x^2 + A \sin(T) \right). \tag{2.19}$$

Note: We choose to use the subscript notation for partial derivatives, $\frac{\partial x}{\partial T} = x_T$. In (2.19), the small quantity Ω^{-1} appears which suggests an asymptotic expansion in powers of this quantity

$$x(t, T) \sim x_0(t, T) + \Omega^{-1} x_1(t, T) + \Omega^{-2} x_2(t, T) + O(\Omega^{-3}). \tag{2.20}$$

Substituting (2.20) into (2.19), we find

$$x_{0T} + \Omega^{-1} x_{0t} + \Omega^{-1} x_{1T} + \ldots = \Omega^{-1}(-\mu - 2x_0 + x_0^2 + A \sin(T)) + \Omega^{-2}(-2x_1 + 2x_1 x_0) + \ldots$$

Here we separate by each order of Ω to find the following system of reduced equations

$$O(1): \quad x_{0T} = 0, \tag{2.21}$$

$$O(\Omega^{-1}): \quad x_{1T} + x_{0t} = -\mu - 2x_0 + x_0^2 + A \sin(T), \tag{2.22}$$

$$O(\Omega^{-2}): \quad x_{2T} + x_{1t} = -2x_1 + 2x_0 x_1. \tag{2.23}$$

With an equation at each order, we must be able to solve each equation to proceed to the next but we must also further restrict our solution from having resonant or linearly

growing terms to prevent any multiplicity or exponential growth. This assures that the terms in the asymptotic expansion are compatible with one another and we are able to find a robust solution. A common method to guarantee compatible solutions with sublinear growth at each order is the Fredholm alternative. This provides a solvability condition for each equation of the form $x_{iT} = R_i(t, T)$ with

$$\lim_{T\to\infty} \frac{1}{T} \int_0^T R_i(t, u)\, du = 0,$$

although for this system we consider the periodic form of the Fredholm alternative

$$\frac{1}{2\pi} \int_0^{2\pi} R_i(t, T)\, dT = 0. \tag{2.24}$$

Both the general and periodic form of the Fredholm alternative have been well studied and a more theoretic approach to the periodic version is discussed in Bensoussan's *Asymptotic analysis for periodic structures* [3]. From (2.21), we learn the leading order term is only dependent on the slow time, $x_0 = x_0(t)$. Applying the Fredholm alternative (2.24) to (2.22) gives an equation for the slow behavior which then implies an equation for the fast behavior with

$$\begin{aligned} 0 &= \frac{1}{2\pi} \int_0^{2\pi} \left(-x_{0t}(t) - \mu - 2x_0(t) + x_0(t)^2 + A\sin(T)\right)\, dT, \\ x_{0t} &= -\mu - 2x_0 + x_0^2, \quad x_{1T} = A\sin(T). \end{aligned} \tag{2.25}$$

Solving for the equilibrium solution of (2.25) leads to the leading order solution, x_0, and also allows us to partially solve for the first correction term x_1 with

$$\begin{aligned} x_0 &= 1 - \sqrt{1+\mu}, \\ x_1(t, T) &= v_1(t) - A\cos(T). \end{aligned}$$

Repeating this procedure in (2.23), as shown in Appendix B, results in the expansion (2.20) written in the original variables

$$x \sim 1 - \sqrt{1+\mu} - \Omega^{-1} A\cos(\Omega t) + O(\Omega^{-2}). \tag{2.26}$$

Once again, the explicit outer solution (2.26) performs well for x away from the axis $x = 0$, we search for when the assumptions of the asymptotic series fail indicating where an inner analysis is needed. This is when $x_0 \sim \epsilon x_1$ which occurs for $\mu \sim O(\Omega^{-1})$.

We consider a general scaling in the form of $x = \Omega^{-\alpha} y$ and $\mu = \Omega^{-\beta} m$ where $\alpha > 0$ and $\beta > 0$ allow for an inner equation to be found. Applying these local variables to (2.1) results in

$$\dot{y} = -\Omega^{\alpha-\beta} m + 2|y| - \Omega^{-\alpha} y|y| + \Omega^{\alpha} A\sin(\Omega t). \tag{2.27}$$

In the local system (2.27), we find similar behavior occurring across multiple scales and thus we are able to use the same time scales from the outer analysis, $t = t$ and $T = \Omega t$. Then we have $y(t) = y(t, T)$ and hence a similar multiple scales argument in (2.27) leads to

$$y_T + \Omega^{-1} y_t = -\Omega^{\alpha-\beta-1} m + \Omega^{-1} 2|y| - \Omega^{-\alpha-1} y|y| + \Omega^{\alpha-1} A\sin(T). \tag{2.28}$$

With a standard balancing argument between the leading order terms in (2.28) y_T and $\Omega^{\alpha-1}A\sin(T)$, we see that $\alpha = 1$. We also want to see the terms $\Omega^{\alpha-\beta-1}m$ balance with $\Omega^{-1}2|y|$, which gives us that $\beta = 1$ as well. This results in the inner equation

$$y_T + \Omega^{-1}y_t = \Omega^{-1}\left(-m + 2|y|\right) - \Omega^{-2}y|y| + A\sin(T). \tag{2.29}$$

Similarly to the outer equation, we approximate the solution with an asymptotic expansion in terms of Ω^{-1}

$$y(t,T) \sim y_0(t,T) + \Omega^{-1}y_1(t,T) + O(\Omega^{-2}). \tag{2.30}$$

Substituting the expansion (2.30) into the inner equation (2.29) we find

$$\begin{aligned} y_{0T} + \Omega^{-1}y_{0t} + \Omega^{-1}y_{1T} + \ldots = \Omega^{-1}(-m + 2|y_0 + \Omega^{-1}y_1 + \ldots|) + A\sin(T) \\ + \Omega^{-2}(y_0 + \Omega^{-1}y_1 + \ldots)|y_0 + \Omega^{-1}y_1 + \ldots|. \end{aligned}$$

Here we then find the following system of equations at each order of Ω

$$O(1): \quad y_{0T} = A\sin(T), \tag{2.31}$$

$$O(\Omega^{-1}): \quad y_{1T} + y_{0t} = -m + 2|y_0|. \tag{2.32}$$

Solving the leading order equation (2.31) gives that the leading order term has the form, $y_0(t,T) = v_0(t) - A\cos(T)$. Applying the Fredholm alternative (2.24) to (2.32) leads to

$$v_{0t}(t) = -m + \frac{1}{\pi}\int_0^{2\pi} |v_0(t) - A\cos(T)|\, dT. \tag{2.33}$$

In this setting, we must consider two cases for $v_0(t)$ that determine the nature of this integrand. Case I: if $v_0(t)$ is large enough to keep y_0 from ever changing sign and Case II: if $v_0(t)$ is too small and y_0 crosses the $x = 0$ axis. In figure 2.3 we show the range of each case, the region on the right is following under case I, the green dotted vertical line defining the parameter range between the cases, the middle region for case II and the blue vertical line giving the bifurcation, μ_{osc}, which is determined below.

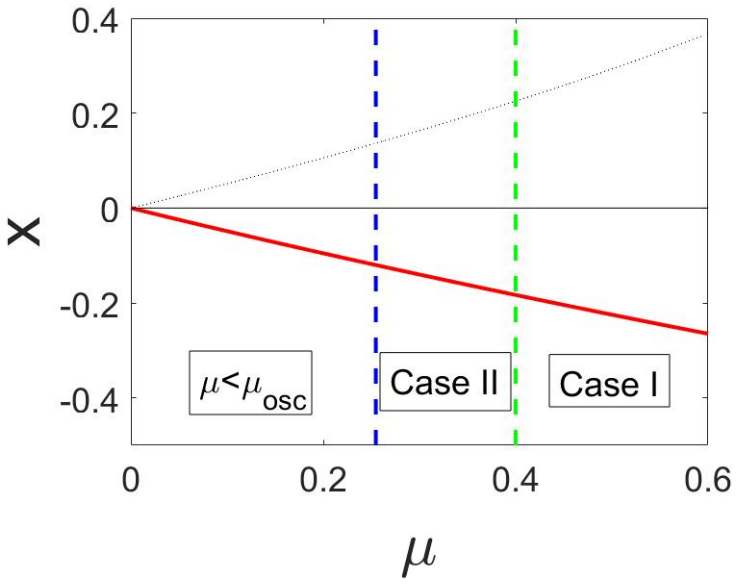

Figure 2.3: The parameter ranges for each case are shown here with $A = 2$. For reference, the original bifurcation diagram is overlayed.

2.3.1 Case I: $v_0(t) \leq -|A|$

We call this the 'below axis' case as the solution stays far from the axis $x = 0$ for most of the oscillation and thus the behavior is not influenced by the non-smooth dynamics. We do not expect to see the bifurcation occur under these conditions but instead we find the parameter range for each of these cases. Here the integral in equation (2.33) is straightforward to evaluate as $v_0(t)$ is a constant with respect to the fast time T, thus we find the inner equation and equilibrium

$$v_{0t} = -m - 2v_0, \quad v_0 = -\frac{m}{2}.$$

This gives the leading order equilibrium solution with oscillations of the local variables for this case which we write in terms of the original variables

$$\begin{aligned} y(t,T) &\sim -\frac{m}{2} - A\cos(T) + O(\Omega^{-1}), \\ x(t) &\sim -\frac{\mu}{2} - \Omega^{-1} A\cos(\Omega t) + O(\Omega^{-2}). \end{aligned} \tag{2.34}$$

The condition $v_0(t) \leq -|A|$ combined with the equilibrium allows us to establish when (2.34) holds

$$\mu \geq \frac{2|A|}{\Omega}. \tag{2.35}$$

Following the equilibrium to (2.35) leads us to case II where the oscillations cross the axis and the assumptions of this case no longer hold.

2.3.2 Case II: $|v_0(t)| < |A|$

We call this the 'crossing' case; here the equilibrium is small enough that the oscillations can now push the solution above the axis. Under these conditions, the solution spends time near the axis $x = 0$ and thus experiences non-smooth influence. As the crossing continues, the non-smooth behavior drives the solution to gradually grow. Therefore we expect to find the bifurcation here. From (2.35), we have a range of μ when this case applies, $\mu < \frac{2|A|}{\Omega}$. It is important to note that the integrand in (2.33) is non-trivial when $|v_0(t)| < |A|$. In order to deal with the sign changing inside the integral, we break the integration into regions based on the sign. Recall that we are searching for equilibrium behavior, and so we may make the assumption that we are dealing with a fixed value of v_0 such that $|v_0| \leq |A|$. In figure 2.4 we observe the function that we are integrating.

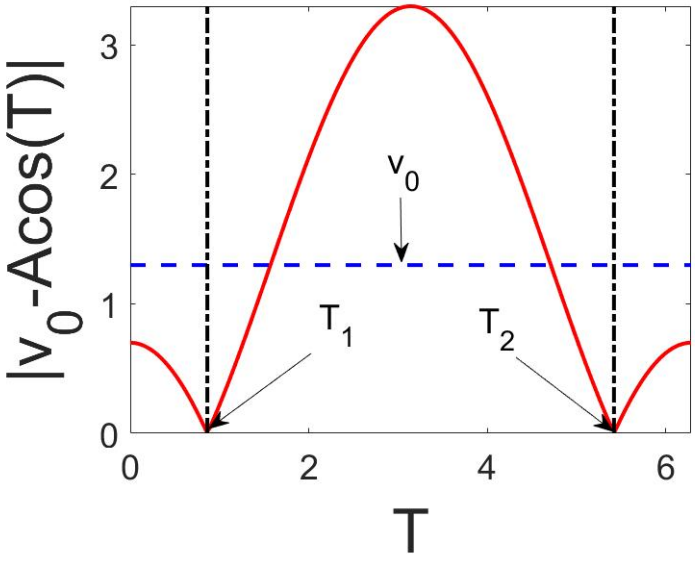

Figure 2.4: The non-smooth function $|y_0(T)| = |v_0 - A\cos(T)|$ that we integrate is shown as a solid red line. We also show an example of v_0 as a horizontal blue dotted line. Here the value of $|v_0| \leq |A|$, which causes kinks to appear at the roots of $|y_0|$: T_1 and T_2 respectively. These are the vertical black dashed dotted lines.

From figure 2.4, the roots of the integrand are

$$T_1 = \arccos(v_0/A), \qquad T_2 = 2\pi - \arccos(v_0/A).$$

Here we notice $0 < T_1 < T_2 < 2\pi$ and that the sign of the integrand stays the same on each interval. We only assume that the first interval $[0, T_1]$ observes a solution while the center is still negative, thus the integrand will also be negative. From this, the integral in (2.33)

is computed as

$$\int_0^{2\pi} |v_0 - A\cos(T)|\, dT = -\int_0^{T_1} (v_0 - A\cos(T))\, dT + \int_{T_1}^{T_2} (v_0 - A\cos(T))\, dT - \int_{T_2}^{2\pi} (v_0 - A\cos(T))\, dT. \tag{2.36}$$

Evaluating (2.36) and using a trigonometric identity, $\sin(\arccos(x)) = \sqrt{1-x^2}$, we find the integral to be

$$\int_0^{2\pi} |v_0 - A\cos(T)|\, dT = \frac{2}{\pi}\left(\arcsin(v_0/A)v_0 + \sqrt{A^2 - v_0^2}\right).$$

Notice that our argument above is simple for fixed v_0, but we have used a multiple scales approach for our fast time with $t \ll T$ implying that $v_0(t)$ is approximately fixed over $T \in [0, 2\pi]$. This holds true due to having a high frequency Ω and otherwise would not be a valid approximation. Thus we can evaluate (2.33) to find the inner equation

$$v_{0t} = -m + \frac{4}{\pi}\left(\arcsin(v_0/A)v_0 + \sqrt{A^2 - v_0^2}\right). \tag{2.37}$$

In its current form, (2.37) prevents $v_0(t)$ to be found analytically, so we use a quadratic Taylor approximation to be able to solve this equation explicitly. This then gives

$$v_{0t} \approx -m + \frac{4|A|}{\pi} + \frac{2}{\pi|A|}v_0^2, \tag{2.38}$$

which has the following equilibrium with positive constant C

$$v_0 = -C\sqrt{m - \frac{4|A|}{\pi}}. \tag{2.39}$$

Thus we have the leading order inner equilibrium (2.39) and writing this in the original variables gives

$$\begin{aligned} y &\sim -C\sqrt{m - \frac{4|A|}{\pi}} - A\cos(T) + O(\Omega^{-1}), \\ x(t) &\sim -C\sqrt{\Omega\left(\mu - \frac{4|A|}{\pi\Omega}\right)} - \Omega^{-1}A\cos(\Omega t) + O(\Omega^{-2}). \end{aligned} \tag{2.40}$$

It then is clear that the bifurcation, μ_{osc}, occurs when (2.40) fails to be real valued. Thus we find μ_{osc} to take the form

$$\mu_{\text{osc}} = \frac{4|A|}{\pi\Omega}. \tag{2.41}$$

From the result (2.41), we gather that the oscillatory forcing in the system causes the bifurcation to occur sooner, $\mu_{\text{osc}} > \mu_{\text{ns}}$, and this is controlled by the size of A and Ω. Heuristically, the model experiences the non-smooth behavior sooner in μ with the oscillations, but we can see as $\Omega \to \infty$ then $\mu_{\text{osc}} \to \mu_{\text{ns}}$. This effect is contrary to the

slow variation where the solution experienced a delayed tipping, $\mu_{\text{slow}} < \mu_{\text{ns}}$. Although our assumption that $\Omega \gg 1$ must be met for our analysis to hold, we may still see a medium-range Ω. From figure 2.5 (d) we may have $\Omega = 5$ and get reasonable approximations with μ_{osc}. This means that our approximation μ_{osc} improves with increasing Ω, but it still provides a reasonable approximation for bifurcations away from μ_{ns} for a range of Ω. Advanced bifurcation also indicates that the region of bi-stability is shrunk with oscillatory forcing and thus can be used to eliminate the region entirely with A and Ω chosen properly, effectively destroying any hysteresis. We compare our estimate to numerical results for varying sizes of Ω^{-1}.

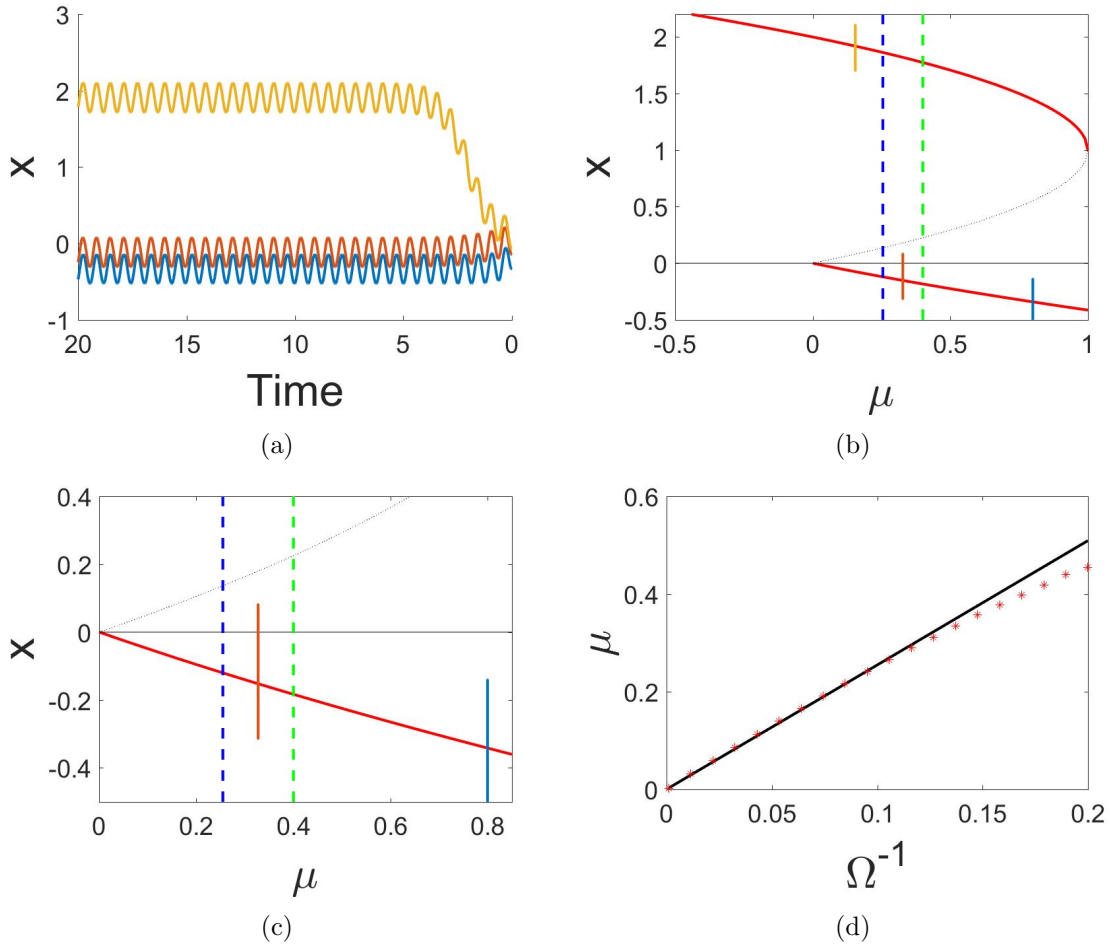

Figure 2.5: In (a) the numerical time series solutions to (2.1) are given from bottom to top with $\mu = \{.8, .33, .15\}$ in case I, case II and $\mu < \mu_{\text{osc}}$ in (2.41) respectively with $A = 2$, $\Omega = 10$ and $\epsilon = 0$. In (b) we show the time series on the bifurcation diagram. In (c), a zoom in closer to the non-smooth bifurcation of (b), where the dotted vertical lines dictate the region between case I and case II (green) as well as the bifurcation estimate (blue) respectively. In (d) a range of Ω^{-1} and the corresponding numerical bifurcations (red stars) are compared to our estimate of the bifurcations (black solid line). We consider the bifurcation criterion to be when the numerical solution has passed $x > .5$.

In figure 2.5 an example is given of the effect oscillatory forcing has on the solution given a choice of A and Ω with (a), (b) and (c), but (d) shows the bifurcation approximation across a range of Ω^{-1}. There is an allowed range of Ω from our assumption of $\Omega \gg 1$ and in this region we see agreement between the numerical results and our approximations. The concavity is well represented and the behavior as $\Omega^{-1} \to 0$ converges to the static bifurcation. Thus we expect that our methodology is valuable for the Stommel model.

2.3.3 Stability

Once more, the outer solution (2.26) is stable from the static model in section 2.1. In this section, we have two regions of interest and establish their stabilities agree with our analysis. Each region has a particular version of the same inner equation dictating the solution's behavior, namely

$$v_{0t} = -m + \frac{1}{\pi}\int_0^{2\pi} |v_0 - A\cos(T)|\, dT. \tag{2.42}$$

Case I: $v_0(t) < -|A|$

In this region we did not find any bifurcation behavior and (2.42) simplifies to the inner equation with equilibrium z^0 as follows

$$v_{0t} = -m - 2v_0 = f(v_0), \quad z^0 = -\frac{m}{2}.$$

Similarly to section 2.2, we have a fixed parameter equation that we have shown to cause perturbations to decay exponentially and hence we find the equilibrium to be hyperbolic and asymptotically stable in the paramter range found in the analysis (2.35)

$$\mu \geq \frac{2|A|}{\Omega}.$$

Case II: $|v_0(t)| < |A|$

For this region we found the bifurcation and hence we should expect to lose stability here. The Taylor approximation (2.38) for the inner equation with equilibrium z^0 is

$$v_{0t} = -m + \frac{4|A|}{\pi} + \frac{2}{\pi|A|}v_0^2, \quad z^0 = -C\sqrt{m - \frac{4|A|}{\pi}}. \tag{2.43}$$

We consider a simple linear perturbation of (2.43), $v_0(t) = z^0 + u(t)$ with $\|u(t)\| \ll 1$. Applying the standard Taylor expansion to determine the equation for the perturbations, we find

$$\begin{aligned} v_{0t} =& f(z^0) + f_{v_0}(z^0)(v_0 - z^0) + O(\|v_0 - z^0\|^2), \\ u_t =& -2\sqrt{m - \frac{4|A|}{\pi}}u. \end{aligned} \tag{2.44}$$

The sign of (2.44) gives that the perturbations decay exponentially and hence the equilibrium is hyperbolic and asymptotically stable as long as $m > \frac{4|A|}{\pi}$ or equivalently $\mu > \frac{4|A|}{\pi\Omega}$.

We find that once μ reaches this value in (2.41), then the stability of (2.44) is non-hyperbolic. When the stability switches like this, we expect a bifurcation. Thus we have further evidence to support that (2.41) is the oscillatory bifurcation we seek.

2.4 Slowly Varying and Oscillatory Forcing

Now that we have established an approach for each feature of the model individually, we combine them in the full one component model (2.1) where $\epsilon \ll 1$ and $A \sim O(1)$. Due to the slow variation in μ, we do not see a bifurcation occur under these conditions but rather a tipping point. Hence we must find the behavior of the solution and search for when a rapid transition towards the upper branch occurs. Since the high frequency could be approximated by a power of slow variation, we choose to relate these mechanisms with a generic polynomial $\Omega = \epsilon^{-\lambda}$ for a parameter $\lambda > 0$. With a general λ, we classify regions of behavior by ranges of λ and are able to determine where mixed behavior occurs or when one of the mechanisms becomes dominant. With both mechanisms in effect, we again choose to use a multiple scales approach to capture both slow behavior and fast oscillations. Although now, we truly have slow behavior, the slowly varying parameter $\mu(t)$, as well as fast behavior, the rapid oscillations $\sin(\Omega t)$. The choice in time scales is then $\tau = \epsilon t$ and $T = \epsilon^{-\lambda} t$, which leads to the system

$$\begin{aligned} x_T + \epsilon^{\lambda+1} x_\tau &= \epsilon^\lambda(-\mu(\tau) + 2|x| - x|x| + A\sin(T)), \\ \mu_\tau &= -1. \end{aligned}$$

Once again, we assume initial conditions satisfying $x < 0$ and starting far enough away from $x = 0$, before any crossing occurs, to find the outer solution. Thus we have the system

$$\begin{aligned} x_T + \epsilon^{\lambda+1} x_\tau &= \epsilon^\lambda(-\mu(\tau) - 2x + x^2 + A\sin(T)), \\ \mu_\tau(\tau) &= -1. \end{aligned} \tag{2.45}$$

We perform an asymptotic expansion in terms of the small quantity ϵ^λ, where we note that this is the same as Ω^{-1},

$$x(\tau, T) \sim x_0(\tau, T) + \epsilon^\lambda x_1(\tau, T) + O(\epsilon^{1+\lambda}, \epsilon^{2\lambda}). \tag{2.46}$$

Introducing the expansion (2.46) into the outer multi-scaled equation (2.45) gives

$$x_{0T} + \epsilon^{\lambda+1} x_{0\tau} + \epsilon^\lambda x_{1T} + \ldots = \epsilon^\lambda(-\mu(\tau) - 2x_0 + x_0^2 + A\sin(T)) + \epsilon^{2\lambda}(-2x_1 + x_1 x_0) + \ldots \tag{2.47}$$

Here we separate (2.47) at each order of ϵ^λ to find the following system of equations

$$O(1): \quad x_{0T} = 0, \tag{2.48}$$

$$O(\epsilon^\lambda): \quad x_{1T} = -\mu(\tau) - 2x_0 + x_0^2 + A\sin(T), \tag{2.49}$$

$$O(\epsilon^{2\lambda}): \quad x_{2T} + \epsilon^{1-\lambda} x_{0\tau} = -2x_1 + 2x_0 x_1. \tag{2.50}$$

Depending on the value of λ, $O(\epsilon^{\lambda+1})$ may be the next order before $O(\epsilon^{2\lambda})$, although considering either produce the same equation at their respective order and hence our choice in λ does not change the calculations up to this correction term. Thus for the outer solution, we consider the system with $O(\epsilon^{2\lambda})$. Each equation gives the behavior of each order of the solution; (2.48) indicates that the leading order term is only slow time dependent, $x_0 = x_0(\tau)$. In Appendix B we apply the Fredholm alternative (2.24) to (2.49) and (2.50) to find the first few terms of the expansion in (2.46) explicitly. The resulting solution is

$$x(t) \sim 1 - \sqrt{1+\mu(t)} - \frac{\epsilon}{4(1+\mu(t))} - \epsilon^{\lambda} A\cos(\Omega t) + O(\epsilon^{1+\lambda}, \epsilon^{2\lambda}). \tag{2.51}$$

In the outer solution (2.51), we consider when the terms violate the assumptions of the expansion to find where we need to use an inner equation. This happens either when $x_0 \sim O(\epsilon)$ or when $x_0 \sim O(\epsilon^{\lambda})$ which is when $\mu \sim O(\epsilon)$ or $\mu \sim O(\epsilon^{\lambda})$ respectively and depends on the value of λ.

To find an inner equation we use a general scaling for both x and μ given the ambiguity of the choice in μ with

$$x(t) = \epsilon^{\alpha} y(t), \quad \mu(t) = \epsilon^{\beta} m(t), \tag{2.52}$$

where $\alpha > 0$ and $\beta > 0$ allow for inner equations to be found. Applying the local variables (2.52) to the canonical equation (2.1) gives

$$\begin{aligned} \epsilon^{\alpha}\dot{y} &= -\epsilon^{\beta} m(t) + \epsilon^{\alpha} 2|y| - \epsilon^{2\alpha} y|y| + A\sin\Big(\epsilon^{-\lambda} t\Big), \\ \dot{m} &= -\epsilon^{1-\beta}. \end{aligned} \tag{2.53}$$

From (2.53) we find the fast time still appears but the slow time has multiple choices depending on λ. For convenience we choose to take a multiple scales approach with scales t and $T = \epsilon^{-\lambda} t$ in (2.53) to find

$$\begin{aligned} \epsilon^{\alpha-\lambda} y_T + \epsilon^{\alpha} y_t &= -\epsilon^{\beta} m(t) + \epsilon^{\alpha} 2|y| - \epsilon^{2\alpha} y|y| + A\sin(T), \\ m_t &= -\epsilon^{1-\beta}. \end{aligned} \tag{2.54}$$

To determine the correct scalings in (2.52), we balance the leading order terms on both sides of (2.54) $\epsilon^{\alpha-\lambda} y_T$ and $A\sin(T)$, which gives us that $\alpha = \lambda$. This suggests that the oscillatory term persists in the inner asymptotic expansion of (2.1) regardless of the choice in λ.

We now consider the same scales t and $T = \epsilon^{-\lambda} t$ on the canonical system (2.1)

$$\begin{aligned} x_T + \epsilon^{\lambda} x_t &= -\epsilon^{\lambda+\beta} m(t) + \epsilon^{\lambda} 2|x| - \epsilon^{\lambda} x|x| + \epsilon^{\lambda} A\sin(T), \\ m_t &= -\epsilon^{1-\beta}. \end{aligned} \tag{2.55}$$

Here we use the expansion

$$x(t,T) = \epsilon^{\lambda} y_0(t,T) + \ldots,$$

where the next terms of this expansion depend on whether $\lambda \leq 1$ or $\lambda > 1$. We consider these ranges in case I and case II respectively.

2.4.1 Case I: $\lambda \leq 1$

We call this the 'mixed effects' case a both slow variation and oscillatory forcing causing noticeable effects on the solution for this range of λ. Hence we consider the expansion

$$x(t,T) \sim \epsilon^{\lambda} y_0(t,T) + \epsilon^{q} y_1(t,T) + \ldots, \tag{2.56}$$

with the next term $q > \lambda$ to be consistent with the scale analysis above that determined inner behavior to start at $O(\epsilon^{\lambda})$. Substituting (2.56) into (2.55) gives

$$\begin{aligned} y_{0T} + \epsilon^{\lambda} y_{0t} + \epsilon^{q-\lambda} y_{1T} + \epsilon^{q} y_{1t} + \ldots = & -\epsilon^{\beta} m(t) + \epsilon^{\lambda} 2|y_0 + \epsilon^{q-\lambda} y_1 + \ldots| + A\sin(T) \\ & + \epsilon^{2\lambda}(y_0 + \epsilon^{q-\lambda} y_1 + \ldots)|y_0 + \epsilon^{q-\lambda} y_1 + \ldots|. \end{aligned}$$

Separating by distinct orders of ϵ then gives the following equations at each order

$$O(1) : y_{0T} = A\sin(T), \tag{2.57}$$

$$O(\epsilon^{\lambda}) : \epsilon^{q-2\lambda} y_{1T} + y_{0t} = -\epsilon^{\beta-\lambda} m(s) + 2|y_0|. \tag{2.58}$$

In (2.58) we find that the appropriate next term in the expansion (2.56) is with $q = 2\lambda$. This choice in q keeps the equations balanced but q implies that $\lambda > \frac{1}{2}$ for an expansion to be found. Otherwise, the quadratic terms must be included and we no longer find local equations. This indicates that the range of $\lambda \leq \frac{1}{2}$ behaves differently. We discuss this further in chapter 4. There is also the choice between $\beta = \lambda$ or $\beta = 1$ and each has a particular appeal. With $\beta = \lambda$, the form of (2.58) is simple, but the equation for the slow variation is $m_t = -\epsilon^{1-\lambda}$. This then suggests a slower time scale to approach the problem. We instead choose to allow $\beta = 1$ for convenience and track a small coefficient on $m(t)$ in exchange for keeping the same time scale with $m_t = -1$. This is valid as long as we are tracking small coefficients and not large ones as this would suggest we used an incorrect scaling, but both of these choices lead to the same conclusion. Using (2.57) gives the appropriate form, $y_0(t,T) = v_0(t) - A\cos(T)$. We then apply the Fredholm alternative (2.24) to (2.58) which gives a similar equation to the integral (2.33) in section 2.3 with

$$v_{0t} = -\epsilon^{1-\lambda} m(t) + \frac{1}{\pi}\int_0^{2\pi} |v_0(t) - A\cos(T)|\, dT. \tag{2.59}$$

The approach developed in section 2.3 is applied here to (2.59), where we separate the behavior of the integral based on the relative size of $v_0(t)$ to A. We have the following situations, sub-case I: $v_0(t) \leq -|A|$ and sub-case II: $|v_0(t)| < |A|$.

Sub-Case I: $v_0(t) \leq -|A|$

Once more, we call this the 'below axis' sub-case and we do not expect tipping to occur under these conditions since the solution is entirely negative and far from the axis $x = 0$ for most of the oscillation. Under these conditions, (2.59) gives the simple inner equation

$$v_{0t} = -\epsilon^{1-\lambda} m(t) - 2v_0. \tag{2.60}$$

Solving (2.60) can be done under our assumptions much like in subsection 2.3.1 but instead we focus on the pseudo-equilibrium. This choice results in finding the effective parameter range for μ which distinguishes these sub-cases and helps to determine when the solution enters sub-case II. Since $m(t)$ is allowed to vary, this must be thought of more as a pseudo-equilibrium and we are only interested in when the pseudo-equilibrium violates the assumptions of this case. Finding the pseudo-equilibrium of (2.60) gives

$$v_0(t) = -\epsilon^{1-\lambda}\frac{m(t)}{2}.$$

Using the condition $v_0(t) \leq -|A|$ gives that $m(t) \geq \epsilon^{\lambda-1}2|A|$. Writing this result in original variables gives us the parameter range

$$\mu(t) \geq \frac{2|A|}{\Omega}, \tag{2.61}$$

for sub-case I which agrees with the range from (2.35) in section 2.3. Following the pseudo-equilibrium to the boundary (2.61), we eventually reach sub-case II where we see the oscillations crossing the axis.

Sub-Case II: $|v_0(t)| < |A|$

Again, we call this the 'crossing' sub-case. Here the behavior of the solution depends strongly on the sign of the solution similarly to section 2.3. We seek the relationship between slow variation and oscillatory forcing on the tipping point. As the pseudo-equilibrium gets closer to the $x = 0$ axis, the solution spends more time above this axis and more complicated contributions from the sign changing appear. We expect tipping to happen under these conditions.

The methodology of solving the integral in (2.59) holds identically to that of subsection 2.3.2. Here, we have a slow time function $v_0(t)$ that is approximately fixed with respect to the fast time T under the multiple scales approach. Thus we evaluate the integral by separating the sign of the integrand with the values $T_1 = \arccos(v_0/A)$ and $T_2 = 2\pi - \arccos(v_0/A)$ to find

$$v_{0t} = -\epsilon^{1-\lambda}m(t) + \frac{4}{\pi}\left(\arcsin(v_0/A)v_0 + \sqrt{A^2 - v_0^2}\right). \tag{2.62}$$

We then choose to find an explicit analytic expression by approximating (2.62) with a quadratic Taylor expansion. This gives

$$\begin{aligned} v_{0t} &= -\epsilon^{1-\lambda}m(t) + \frac{4|A|}{\pi} + \frac{2}{\pi|A|}v_0^2, \\ m_t &= -1. \end{aligned} \tag{2.63}$$

With (2.63) in terms of slow time, it restricts any analytical approaches that link the effects of the varying parameter. Instead we take the same approach from [7] and switch the differentiation onto the slow varying parameter m with

$$v_{0m} = \epsilon^{1-\lambda}m - \frac{4|A|}{\pi} - \frac{2}{\pi|A|}v_0^2. \tag{2.64}$$

It is here where we take advantage of the form of (2.64) with the form from (1.3) to solve, resulting in

$$v_0(m) \sim \epsilon^{(1-\lambda)/3} \left(\frac{\pi|A|}{2}\right)^{2/3} \frac{Ai'\left(\epsilon^{2(\lambda-1)/3}\left(\frac{2}{\pi|A|}\right)^{1/3}(\epsilon^{1-\lambda}m - \frac{4|A|}{\pi})\right)}{Ai\left(\epsilon^{2(\lambda-1)/3}\left(\frac{2}{\pi|A|}\right)^{1/3}(\epsilon^{1-\lambda}m - \frac{4|A|}{\pi})\right)}.$$

With the solution to (2.56) we rewrite back into the original variables

$$\begin{aligned} y_0(t,T) \sim & C\frac{Ai'\left(\epsilon^{2(\lambda-1)/3}\left(\frac{2}{\pi|A|}\right)^{1/3}(\epsilon^{1-\lambda}m(t) - \frac{4|A|}{\pi})\right)}{Ai\left(\epsilon^{2(\lambda-1)/3}\left(\frac{2}{\pi|A|}\right)^{1/3}(m(t) - \frac{4|A|}{\pi})\right)} - \epsilon^{\lambda} A\cos(T) + \ldots, \\ x(t) \sim & C\frac{Ai'\left(\left(\frac{\Omega}{\epsilon^2}\right)^{1/3}\left(\frac{2}{\pi|A|}\right)^{1/3}(\mu(t) - \frac{4|A|}{\pi\Omega})\right)}{Ai\left(\left(\frac{\Omega}{\epsilon^2}\right)^{1/3}\left(\frac{2}{\pi|A|}\right)^{1/3}(\mu(t) - \frac{4|A|}{\pi\Omega})\right)} - \epsilon^{\lambda} A\cos(\Omega t) + \ldots \end{aligned} \tag{2.65}$$

Given the inner solution (2.65), we search for the singularity of this solution in order to identify tipping. Recall from (1.4) that the singularity relates to the first root of the Airy equation. Here we find the singularity μ_{mixed} to be

$$\mu_{\text{mixed}} = \left(\frac{\epsilon^2}{\Omega}\right)^{1/3}\left(\frac{\pi|A|}{2}\right)^{1/3}(-2.33811\ldots) + \frac{4|A|}{\pi\Omega}. \tag{2.66}$$

The value μ_{mixed} which causes this singularity is our tipping point. We rewrite (2.66) to emphasize the contributions from the slow variation of the parameter and the oscillatory forcing

$$\mu_{\text{mixed}} = \left(\frac{\pi|A|}{2\Omega}\right)^{1/3}\mu_{\text{smooth}} + \mu_{\text{osc}}, \tag{2.67}$$

with $\mu_{\text{smooth}} = \epsilon^{2/3}(-2.33811\ldots)$, similarly to the smooth problem from [24], and μ_{osc} from (2.41) respectively.

The resulting tipping approximation (2.67) indicates that the size of the amplitude A determines whether the tipping occurs early or late relative to the bifurcation. Naturally we see a larger amplitude cause more contribution from the oscillations and hence an earlier tipping. On the other hand, larger values in ϵ cause this tipping to occur later. So these effects have opposite pulls on the tipping and can effectively cancel one another out under proper conditions. It would even be possible to break the hysteresis cycle by eliminating the region of bi-stability in this model with sufficiently large amplitude and small ϵ. The tipping point holds for any $\lambda \in (\frac{1}{2}, 1]$ and we see different behavior for larger λ.

2.4.2 Case II: $\lambda > 1$

We call this the 'slowly varying dominant' case as this is when we see that the oscillations contribute less than the slow variation. For this range of λ the scaling for μ is simple,

$\mu = \epsilon m$. Thus we expect to see integer powers in the leading order along with powers of λ so we choose the expansion

$$x(t,T) \sim \epsilon^{\lambda} y_0(t,T) + \epsilon y_1(t,T) + \epsilon^q y_2(t,T) + \dots, \tag{2.68}$$

where $q > \lambda$ to allow for consistency with the scale analysis but not necessarily the same value as in case I. Substituting (2.68) into (2.55) gives

$$\begin{aligned}\epsilon y_{0T} + \epsilon^{\lambda+1} y_{0t} + \epsilon^{\lambda} y_{1T} + \epsilon^q y_{2T} + \dots = &- \epsilon^{\lambda+1} m(t) + \epsilon^{\lambda+1} 2|y_0 + \epsilon^{\lambda-1} y_1 + \dots| \\ &+ \epsilon^{\lambda+2}(y_0 + \epsilon^{\lambda-1} y_1 + \dots)|y_0 + \epsilon^{\lambda-1} y_1 + \dots| \\ &+ \epsilon^{\lambda} A \sin(T)\end{aligned}$$

Here we separate out each order of ϵ to find the equations at each order

$$O(\epsilon) : y_{0T} = 0, \tag{2.69}$$

$$O(\epsilon^{\lambda}) : y_{1T} = A\sin(T), \tag{2.70}$$

$$O(\epsilon^{\lambda+1}) : \epsilon^{q-\lambda-1} y_{2T} + y_{0t} = -m(t) + 2|y_0 + \epsilon^{\lambda-1} y_1|. \tag{2.71}$$

We learn in (2.71) that $q = \lambda + 1$ keeps the terms balanced. From (2.69) we find that the dominant behavior for this case is only slow time dependent, $y_0 = y_0(t)$ and from (2.70) that the oscillatory behavior occurs in y_1 with $y_1(t,T) = v_1(t) - A\cos(T)$. Since we have y_1 as a correction to y_0, we may absorb the slow behavior into y_0. Thus we treat $y_0(t) = y_0(t) + \epsilon^{\lambda+1} v_1(t) \approx y_0(t)$. Applying Fredholm to (2.71) gives

$$y_{0t} = -m(t) + \frac{1}{\pi}\int_0^{2\pi} |y_0(t) - \epsilon^{\lambda-1} A\cos(T)|\, dT. \tag{2.72}$$

With $\lambda \approx 1$, we see nearly identical behavior in (2.72) as that of what we explored in subsection 2.4.1. As long as the amplitude of oscillations inside the integral are $\epsilon^{\lambda-1}A \sim O(1)$, then this integral is similar to the integral in Case I (2.59). To see this, we follow the same approach as to integrate (2.72) with $T_1 = \arccos\big(y_0/\epsilon^{\lambda-1}A\big)$ and $T_2 = 2\pi - \arccos\big(y_0/\epsilon^{\lambda-1}A\big)$ which gives

$$y_{0t} = -m(t) + \frac{4}{\pi}\left(\arcsin\Big(y_0/\epsilon^{\lambda-1}A\Big) y_0 + \sqrt{(\epsilon^{\lambda-1}A)^2 - y_0^2}\right). \tag{2.73}$$

Here we apply the same quadratic Taylor approximation to (2.73) to find

$$\begin{aligned} y_{0t} &= -m(t) + \epsilon^{\lambda-1}\frac{2|A|}{\pi} + \epsilon^{1-\lambda}\frac{2}{\pi|A|} y_0^2, \\ m &= -1. \end{aligned} \tag{2.74}$$

We again use the result from (1.4) to find the tipping, which we then write into original variables

$$m_{\text{mixed}} = \epsilon^{(\lambda-1)/3}\left(\frac{\pi|A|}{2}\right)^{1/3}(-2.33811\ldots) + \epsilon^{\lambda-1}\frac{4|A|}{\pi},$$
$$\mu_{\text{mixed}} = \left(\frac{\pi|A|}{2\Omega}\right)^{1/3}\mu_{\text{smooth}} + \mu_{\text{osc}}.$$

Thus we conclude that there is a natural transition into case II from case I with almost the same behavior and identical tipping as in (2.67). As λ continues to grow, the amplitude of oscillation in (2.72) decays and the contribution from the oscillations weaken. This allows us to say that the integral is approaching

$$y_{0t} = -m(t) + 2|y_0|. \tag{2.75}$$

With (2.75) taking the same form as in section 2.2, this allows us to use the results there to find the solution. We write this in terms of the original variables

$$\begin{aligned} y_0(t,T) \sim& Ce^{-2m(t)} + \frac{m(t)}{2} - 1/4 + \epsilon^{\lambda}A\cos(T), \\ x(t) \sim& Ce^{-2\mu(t)/\epsilon} + \frac{\mu(t)}{2} - \epsilon^{\lambda}A\cos(\Omega t) + O(\epsilon^{2\lambda}). \end{aligned} \tag{2.76}$$

This then leads to the same tipping as in the slowly varying model with

$$\mu_{\text{slow}} = \frac{1}{2}\epsilon\log\epsilon.$$

Thus we find that in this case and with λ near 1, the same tipping point μ_{mixed} in (2.67) from subsection 2.4.1 is found. For large λ, the oscillations have less of an impact and the solution tips entirely like μ_{slow} in (2.14) from section 2.2. For convenience, this is summarized in the following table.

One Component Tipping Points	
$\epsilon > 0$ and $A = 0$:	$\mu_{\text{slow}} = \epsilon\ln(\epsilon)/2$
$\epsilon = 0$ and $A \neq 0$ with $\Omega \gg 1$:	$\mu_{\text{osc}} = \frac{4\lvert A\rvert}{\pi\Omega}$
$\epsilon > 0$, $A \neq 0$ and $\lambda \leq 1$:	$\mu_{\text{mixed}} = \left(\frac{\pi\lvert A\rvert}{2\Omega}\right)^{1/3}\mu_{\text{smooth}} + \mu_{\text{osc}}$
$\epsilon > 0$, $A \neq 0$ and $\lambda > 1$ with $\lambda \approx 1$:	$\mu_{\text{mixed}} = \left(\frac{\pi\lvert A\rvert}{2\Omega}\right)^{1/3}\mu_{\text{smooth}} + \mu_{\text{osc}}$
$\epsilon > 0$, $A \neq 0$ and $\lambda > 1$:	$\mu_{\text{slow}} = \epsilon\ln(\epsilon)/2$

Table 2.1: Overview of the tipping points of the one component model for each mechanism and case.

In figure 2.6, we see an example of the numerical solution to the canonical system (2.1) with slow variation and oscillatory forcing. This example has a tipping point occurring in case I due to $\lambda \in (\frac{1}{2}, 1]$ allowing the slow variation and oscillatory forcing to produce a mixed effect on the tipping point. Although we see noticeable contributions from the slow varying parameter the tipping point still occurs near the oscillatory bifurcation. This tells

us that for these choices in the values the strongest effect is the oscillatory forcing. It is possible to find values of ϵ, A and λ that cause the non-smooth tipping to occur at the same place as the smooth bifurcation. This would eliminate the region of bi-stability and destroy the hysteresis curve entirely for this model.

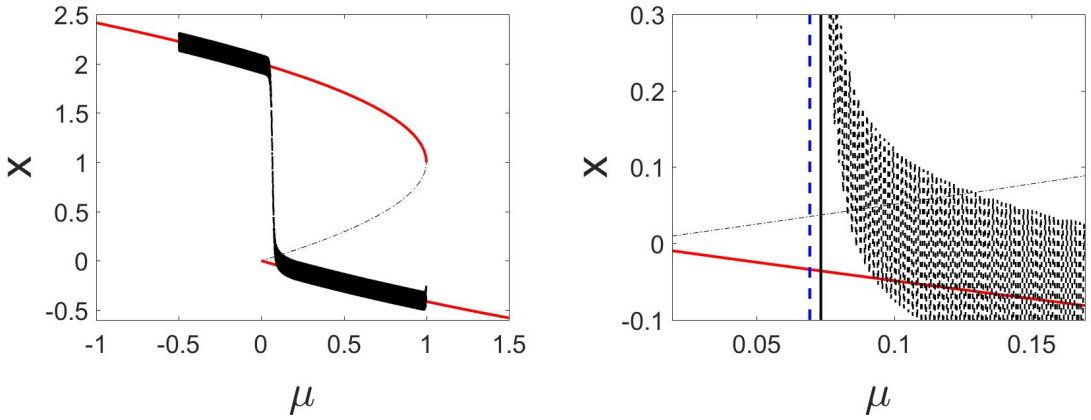

(a) (b)

Figure 2.6: On the left, one can see the bifurcation diagram for the canonical system (2.1) with the numerical solution (black dotted line). On the right, a zoom in around the non-smooth bifurcation. The dotted vertical line is the tipping point μ_{mixed} (2.66) (blue). The vertical line (black) is the when the numerical solution has passed the tipping criterion $x > .5$. The parameter values are $\epsilon = .05$, $\lambda = .8$ and $A = 4$.

In figure 2.7, we see an example of λ falling into case II yet close enough to 1 that we see mixed behavior in the tipping. Here the slow variation is dominant and the oscillations are only noticeable in the zoom in. The green dotted line is the tipping point approximation (2.14) from section 2.2 and μ_{mixed} is still approximating the tipping point well.

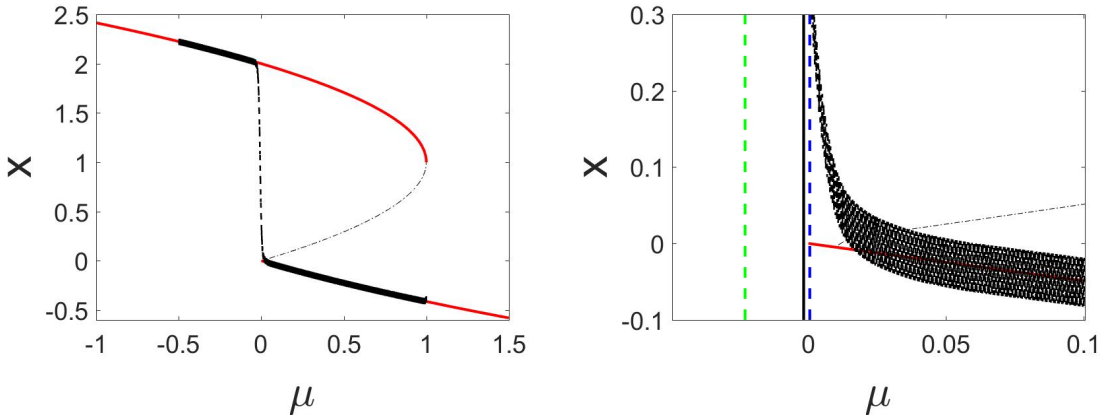

(a) (b)

Figure 2.7: On the left, one can see the bifurcation diagram for the canonical system (2.1) with the numerical solution (black dotted line). On the right, a zoom in about the non-smooth bifurcation. The dotted vertical lines are the tipping point μ_{mixed} (2.66) (blue) and slowly varying tipping μ_{slow} (2.14) (green). The vertical line (black) is the when the numerical solution has passed the tipping criterion $x > .5$. The parameter values are $\epsilon = .05$, $\lambda = 1.05$ and $A = 4$.

In figure 2.8, we see an example of λ falling into case II but large enough that we see almost entirely slow behavior in the tipping. Even upon closer inspection it is hardly noticeable that oscillations are present in the model. The green dotted line is the tipping approximation (2.14) from section 2.2, and it is clear that this is a better approximation than the mixed tipping point.

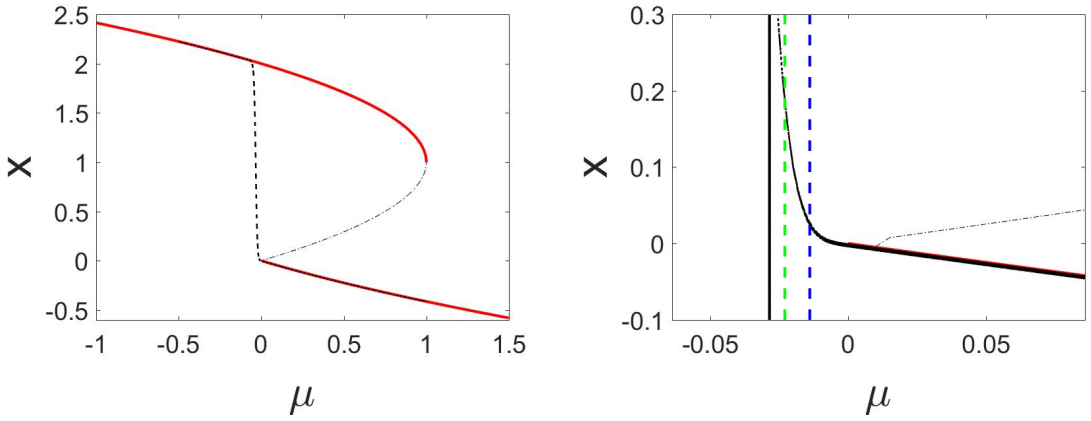

(a) (b)

Figure 2.8: On the left, one can see the bifurcation diagram for the canonical system (2.1) with the numerical solution(black dotted line). On the right, a zoom in around the non-smooth bifurcation. The dotted vertical lines are the tipping point μ_{mixed} (2.66) (blue) and slowly varying tipping μ_{slow} (2.14) (green). The vertical line (black) is the when the numerical solution has passed the tipping criterion $x > .5$. The parameter values are $\epsilon = .05$, $\lambda = 1.6$ and $A = 4$.

In figure 2.9 we compare the tipping between case I and case II with the numerical tipping. For smaller λ, the frequency Ω gets smaller and the case I tipping becomes more predominant. For the analysis performed in this section, $\Omega \gg 1$ and for $\lambda \leq \frac{1}{2}$ we have $\Omega \sim O(1)$. We do not consider a low frequency corresponding to $\lambda \leq \frac{1}{2}$ in this thesis. The larger λ becomes, the less effect we see due to the oscillatory forcing until it is negligible for some $\lambda > 1$. This is also seen in the asymptotic solution for each case, (2.51), (2.65), and (2.76), where the oscillatory component of the term has a ϵ^{λ} coefficient and shrinks the effects as λ grows.

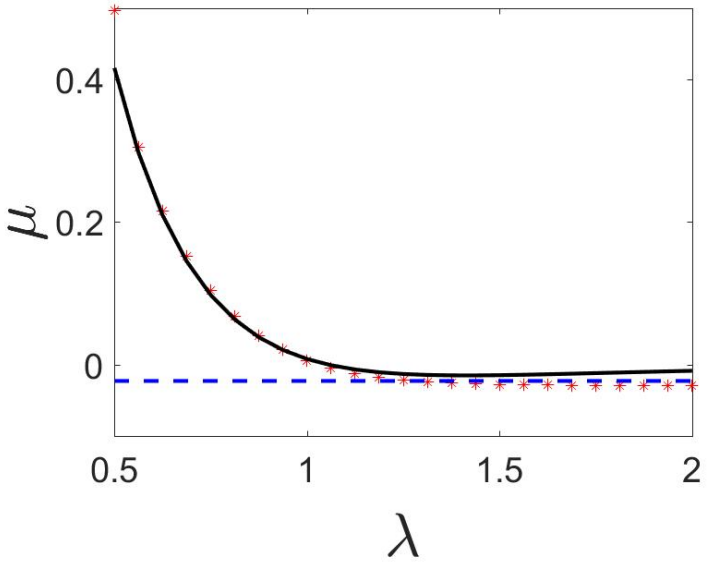

Figure 2.9: An example of numerical tipping (red stars) as the numerical solution to (2.1) passes the tipping criterion $x = .5$ for the last time. The parameter values are $\epsilon = .01$ and $A = 4$. The lines are the case I tipping estimate (2.66) (black solid line) and the case II tipping estimate (2.14) (blue dotted line).

The performance of our estimates are seen in figure 2.10. For case I tipping, the range of appropriate ϵ is highly dependent on the choice in λ. Often, the range is quite small for accurate estimates, but with this in mind both case approximations have good performance over a reasonable range of ϵ.

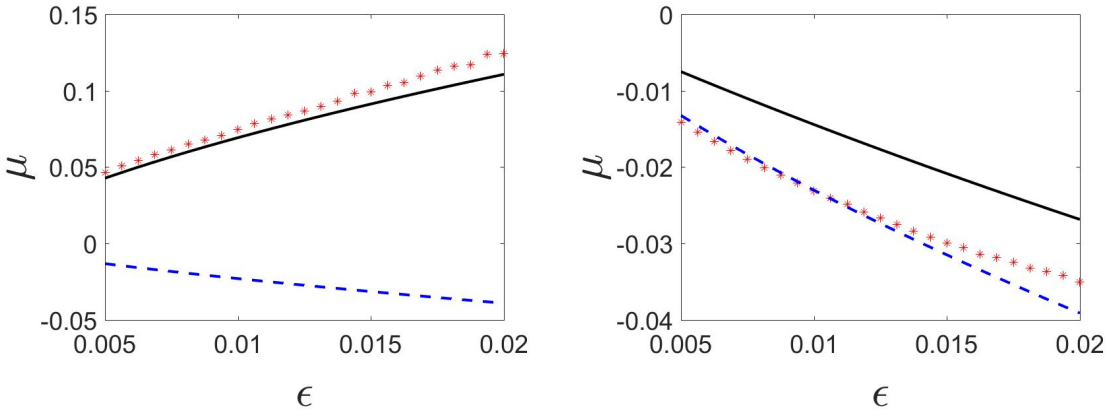

(a) $\lambda = .8$ (b) $\lambda = 1.3$

Figure 2.10: The numerical tipping (red stars) follows the appropriate case depending on λ. The case I tipping estimate (black solid line) and the case II tipping estimate (blue dotted line) are shown.

2.4.3 Stability

Similarly to section 2.3, there are two ranges for λ that govern the stability of solutions found in our analysis, namely $\lambda \leq 1$ and $\lambda > 1$.

Case I: $\lambda \leq 1$

Recall that for this case, we must have $\lambda \in (\frac{1}{2}, 1]$ and for this range, we found the inner equation

$$v_{0t} = -\epsilon^{1-\lambda} m(t) + \frac{1}{\pi} \int_0^{2\pi} |v_0(t) - A\cos(T)|\, dT = f(t, v_0). \tag{2.77}$$

As in our previous analysis, we consider two regions of the solution $v_0(t)$ for this integral, in subsection 2.4.1 with sub-case I: $v_0(t) \leq -|A|$ and in subsection 2.4.2 with sub-case II: $|v_0(t)| \leq |A|$ where each these sub-cases deal with the respective size of $v_0(t)$ to the amplitude of the effective oscillations.

Sub-Case I: $v_0(t) \leq -|A|$

Recall from the analysis that equation (2.77) simplifies in this region of $v_0(t)$ and has the following inner equation and pseudo-equilibrium $z^0(t)$

$$v_{0t} = -\epsilon^{1-\lambda} m(t) - 2v_0 = f(t, v_0), \quad z^0(t) = -\epsilon^{1-\lambda} \frac{m(t)}{2}. \tag{2.78}$$

As we saw in section 2.2, special treatment of the pseudo-equilibrium stability analysis is needed with linear perturbations $v_0(t) = z^0(t) + u(t)$, where $\|u(t)\| \ll 1$ and $z_t^0 = -\epsilon^{1-\lambda} \frac{m_t}{2} = \frac{\epsilon^{1-\lambda}}{2}$. The resulting Taylor expansion is thus

$$\begin{aligned} v_{0t} =& f(t, z^0) + f_{v_0}(t, v_0)(v_0(t) - z^0(t)) + O(\|v_0(t) - z^0(t)\|^2), \\ u_t =& -\frac{\epsilon^{1-\lambda}}{2} - 2u. \end{aligned}$$

This leads to the conclusion that equation (2.78) causes perturbations to decay exponentially to just below the pseudo-equilibrium. Hence we find the pseudo-equilibrium to be a hyperbolic and asymptotically attracting solution.

Sub-Case II: $v_0(t) \leq |A|$

With the Taylor approximation from the analysis (2.63), we have the following inner equation and pseudo-equilibrium $z^0(t)$

$$v_{0t} = -\epsilon^{1-\lambda} m(t) + \frac{4|A|}{\pi} + \frac{2}{\pi|A|} v_0^2 = f(t, v_0), \quad z^0(t) = -C\sqrt{\epsilon^{1-\lambda} m(t) - \frac{4|A|}{\pi}}. \tag{2.79}$$

We consider simple linear perturbations to this pseudo-equilibrium (2.79), $v_0(t) = z^0(t) + u(t)$ with $\|u(t)\| \ll 1$. Treating the pseudo-equilibrium carefully, we find that the slowly varying component of the equilibrium contributes to the derivative. Thus we have

$$\begin{aligned} v_{0t} =& z_t^0(t) + u_t, \\ z_t^0(t) =& \begin{cases} \frac{\epsilon^{1-\lambda}}{2C\sqrt{\epsilon^{1-\lambda}m(t) - \frac{4|A|}{\pi}}} & \epsilon^{1-\lambda}m(t) > \frac{4|A|}{\pi}, \\ 0 & \epsilon^{1-\lambda}m(t) = \frac{4|A|}{\pi}. \end{cases} \end{aligned} \tag{2.80}$$

Now applying a Taylor expansion, we find the following behavior of perturbations

$$\begin{aligned} v_{0t} =& f(t, z^0) + f_{v_0}(t, z^0)(v_0 - z^0(t)) + O(\|v_0(t) - z^0(t)\|), \\ u_t =& \begin{cases} -\frac{\epsilon^{1-\lambda}}{2C\sqrt{\epsilon^{1-\lambda}m(t) - \frac{4|A|}{\pi}}} - 2\sqrt{\epsilon^{1-\lambda}m(t) - \frac{4|A|}{\pi}}u & \epsilon^{1-\lambda}m(t) > \frac{4|A|}{\pi}, \\ 0 & \epsilon^{1-\lambda}m(t) = \frac{4|A|}{\pi}. \end{cases} \end{aligned} \tag{2.81}$$

From (2.81), we find that the perturbations decay to a fixed negative quantity. This indicates, much like in section 2.2, that there is an attracting solution below the pseudo-equilibrium. The negative sign describes exponential decay and hence this equilibrium is hyperbolic and asymptotically stable for $\epsilon^{1-\lambda}m(t) > \frac{4|A|}{\pi}$ or $\mu(t) > \frac{4|A|}{\pi\Omega}$. For $\epsilon^{1-\lambda}m(t) = \frac{4|A|}{\pi}$ or $\mu(t) = \mu_{\text{osc}}$, the stability of (2.81) suddenly becomes non-hyperbolic. This tells us that we lose stability at the oscillatory bifurcation but the tipping point occurs afterwards, which agrees with the conclusion in the tipping approximation from (2.67).

Case II: $\lambda > 1$

From the analysis, we discovered that as long as $\epsilon^{\lambda-1}A \sim O(1)$, then we have a similar behavior in the tipping point. With the Taylor approximation from the analysis (2.72), the inner equation and pseudo-equilibrium $z^0(t)$ are

$$\begin{aligned} y_0 =& -m(t) + \epsilon^{\lambda-1}\frac{2|A|}{\pi} + \epsilon^{1-\lambda}\frac{2}{\pi|A|}y_0^2 = f(t, y), \\ z^0(t) =& -\epsilon^{\lambda-1}C\sqrt{m(t) - \epsilon^{\lambda-1}\frac{4|A|}{\pi}}. \end{aligned} \tag{2.82}$$

Similarly to Case I, we consider simple linear perturbations to this pseudo-equilibrium (2.85), $y_0(t) = z^0(t) + u(t)$ with $\|u(t)\| \ll 1$. Treating the pseudo-equilibrium carefully, we find that the slowly varying component of the equilibrium contributes to the derivative. Thus we have

$$\begin{aligned} y_{0t} =& z_t^0(t) + u_t, \\ z_t^0(t) =& \begin{cases} \frac{\epsilon^{\lambda-1}}{2C\sqrt{m(t) - \epsilon^{\lambda-1}\frac{4|A|}{\pi}}} & m(t) > \epsilon^{\lambda-1}\frac{4|A|}{\pi}, \\ 0 & m(t) = \epsilon^{\lambda-1}\frac{4|A|}{\pi}. \end{cases} \end{aligned} \tag{2.83}$$

Now applying a Taylor expansion, we find the following behavior of perturbations

$$\begin{aligned} y_{0t} =& f(t, z^0) + f_{y_0}(t, z^0)(y_0 - z^0(t)) + O(\|y_0 - z^0(t)\|^2), \\ u_t =& \begin{cases} -\frac{\epsilon^{\lambda-1}}{2C\sqrt{m(t)-\epsilon^{\lambda-1}\frac{4|A|}{\pi}}} - 2\sqrt{m(t) - \epsilon^{\lambda-1}\frac{4|A|}{\pi}}u & m(t) > \epsilon^{\lambda-1}\frac{4|A|}{\pi}, \\ 0 & m(t) = \epsilon^{\lambda-1}\frac{4|A|}{\pi}. \end{cases} \end{aligned} \tag{2.84}$$

The conclusions from case I still apply to (2.84) and thus we still have an attracting solution until $\mu(t) = \mu_{\text{osc}}$ and expect to see tipping occurring after the oscillatory bifurcation which is consistent with our tipping approximation for this case.

On the other hand, for large λ the integral (2.72) approaches

$$y_{0t} = -m(t) + 2|y_0|. \tag{2.85}$$

This is the same type of behavior from section 2.2, where we found that for $m(t) \geq 0$ our pseudo-equilibrium was attracting and for $m(t) < 0$ searching for the pseudo-equilibrium caused a contradiction. Thus, we conclude that the tipping point occurs in the region of $m(t) < 0$ which agrees with (2.14).

Chapter 3

Two Component Model

With the methods and approaches developed in chapter 2 for the one component model, we have an expectation of the behavior of the two component Stommel model around the non-smooth bifurcation under similar conditions. Recall that we study the non-dimensionalized model (1.6) and η_2 is the control parameter linked to the flow rate. With the bifurcation structure we explored in chapter 1, we consider a generalization of the Stommel model

$$\begin{aligned} \dot{V} &= \eta_1 - \eta_2 + \eta_3(T - V) - T - V|V| + A\sin(\Omega t), \\ \dot{T} &= \eta_1 - T(1 + |V|) + B\sin(\Omega t), \\ \dot{\eta_2} &= -\epsilon \\ V(0) = V^0, &\quad T(0) = T^0, \quad \eta_2(0) = {\eta_2}^0, \end{aligned} \tag{3.1}$$

with slow variation $\epsilon \ll 1$, high frequency $\Omega \gg 1$, amplitudes of oscillation A and B, and model parameters η_1 and η_3 as positive constants. We assume the initial conditions V^0, T^0 and $\eta_2^0 > \eta_{2_{\text{ns}}}$ are along the lower equilibrium branch which puts emphasis on the non-smooth behavior of the Stommel model with two additional features. First, we allow for slow variation in the bifurcation parameter which has been shown to be realistic since η_2 is related to the freshwater flux and therefore not a fixed parameter; the same assumption is made in [19]. Second, we consider periodic forcing in the additive parameter η_1 to account for oscillations in seasonal effects, annual effects as well as tidal currents. This same approach is taken in [16] to look into idealized forcing in the Atlantic Meridonal Overturning Circulation (AMOC). It should be noted that although oscillatory forcing is present, there is strong evidence to believe that stochastic forcing is also present in the AMOC [4] and [16] which is suggestive of the same being true for the THC. Thus we consider periodic forcing in the Stommel model, but we discuss stochastic forcing in the future work section. To fully understand the effects of each component on the model, we consider them individually before putting them together.

For the remainder of this thesis, we make two assumptions: first that $\eta_3 < 1$ which gives the smooth bifurcation V_{smooth} of (3.1) in the region $V > 0$. The value of η_3 describes the relative strength of the temperature relaxation to that of salinity, and it is frequently assumed that salinity has a slower relaxation, giving $\eta_3 < 1$. Thus we restrict our attention to $\eta_3 < 1$ and the case of $\eta_3 > 1$ follows similarly. The second assumption we make is that even though we have a model in terms of V and T, the variable V is driving the dynamics of the system as confirmed in the analysis below. This assumption means that we want to understand the non-smooth behavior in V where T follows in response to the effects of V. The evidence below shows that change in temperature respond to change in salinity. This assumption reduces the model, expressing the behavior of T in terms of V to find equations in only one variable.

3.1 Slowly Varying Bifurcation Parameter

We consider the slow variation mechanism to understand the effects on the Stommel model (3.1) with $\epsilon \ll 1$ and $A = B = 0$, where the bifurcation parameter η_2 slowly varies without oscillatory forcing. We expect to find a tipping point in the neighborhood of the aforementioned non-smooth bifurcation at $\eta_{2_{\text{ns}}} = \eta_1\eta_3$. With the choice of $\eta_3 < 1$, the lower branch with $V < 0$ is the branch we focus on in order to approach the non-smooth behavior, thus (3.1) is

$$\begin{aligned} \dot{V} &= \eta_1 - \eta_2(t) + \eta_3(T - V) - T + V^2, \\ \dot{T} &= \eta_1 - T(1 - V), \\ \dot{\eta_2} &= -\epsilon. \end{aligned} \tag{3.2}$$

From section 2.2, we learned that the one component model had a solution that displayed one type of behavior away from the non-smooth axis $x = 0$ and another type close to $x = 0$ thus a local analysis gave insight into the tipping. Here we search for an outer solution to (3.2) that helps us understand the behavior of the system away from the non-smooth $V = 0$. Since we have slow variation in η_2, we choose to scale the system (3.2) with the slow time $\tau = \epsilon t$

$$\begin{aligned} \epsilon V_\tau =& \eta_1 - \eta_2(\tau) + \eta_3(T - V) - T + V^2, \\ \epsilon T_\tau =& \eta_1 - T(1 - V), \\ \eta_{2\tau} =& -1. \end{aligned} \tag{3.3}$$

We use asymptotic expansions in terms of the small quantity ϵ to look for slowly varying solutions. Here we choose

$$\begin{aligned} V(\tau) \sim& V_0(\tau) + \epsilon V_1(\tau) + \epsilon^2 V_2(\tau) + \dots, \\ T(\tau) \sim& T_0(\tau) + \epsilon T_1(\tau) + \epsilon^2 T_2(\tau) + \dots, \end{aligned} \tag{3.4}$$

and substitute (3.4) into (3.3) to find

$$\begin{aligned} \epsilon V_{0\tau} + \epsilon^2 V_{1\tau} + \dots =& \eta_1 - \eta_2(\tau) + \eta_3(T_0 - V_0) - T_0 + V_0^2 \\ &+ \epsilon(\eta_3(T_1 - V_1) - T_1 - 2V_1V_0) + \dots \\ \epsilon T_{0\tau} + \epsilon^2 T_{1\tau} + \dots =& \eta_1 - T_0(1 - V_0) + \epsilon(-T_1(1 - V_0) + V_1T_0) + \dots. \end{aligned}$$

Separating at each order of ϵ then gives the following system of equations

$$O(1): \quad \begin{cases} 0 = & \eta_1 - \eta_2(\tau) + \eta_3(T_0 - V_0) - T_0 + V_0^2, \\ 0 = & \eta_1 - T_0(1 - V_0), \end{cases} \tag{3.5}$$

$$O(\epsilon): \quad \begin{cases} V_{0\tau} = & \eta_3(T_1 - V_1) - T_1 + 2V_1V_0, \\ T_{0\tau} = & -T_1(1 - V_0) + V_1T_0. \end{cases} \tag{3.6}$$

We then solve (3.5) simultaneously for the pseudo-equilibria noting that T_0 is explicitly in terms of V_0

$$\begin{aligned} T_0(V_0) =& \frac{\eta_1}{1-V_0}, \\ 0 =& \eta_1 - \eta_2(\tau) - T_0(V_0) + \eta_3(T_0(V_0) - V_0) + V_0^2. \end{aligned} \tag{3.7}$$

With T_0 and V_0 found, we solve (3.6) for T_1 explicitly in terms of V_1

$$\begin{aligned} T_1(V_1) =& \frac{T_{0\tau} - T_0(V_0)V_1}{1-V_0}, \\ V_1 =& \frac{-(1-V_0)V_{0\tau} + (1-\eta_3)T_{0\tau}(V_{0\tau})}{(1-\eta_3)T_0(V_0) + (\eta_3 - 2V_0)(1-V_0)}. \end{aligned} \tag{3.8}$$

This gives the first few terms of the asymptotic expansion (3.4) with (3.7) and (3.8). Given these expressions, in the two component problem it is not immediately obvious when the outer solution breaks down. However, noting that for $V_0 \to 0$ the asymptotic expansion for V is no longer valid, we rescale the system to find an inner equation in this region.

Analogously to section 2.2, this corresponds to the non-smooth bifurcation at $(\eta_{2\text{ns}}, V_{\text{ns}}, T_{\text{ns}}) = (\eta_1\eta_3, 0, \eta_1)$, so we rescale (3.1) around these values. This results in the local variables

$$\begin{aligned} \eta_2 =& \eta_{2\text{ns}} + \epsilon n, \\ V =& \epsilon X, \\ T =& \eta_1 + \epsilon Y. \end{aligned} \tag{3.9}$$

Then we introduce these local variables (3.9) into the Stommel model (3.1) to find the following inner system

$$\begin{aligned} \dot{X} &= -n(t) - \eta_3 X - (1-\eta_3)Y - \epsilon X|X|, \\ \dot{Y} &= -\eta_1|X| - Y - \epsilon|X|Y, \\ \dot{n} &= -1. \end{aligned} \tag{3.10}$$

Here we outline the influence of the parameters η_1 and η_3 on the behavior of a solution. We already determined in the introduction that η_3 determines the orientation of the problem. By viewing (3.10) as a 2×2 system of spatial variables, we find an interaction between the parameters η_1 and η_3 in the eigenvalues of this system. Linearizing then gives

$$\begin{pmatrix} \dot{X} \\ \dot{Y} \end{pmatrix} = \begin{pmatrix} -\eta_3 & -(1-\eta_3) \\ -\eta_1 \text{sgn}(X) & -1 \end{pmatrix} \begin{pmatrix} X \\ Y \end{pmatrix} - \begin{pmatrix} n(t) \\ 0 \end{pmatrix}. \tag{3.11}$$

A linearized stability analysis about the pseudo-equilibria similar to [21] is needed to determine the stability of the lower pseudo-equilibria. This is performed in [5] and hence we note that both stability of the lower branch and non-hyperbolic behavior at $(\eta_{2\text{ns}}, V_{\text{ns}}, T_{\text{ns}})$ is observed. Thus we expect our tipping point to occur just after the static non-smooth

bifurcation $\eta_{2\text{ns}}$. With this in mind, we consider $V > 0$ and with (3.11) we find the inner system

$$\begin{aligned}\dot{X} &= -n(t) - \eta_3 X - (1-\eta_3)Y - \epsilon X^2,\\ \dot{Y} &= -\eta_1 X - Y - \epsilon XY,\\ \dot{n} &= -1.\end{aligned} \tag{3.12}$$

Following the approach from section 2.2, we change the differentiation to be in terms of n to find

$$\begin{pmatrix} X_n \\ Y_n \end{pmatrix} = \begin{pmatrix} \eta_3 & 1-\eta_3 \\ \eta_1 & 1 \end{pmatrix} \begin{pmatrix} X \\ Y \end{pmatrix} + \begin{pmatrix} n + \epsilon X^2 \\ \epsilon XY \end{pmatrix}.$$

Seeking a leading order solution in this region, we drop the ϵ order terms to give

$$\begin{pmatrix} X_n \\ Y_n \end{pmatrix} = \begin{pmatrix} \eta_3 & 1-\eta_3 \\ \eta_1 & 1 \end{pmatrix} \begin{pmatrix} X \\ Y \end{pmatrix} + \begin{pmatrix} n \\ 0 \end{pmatrix}. \tag{3.13}$$

For the system (3.13), we find the eigenvalues

$$\lambda_{1,2} = \frac{\eta_3 + 1}{2} \pm \frac{1}{2}\sqrt{(1+\eta_3)^2 + 4(\eta_1(1-\eta_3) - \eta_3)}. \tag{3.14}$$

The eigenvalues in (3.14) must be real as $\eta_3 < 1$ guarantees the discriminant is always positive. The type of stability also follows as one of the eigenvalues is positive and the other is negative. This causes the solution to be unstable, which confirms tipping to occur in the region $V > 0$. With real eigenvalues, the solution in the $V > 0$ region takes the following exponential form with constants $K_{i,j}$ being component j of the corresponding i-th eigenvector

$$\begin{aligned}X(n) \sim& K_{1,1}e^{\lambda_1 n} + K_{2,1}e^{\lambda_2 n} + C_1 n + C_2,\\ Y(n) \sim& K_{1,2}e^{\lambda_1 n} + K_{2,2}e^{\lambda_2 n} + C_3 n + C_4.\end{aligned} \tag{3.15}$$

Translating both solutions in (3.10) back to our original variables we find

$$\begin{aligned}V(t) \sim& \epsilon K_{1,1}e^{\lambda_1(\eta_2(t) - \eta_1\eta_3)/\epsilon} + \epsilon K_{2,1}e^{\lambda_1(\eta_2(t) - \eta_1\eta_3)/\epsilon} + O(\epsilon),\\ T(t) \sim& \eta_1 + \epsilon K_{1,2}e^{\lambda_1(\eta_2(t) - \eta_1\eta_3)/\epsilon} + \epsilon K_{2,2}e^{\lambda_2(\eta_2(t) - \eta_1\eta_3)/\epsilon} + O(\epsilon).\end{aligned} \tag{3.16}$$

With (3.16) admitting the solution in the region $V > 0$, we determine the system to tip once one of these exponentials becomes large (i.e $O(1/\epsilon)$). This causes the system to abruptly transition away from our lower branch towards the upper stable branch. The tipping point $\eta_{2\text{slow}}$ is then

$$\eta_{2\text{slow}} = \min_i\{\eta_{2\text{ns}} - \epsilon \ln(\epsilon)/\lambda_i\}, \quad i = 1, 2. \tag{3.17}$$

Thus we have the tipping for this problem with (3.17) and this has a similar form to the tipping point from section 2.2. As we found in (3.14), one of the eigenvalues is always positive and thus $\eta_{2\text{slow}} < \eta_{2\text{ns}}$. This means the slow variation causes a delay in the rapid transition from the lower branch to the upper branch and the solution spends more time

around the lower branch. These effects shrink as $\epsilon \to 0$ until we return to the static problem with $\epsilon = 0$.

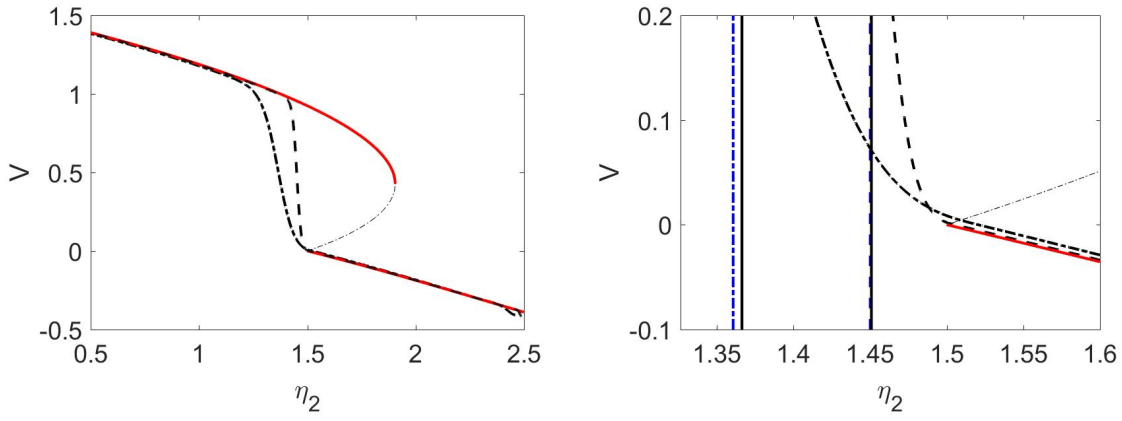

(a) (b)

Figure 3.1: In (a) the numerical solutions (black dotted and dash-dotted lines) to (3.1) are given with $\eta_1 = 4$, $\eta_3 = .375$, and $\epsilon = \{.01, .04\}$ respectively. In (b) a zoom is given closer to the non-smooth bifurcation region. The blue vertical lines are the predictions (3.17) against the black solid vertical lines which are the tipping points with the tipping criterion $V > V_{\text{smooth}}$ on the numerical solution.

In figure 3.1 the numerical solution with a slowly varying η_2 is given for two choices of ϵ in (a) and we zoom in around the non-smooth bifurcation in (b). Here we use the tipping criterion to be whenever $V > V_{\text{smooth}}$ which is large enough that the numerical solution is strongly moving towards the upper branch. The delay in moving towards the upper branch in the V solution causes a similar delay in T, as seen in figure 3.2. This is best seen with the outer solution (3.4) as the correction terms are negative. Thus, when the tipping point in V is reached, the solution for T has yet to reach the maximum value. Notice that after the tipping occurs, the numerical solution passes entirely over the unstable branch and even some of the upper stable branch before following the upper branch closely.

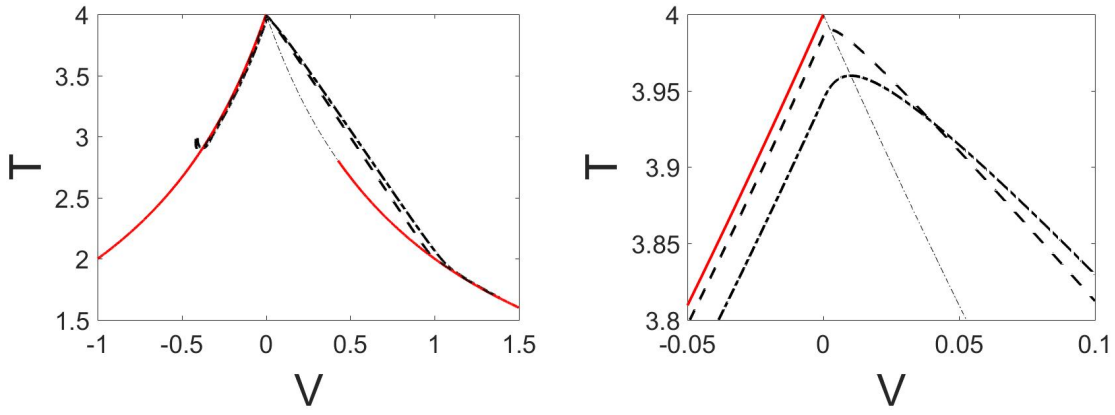

(a) (b)

Figure 3.2: In (a) we have the numerical solutions (black dotted and dash-dotted) over the standard equilibrium plot for V vs. T. In (b) a zoom in closer to the bifurcation area.

In figure 3.3 we compare the numerical tipping to the predicted tipping in (3.17) over a range of ϵ. Here we see performance even better than in section section 2.2 as even for relatively large ϵ the prediction has a small error. This is an artifact of having a higher dimensional problem, where now two exponentials in (3.16) are dominating the behavior of the solution in the $V > 0$ region. As in section 2.2, the concavity of the predicted tipping against the numerical tipping matches very well and we can expect the prediction to hold for reasonably small values of ϵ.

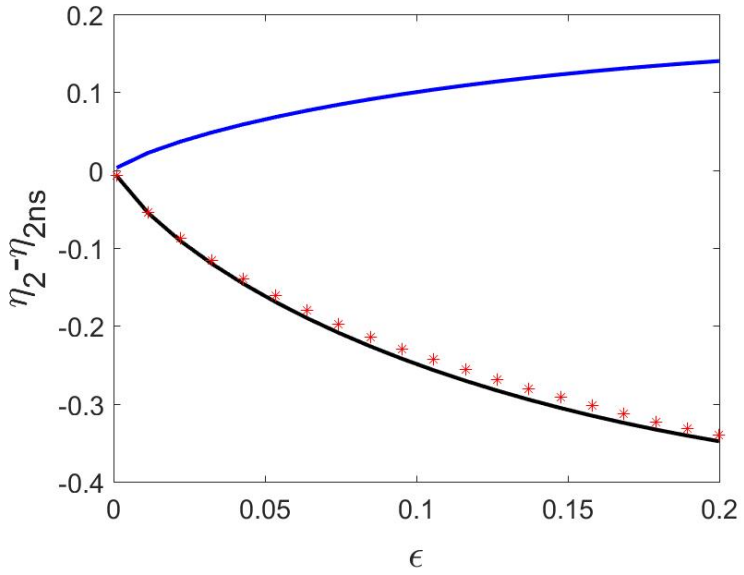

Figure 3.3: The numerical tipping (red stars) vs. the estimate $\eta_{2\text{slow}}$ (black line) with $\eta_1 = 4$ and $\eta_3 = .375$. The top blue line is the tipping of the second eigenvalue. The tipping criterion on the numerical solution is $V > V_{\text{smooth}}$.

3.2 High Frequency Oscillatory Forcing

We consider oscillations occurring in the dynamics of the THC that are not originally encompassed by the Stommel model [1, 9, 14, 17, 18, 22]. We allow η_1 to exhibit oscillatory behavior to account for this. As η_1 appears in both equations for V and T, we consider oscillatory forcing on both, but permit their amplitudes to be different. In other words, the canonical system (3.1) with $A, B \sim O(1)$, $\Omega \gg 1$ and $\epsilon = 0$ which is the purely oscillatory forcing problem. Under these conditions, like with the one component model in section 2.3, we expect to find oscillations that are attracting. Here stable behavior should act like oscillations about the equilibria of a reduced inner problem. Thus our analysis must locate these equilibria as a function of η_2 in order to find the bifurcation.

To begin our analysis, we note that the dynamics occur on multiple time scales, a slow t and fast $R = \Omega t$. Following a multiple scales approach, we consider $V(t) = V(t, R)$ and $T(t) = T(t, R)$ and substituting this into (3.1), we get the system

$$\begin{aligned} V_R + \Omega^{-1} V_t =& \Omega^{-1} \left(\eta_1 - \eta_2 + \eta_3(T - V) - T - V|V| + A\sin(R)\right), \\ T_R + \Omega^{-1} T_t =& \Omega^{-1} \left(\eta_1 - T(1 + |V|) + B\sin(R)\right). \end{aligned} \tag{3.18}$$

We follow the lower branch to study dynamics near the non-smooth bifurcation. Thus we consider the system (3.18) with $V < 0$

$$\begin{aligned} V_R + \Omega^{-1} V_t =& \Omega^{-1} \left(\eta_1 - \eta_2 + \eta_3(T - V) - T + V^2 + A\sin(R)\right), \\ T_R + \Omega^{-1} T_t =& \Omega^{-1} \left(\eta_1 - T(1 - V) + B\sin(R)\right). \end{aligned} \tag{3.19}$$

From (3.19), it makes sense to consider an asymptotic expansion for both V and T in terms of the small quantity, Ω^{-1}, with

$$\begin{aligned} V(t,R) &\sim V_0(t,R) + \Omega^{-1}V_1(t,R) + \Omega^{-2}V_2(t,R) + O(\Omega^{-3}), \\ T(t,R) &\sim T_0(t,R) + \Omega^{-1}T_1(t,R) + \Omega^{-2}T_2(t,R) + O(\Omega^{-3}). \end{aligned} \tag{3.20}$$

Substituting (3.20) into the system (3.19) gives

$$\begin{aligned} V_{0R} + \Omega^{-1}V_{0t} + \Omega^{-1}V_{1R} + \ldots =& \Omega^{-1}(\eta_1 - \eta_2 + \eta_3(T_0 - V_0) - T_0 + V_0^2 + A\sin(R)) \\ &+\Omega^{-2}(\eta_3(T_1 - V_1) - T_1 + 2V_1V_0) + \ldots, \\ T_{0R} + \Omega^{-1}T_{0t} + \Omega^{-1}T_{1R} + \ldots =& \Omega^{-1}(\eta_1 - T_0(1 - V_0) + B\sin(R)) \\ &+\Omega^{-2}(-T_1(1 - V_0) + T_0V_1) + \ldots. \end{aligned}$$

Here we find the following equations separated by order of Ω^{-1} with

$$O(1): \quad \begin{cases} V_{0R} = & 0, \\ T_{0R} = & 0, \end{cases} \tag{3.21}$$

$$O(\Omega^{-1}): \quad \begin{cases} V_{1R} + V_{0t} = & \eta_1 - \eta_2 + \eta_3(T_0 - V_0) - T_0 + V_0^2 + A\sin(R), \\ T_{1R} + T_{0t} = & \eta_1 - T_0(1 - V_0) + B\sin(R), \end{cases} \tag{3.22}$$

$$O(\Omega^{-2}): \quad \begin{cases} V_{2R} + V_{1t} = & \eta_3(T_1 - V_1) - T_1 + 2V_0V_1, \\ T_{2R} + T_{1t} = & -T_1(1 - V_0) + T_0V_1. \end{cases} \tag{3.23}$$

We learn from (3.21) that both our leading order terms are only dependent on the slow time, $V_0 = V_0(t)$, $T_0 = T_0(t)$. Much like section 2.3, we must introduce a solvability condition on the resonant terms to be able to solve for the correction terms, ensuring for the sub-linear growth resulting in a stable solution. Here, we use the Fredholm alternative (2.24) on (3.22)-(3.23) and search for the equilibrium solutions. This is shown in Appendix C. Collecting these solutions leads to the outer solution in original variables

$$\begin{aligned} V \sim& V_0 - \Omega^{-1}A\cos(\Omega t) + \ldots, \\ T \sim& T_0 - \Omega^{-1}B\cos(\Omega t) + \ldots. \end{aligned} \tag{3.24}$$

Here both V_0 and T_0 are the same equilibrium solutions from the static model in the introduction with

$$\begin{aligned} T_0(V_0) =& \frac{\eta_1}{1 - V_0}, \\ 0 =& \eta_1 - \eta_2 + \eta_3(T_0(V_0) - V_0) - T_0(V_0) + V_0^2. \end{aligned}$$

For the one component model in section 2.3, we had to use a local expansion so we needed to scale both the variable x as well as the parameter μ and analyze the local behavior around the axis $x = 0$. Since we again have non-smooth dynamics at the axis $V = 0$, we expect to use a local expansion for the two component model as well. While the precise scaling of the breakdown of the outer solution (3.24) is too complex for us to search for, we instead observe that once $V_0 \to 0$ the oscillations begin to dominate the solution and this is not consistent

with our assumptions of the expansion. So we introduce the local variables analogously to section 2.3

$$\begin{aligned} V =&\Omega^{-1}X, \\ T =&\eta_1 + \Omega^{-1}Y, \\ \eta_2 =&\eta_{2\text{ns}} + \Omega^{-1}n. \end{aligned} \tag{3.25}$$

Substituting (3.25) into (3.1) leads to the inner system

$$\begin{aligned} \dot{X} =& -n + \eta_3(Y - X) - Y - \Omega^{-1}X|X| + \Omega A\sin(\Omega t), \\ \dot{Y} =& -\eta_1|X| - Y - \Omega^{-1}|X|Y + \Omega A\sin(\Omega t). \end{aligned} \tag{3.26}$$

The form suggests behavior on the same time scales in (3.26), the slow t and the fast $R = \Omega t$. Considering $X(t) = X(t, R)$ and $Y(t) = Y(t, R)$ gives the multiple scales inner system

$$\begin{aligned} X_R + \Omega^{-1}X_t =&\Omega^{-1}\left(-n + \eta_3(Y - X) - Y\right) - \Omega^{-2}X|X| + A\sin(R), \\ Y_R + \Omega^{-1}Y_t =&\Omega^{-1}\left(-\eta_1|X| - Y\right) - \Omega^{-2}|X|Y + B\sin(R). \end{aligned} \tag{3.27}$$

Once more, as we see the small quantity Ω^{-1} appearing in (3.27), we choose an expansion of the form

$$\begin{aligned} X(t, R) \sim& X_0(t, R) + \Omega^{-1}X_1(t, R) + O(\Omega^{-2}), \\ Y(t, R) \sim& Y_0(t, R) + \Omega^{-1}Y_1(t, R) + O(\Omega^{-2}), \end{aligned} \tag{3.28}$$

where we then substitute (3.28) into (3.27) to get

$$\begin{aligned} X_{0R} + \Omega^{-1}X_{0t} + \Omega^{-1}X_{1R} + \ldots =&\Omega^{-1}(-n + \eta_3(Y_0 - X_0) - Y_0) + A\sin(R) \\ &+\Omega^{-2}(X_0|X_0 + \Omega^{-1}X_1 + \ldots| + \eta_3(Y_1 - X_1) - Y_1) + \ldots \\ Y_{0R} + \Omega^{-1}Y_{0t} + \Omega^{-1}Y_{1R} + \ldots =&\Omega^{-1}(-\eta_1|X_0 + \Omega^{-1}X_1 + \ldots| - Y_0) + B\sin(R) \\ &+\Omega^{-2}(-|X_0 + \Omega^{-1}X_1 + \ldots| - Y_0 - Y_1) + \ldots \end{aligned}$$

We then separate the terms by their orders of Ω^{-1} to find the equations

$$O(1): \quad \begin{cases} X_{0R} &= A\sin(R), \\ Y_{0R} &= B\sin(R), \end{cases} \tag{3.29}$$

$$O(\Omega^{-1}): \quad \begin{cases} X_{1R} + X_{0t} &= -n - \eta_3 X_0 - (1 - \eta_3)Y_0, \\ Y_{1R} + Y_{0t} &= -\eta_1|X_0| - Y_0. \end{cases} \tag{3.30}$$

From (3.29) we find that the leading order terms of (3.28) have the form

$$X_0 = P_0(t) - A\cos(R), \quad Y_0 = Q_0(t) - B\cos(R), \tag{3.31}$$

where Q and P track the slow time components for their respective variables. Substituting (3.31) into (3.30), we apply the Fredholm alternative (2.24) to derive equations for the slow functions $P_0(t)$ and $Q_0(t)$. This gives

$$\begin{aligned} P_{0t} =& -n - \eta_3 P_0 - (1-\eta_3)Q_0, \\ Q_{0t} =& -\frac{\eta_1}{2\pi}\int_0^{2\pi} |P_0 - A\cos(R)|dR - Q_0. \end{aligned} \tag{3.32}$$

As we are concerned with finding the bifurcation, we search for the equilibrium solutions to (3.32). We notice that in the equation for Q_0 we find a similar integral equation to the inner equation (2.33) in section 2.3. This leads us again to two cases, Case I: $|P_0(t)| \leq -|A|$ where the sign of the integrand does not change, and Case II: $|P_0(t)| < |A|$ where the integrand changes and the integral has a non-trivial solution. These cases can be seen in figure 3.4.

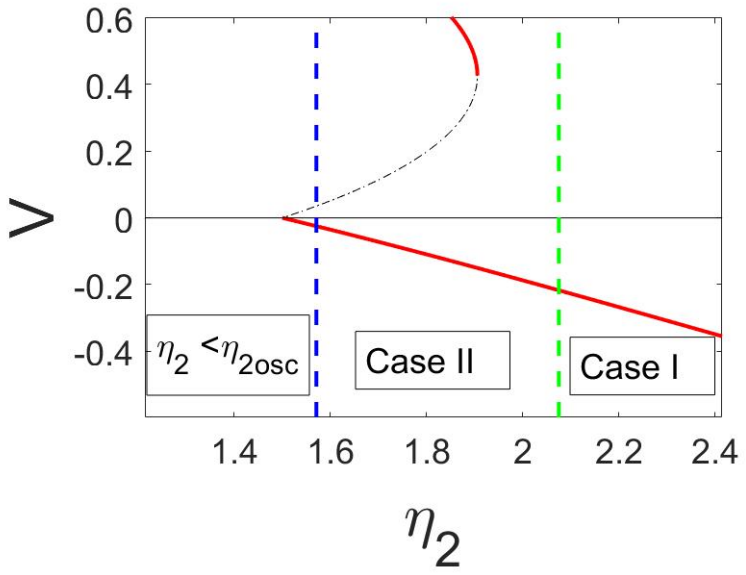

Figure 3.4: Here we have the parameter ranges for case I and case II shown as the right most green vertical line and the bifurcation value as the left blue vertical line respectively.

3.2.1 Case I: $P_0(t) \leq -|A|$

We call this the 'below axis' case, with the solution X_0 below the axis $V = 0$ so we do not expect a bifurcation here. Instead this case helps to simplify the integration in (3.32) but also helps us to determine when the solution acts differently under case II. We use the equilibria of X and Y to define a parameter range in η_2 between case I and case II. Under the conditions of this case, the system (3.32) simplifies to

$$\begin{aligned} P_{0t}(t) =& -n - \eta_3 P_0(t) - (1-\eta_3)Q_0(t), \\ Q_{0t}(t) =& \eta_1 P_0(t) - Q_0(t). \end{aligned} \tag{3.33}$$

Solving for the equilibria in (3.33) results in

$$Q_0(P_0) = \eta_1 P_0, \quad P_0 = -\frac{n}{\eta_1(1-\eta_3)+\eta_3}.$$

Together with these equilibria and with the condition $P_0(t) \leq -|A|$, we find the parameter range that distinguishes between case I and case II in terms of our inner parameter, which we then rewrite in original variables with

$$\begin{aligned} n \geq & (\eta_1(1-\eta_3)+\eta_3)|A|, \\ \eta_2 \geq & \eta_{2_{\text{ns}}} + \frac{(\eta_1(1-\eta_3)+\eta_3)|A|}{\Omega}. \end{aligned} \tag{3.34}$$

For values of η_2 below the values given in (3.34), we see the oscillations crossing above the axis $V = 0$ and hence more contribution from the integral in (3.32). We use a separate case to deal with this behavior.

3.2.2 Case II: $|P_0(t)| < |A|$

We call this the 'crossing' case; here the solution oscillates about the axis $V = 0$ while the center of the solution approaches this axis. With this behavior, we expect a bifurcation to occur in this region and use the equilibria for (3.32) to determine the location. While this problem is two-dimensional in nature, the integral in (3.32) is nearly identical to the integral (2.33) in section 2.3. So we may use the ideas of that section here to get an approximate solution. Thus, under the assumptions of this case, we fix a value of P_0 and integrate (3.32) over the regions defined by

$$R_1 = \arccos(P_0/A), \quad R_2 = 2\pi - \arccos(P_0/A).$$

As in section 2.3, the solution to (3.32) is negative for $P_0(t)$ the region $R \in [0, R_1]$ and alternates sign for the regions $R \in (R_1, R_2]$ and $R \in (R_2, 2\pi]$. We follow the same procedure of integrating over each region to get the exact form for (3.32) with

$$\begin{aligned} P_{0t} = & -n - \eta_3 P_0(t) - (1-\eta_3)Q_0, \\ Q_{0t} = & -\frac{2\eta_1}{\pi}\left(\arcsin(P_0/A)P_0 + \sqrt{A^2 - P_0^2}\right) - Q_0. \end{aligned} \tag{3.35}$$

Although this is the explicit inner equation from (3.35), it is analytically too complex to find an explicit form for a bifurcation and thus we use a second order Taylor approximation to give an approximate system

$$\begin{aligned} P_{0t} = & -n - \eta_3 P_0 - (1-\eta_3)Q_0, \\ Q_{0t} = & -\frac{2\eta_1|A|}{\pi} - Q_0 - \frac{\eta_1}{\pi|A|}P_0^2. \end{aligned} \tag{3.36}$$

We solve for the equilibria of (3.36) in order to locate the bifurcation. For simplicity, we define $a = \frac{\eta_1}{\pi|A|}$, and $c = \frac{2\eta_1|A|}{\pi}$. Thus the equilibria satisfy

$$\begin{aligned} Q_0(P_0) = & -aP_0^2 - c, \\ 0 = & -n + (1-\eta_3)c - \eta_3 P_0 + aP_0^2. \end{aligned} \tag{3.37}$$

Here the equation for P_0 in (3.37) is a quadratic that would have two solutions, with the situation of following the lower branch given by the negative solution with

$$P_0 = \frac{\eta_3}{2a(1-\eta_3)} - \frac{1}{2a(1-\eta_3)}\sqrt{\eta_3^2 + 4a(1-\eta_3)(n-c(1-\eta_3))}. \tag{3.38}$$

The equilibrium for P_0 in (3.38) is real only for positive discriminant. Then the local bifurcation, n_{osc}, is given for vanishing discriminant

$$n_{osc} = \frac{\eta_1(1-\eta_3)|A|}{\pi}\left[2 - \left(\frac{\pi\eta_3}{2\eta_1(1-\eta_3)}\right)^2\right]. \tag{3.39}$$

Here the equilibria in (3.37) are given in terms of the local variables. We write the solution for V, T and bifurcation, $\eta_{2_{\text{osc}}}$, in the original variables

$$\begin{aligned} V(t) \sim & \Omega^{-1}\left(P_0 - A\cos(\Omega t)\right), \\ T(t) \sim & \eta_1 - \Omega^{-1}\left(\frac{\eta_1}{\pi|A|}P_0^2 + \frac{2\eta_1|A|}{\pi} + B\cos(\Omega t)\right), \end{aligned} \tag{3.40}$$

$$\eta_{2osc} = \eta_{2\text{ns}} + \frac{\eta_1(1-\eta_3)|A|}{\pi\Omega}\left[2 - \left(\frac{\pi\eta_3}{2\eta_1(1-\eta_3)}\right)^2\right]. \tag{3.41}$$

With (3.41) we have found the bifurcation induced by the addition of oscillatory forcing in the Stommel model. As we learned from the one component model in section 2.3, the effect of oscillatory forcing is early bifurcations where $\eta_{2\text{osc}} > \eta_{2\text{ns}}$. Our result in (3.41) holds under the caveat that we restrict the parameters with

$$\eta_3 < \frac{2\sqrt{2}\eta_1}{\pi + 2\sqrt{2}\eta_1},$$

which is the condition to guarantee the second term in (3.41) is positive. This restriction is reasonable as generally the parameters have the behavior of $\eta_3 < 1$ and $\eta_3 \ll \eta_1$ as the thermal variation is much larger in real ocean dynamics than the ratio of relaxation times.

In figure 3.5 the numerical solution to (3.1) for V and a zoom of the solution around the numerical bifurcation is shown. The static bifurcation diagram is underlayed as well for comparison. We contrast the result in (3.41) to these numerics and find that the bifurcation prediction from our analysis agrees. Notice that there is a bifurcation for $\eta_2 > \eta_{2\text{ns}}$ with the oscillations present, this causes a region of the static lower branch in V to never be followed. In figure 3.6 the numerical solution to (3.1) for T and a zoom in around the bifurcation is shown with the static bifurcation diagram underlayed. Due to the bifurcation $\eta_{2\text{osc}} > \eta_{2\text{ns}}$ in V, the maximum value of T is never reached in (b).

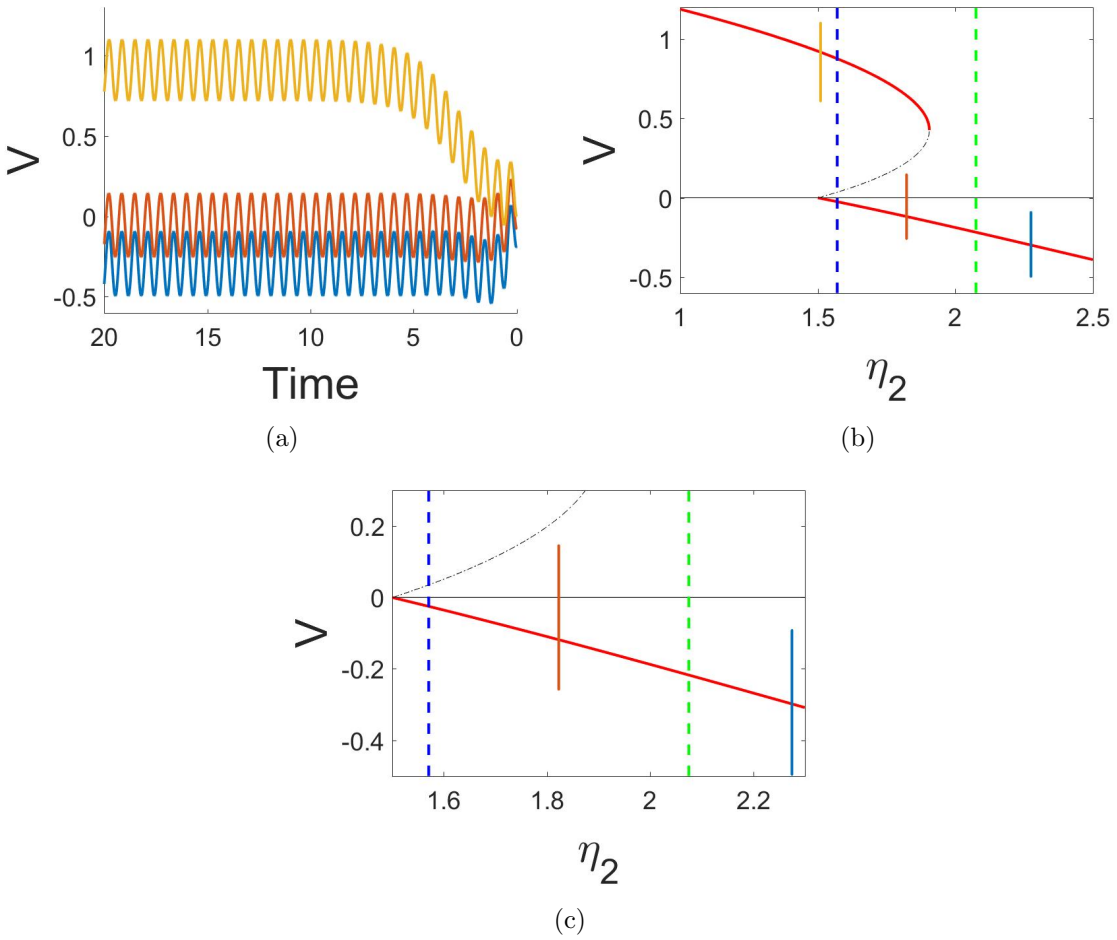

Figure 3.5: In (a) the numerical time series solutions to (3.1) is given with parameters in each qualitatively different case of $\eta_2 = \{2.3, 1.8, 1.51\}$ with $\eta_1 = 4$, $\eta_3 = .375$, $A = B = 2$ and $\Omega = 10$. In (b) these same solutions are shown on the bifurcation diagram. In (c) a zoom in closer to the non-smooth bifurcation region where the blue vertical line is the estimated bifurcation (3.41).

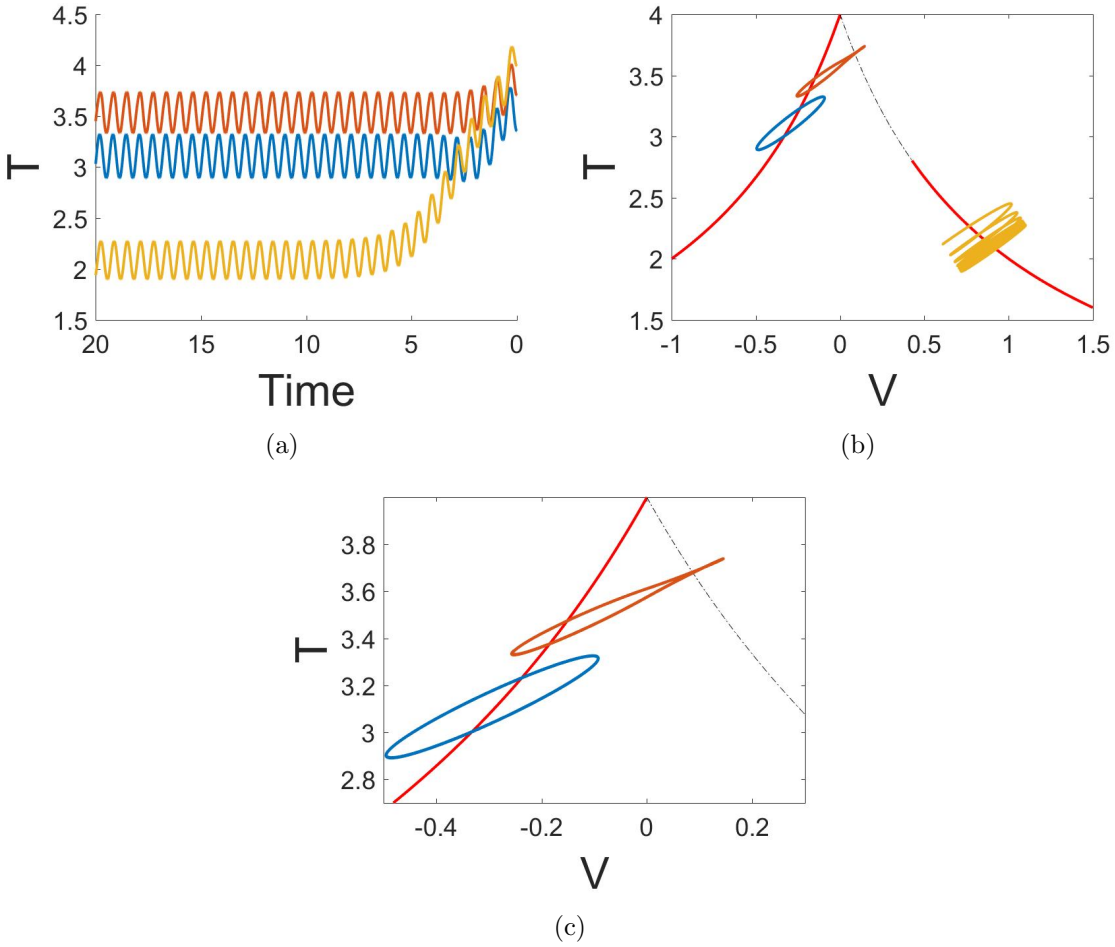

Figure 3.6: In (a) we have the same numerical time series solutions for the qualitatively different cases $\eta_2 = \{2.3, 1.8, 1.51\}$. In (b) we plot these solutions over the standard equilibrium plot for V vs. T. In (c) a zoom closer to the bifurcation area is provided.

To evaluate the performance of this prediction, we compare (3.41) to the numerical bifurcation over a range of Ω^{-1}. In figure 3.7 we allow for this range to be $\Omega^{-1} \in (0, .2)$. For small values, the two agree very well and as we expect, they begin to diverge once the values of Ω^{-1} become too large from the assumption that $\Omega \gg 1$ and the asymptotics cannot capture the behavior for low frequency oscillations. This outperforms the approximation from the one component model in section 2.3.

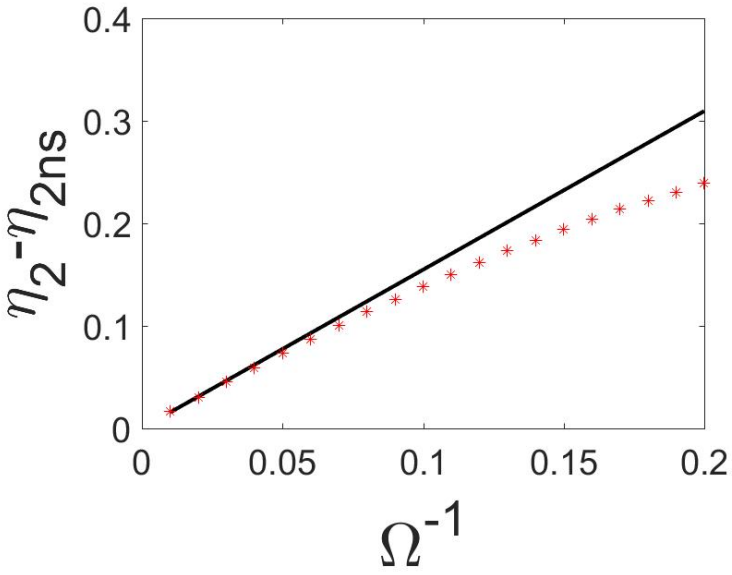

Figure 3.7: The numerical tipping (red stars) vs. the estimate (black line). The model parameters are $\eta_1 = 4$,$\eta_3 = .375$ and $A = B = 2$. The bifurcation criterion for the numerical solution is $V > V_{\text{smooth}}$.

3.2.3 Stability

Since we have a non-autonomous system when $A \neq 0$, we approach the stability with a linearized analysis about the equilibria much like in section 2.3. To do this, recall from (3.32) that we found the system

$$\begin{aligned} P_{0t} =& - n - \eta_3 P_0 - (1-\eta_3)Q_0, \\ Q_{0t} =& -\frac{\eta_1}{2\pi}\int_0^{2\pi} |P_0 - A\cos(R)|\, dR - Q_0. \end{aligned} \tag{3.42}$$

We must consider the stability of solutions over the relative sizes of $P_0(t)$ with Case I: $P_0(t) \leq -|A|$ and Case II: $|P_0(t)| \leq |A|$.

Case I: $v_0(t) \leq -|A|$

For the 'below-axis' case the solution spends most of its time away from the axis $V = 0$. We expect to find attraction around the lower branch and thus we expect stability there. Under these conditions, the inner equation (3.42) simplifies to the equations

$$\begin{aligned} P_{0t} =& - m - \eta_3 P_0 - (1-\eta_3)Q_0, \\ Q_{0t} =& \eta_1 P_0 - Q_0. \end{aligned} \tag{3.43}$$

The equilibria of (3.43) is found with $Q_0(P_0) = \eta_1 P_0$. Thus we find the following reduced

one component equation and equilibrium Z^0 with

$$P_{0t} = -n - (\eta_3 + (1-\eta_3))Q_0 = f(P_0), \quad Z^0 = -\frac{n}{\eta_3 + \eta_1(1-\eta_3)}. \tag{3.44}$$

Now we consider a simple linear perturbation about this equilibrium with $P_0(t) = Z^0 + U(t)$ where $\|U(t)\| \ll 1$. Our standard Taylor expansion about the equilibrium Z^0 results in

$$\begin{aligned} f(P_0) =& f(Z^0) + f_{P_0}(Z^0)(P_0 - Z^0) + O((P_0 - Z^0)^2), \\ U_t =& -(\eta_3 + \eta_1(1-\eta_3))U \end{aligned} \tag{3.45}$$

From (3.45) we now conclude the equilibrium Z^0 is hyperbolic and attracting due to the exponential decay in perturbations. Thus we find that no bifurcation occurs for this case which agrees with our findings from the analysis above. This holds for η_2 in (3.34)

$$\eta_2 \geq \eta_{2\text{ns}} + \frac{(\eta_3 + \eta_1(1-\eta_3))|A|}{\Omega}.$$

Case II: $|P_0(t)| < |A|$

We called this case the 'crossing' case and here the solution experiences the non-smooth behavior when it crosses $V = 0$. We expect the stability to fail under these conditions and we found in the analysis that the crossing $V = 0$ gives (3.42) in the form

$$\begin{aligned} P_{0t} =& -n - \eta_3 P_0 - (1-\eta_3)Q_0, \\ Q_{0t} =& -\frac{2\eta_1|A|}{\pi} - \frac{\eta_1}{\pi|A|}P_0^2 - Q_0. \end{aligned} \tag{3.46}$$

As we search for the equilibria of (3.46), we find the equilibrium for Q_0 in terms of P_0

$$Q_0(P_0) = -\frac{2\eta_1|A|}{\pi} - \frac{\eta_1}{\pi|A|}P_0^2,$$

which then gives the following inner equation with the equilibrium Z^0 for $P_0 < 0$

$$\begin{aligned} P_{0t} =& -n + \frac{2\eta_1|A|}{\pi} - \eta_3 P_0 + \frac{\eta_1}{\pi|A|}P_0^2 = f(P_0), \\ Z^0 =& \frac{\pi|A|}{2\eta_1(1-\eta_3)}\left(\eta_3 - \sqrt{\frac{4\eta_1(1-\eta_3)}{\pi|A|}(n - n_{\text{osc}})}\right). \end{aligned} \tag{3.47}$$

For simplicity we write Z^0 in terms of the local bifurcation n_{osc} we found in the analysis with (3.39). We now consider a simple linear perturbation about this equilibrium in (3.47) with $P_0(t) = Z^0 + U(t)$ where $\|U(t)\| \ll 1$. The standard Taylor expansion about the equilibrium is thus

$$\begin{aligned} f(P_0) =& f(Z^0) + f_{P_0}(Z^0)(P_0 - Z^0) + O((P_0 - Z^0)^2), \\ U_t =& -2\sqrt{\frac{\eta_1(1-\eta_3)}{\pi|A|}(n - n_{\text{osc}})}U. \end{aligned} \tag{3.48}$$

Thus with (3.48) we learn that the perturbations $U(t)$ decay exponentially as long as the square-root is non-zero. We restrict our attention to real solutions so that our perturbations are real. Thus we have that Z^0 is a hyperbolic and asymptotically stable equilibrium for P_0 and find stability in Q_0 as well. This gives an attracting solution for this region but we lose this stability once the square-root becomes zero, here when

$$n_{osc} = \frac{\eta_1(1-\eta_3)|A|}{\pi}\left[2 - \left(\frac{\pi\eta_3}{2\eta_1(1-\eta_3)}\right)^2\right].$$

This indicates the equilibrium Z^0 at this point is non-hyperbolic which is indicative of a bifurcation. The results here are in agreement with our analysis and thus we can say that the value found in (3.41) is the bifurcation under the oscillatory forcing.

3.3 Slow Variation with Oscillatory Forcing

With the one component model solved and both the slowly varying and high oscillatory two component models analyzed, we have all of the tools needed to analyze the full system (3.1) with both $\epsilon \ll 1$ and $A, B \sim O(1)$ simultaneously. This is the most general setting we discuss in this thesis by accounting for both, slowly varying η_2 that leads to abrupt changes seen in [1, 14, 17] as well as the oscillatory forcing seen in [19, 9]. Our goal is to study the interaction of these mechanisms in the physical Stommel model and give an approximation on catastrophic behavior in the model. Under the framework of slowly varying parameters we expect to find a tipping point instead of a bifurcation. Hence our method for finding the tipping point follows a mixture of both section 3.1 and section 3.2. This procedure dictates that we search for inner behavior about the non-smooth bifurcation and to do so we need to solve the inner equation and estimate when this solution abruptly transitions towards the upper branch. Ultimately, we provide a solution that captures the abrupt change from the lower stable branch to the upper branch in the full Stommel model.

To begin, we take our standard approach of following the lower branch towards the non-smooth behavior with $V < 0$ in (3.1) which gives the following system

$$\begin{aligned} \dot{V} &= \eta_1 - \eta_2 - T + \eta_3(T-V) + V^2 + A\sin(\Omega t), \\ \dot{T} &= \eta_1 - T(1-V) + B\sin(\Omega t), \\ \dot{\eta_2} &= -\epsilon. \end{aligned} \tag{3.49}$$

As in section 2.4, we write the frequency in terms of the slow variation, $\Omega = \epsilon^{-\lambda}$ with exponent $\lambda > 0$. This assumption allows us to find the relative influence of the slowly varying parameter and fast oscillations on the tipping. We notice in (3.49) that there is variation on a slow scale in $\eta_2(t)$ and on a fast scale in $\sin(\Omega t)$, so this suggests a multiple scales approach with slow time $\tau = \epsilon t$ and fast time $R = \epsilon^{-\lambda} t$. Using this approach in (3.49) yields

$$\begin{aligned} V_R + \epsilon^{\lambda+1} V_\tau &= \epsilon^\lambda \left(\eta_1 - \eta_2 - T + \eta_3(T-V) + V^2 + A\sin(R)\right), \\ T_R + \epsilon^{\lambda+1} T_\tau &= \epsilon^\lambda \left(\eta_1 - T(1-V) + B\sin(R)\right), \\ \eta_{2\tau} &= -1. \end{aligned} \tag{3.50}$$

To approach the solution to the outer equations in (3.50), we use an asymptotic expansion with both ϵ^λ and integer powers as we have not specified the range of λ and both could be significant. Thus our expansion is

$$\begin{aligned} V(\tau,R) \sim& V_0(\tau,R) + \epsilon^\lambda V_1(\tau,R) + O(\epsilon^{2\lambda}, \epsilon^{\lambda+1}), \\ T(\tau,R) \sim& T_0(\tau,R) + \epsilon^\lambda T_1(\tau,R) + O(\epsilon^{2\lambda}, \epsilon^{\lambda+1}). \end{aligned} \tag{3.51}$$

Here we substitute (3.51) into (3.50) to give

$$\begin{aligned} V_{0R} + \epsilon^{\lambda+1} V_{0\tau} + \epsilon^\lambda V_{1R} + \ldots =& \epsilon^\lambda \left(\eta_1 - \eta_2 - T + \eta_3(T_0 - V_0) + V_0^2 + A\sin(R)\right) \\ &+ \epsilon^{2\lambda}\left(-\eta_3 V_1 - (1-\eta_3)T_1 + 2V_0V_1\right) + \ldots, \\ T_{0R} + \epsilon^{\lambda+1} T_{0\tau} + \epsilon^\lambda T_{1R} + \ldots =& \epsilon^\lambda \left(\eta_1 - T_0(1-V_0) + B\sin(R)\right) \\ &+ \epsilon^{2\lambda}\left(-T_1 + T_0V_1 + T_1V_0\right) + \ldots. \end{aligned}$$

Separating the equation at each order of ϵ then gives the following sets of equations

$$O(1): \quad \begin{cases} V_{0R} = & 0, \\ T_{0R} = & 0, \end{cases} \tag{3.52}$$

$$O(\epsilon^\lambda): \quad \begin{cases} V_{1R} = & \eta_1 - \eta_2(\tau) + \eta_3(T_0 - V_0) - T_0 + V_0^2 + A\sin(R), \\ T_{1R} = & \eta_1 - T_0(1-V_0) + B\sin(R), \end{cases} \tag{3.53}$$

$$O(\epsilon^{2\lambda}): \quad \begin{cases} V_{2R} + \epsilon^{1-\lambda} V_{0\tau} = & \eta_3(T_1 - V_1) - T_1 + 2V_0V_1, \\ T_{2R} + \epsilon^{1-\lambda} T_{0\tau} = & -T_1(1-V_0) + T_0V_1. \end{cases} \tag{3.54}$$

We consider a λ where the next order in (3.51) is $O(\epsilon^{2\lambda})$. Similar results follow from a choice in λ where $O(\epsilon^{\lambda+1}) < O(\epsilon^{2\lambda})$. From (3.52) the leading order terms in our expansion are only dependent on slow time, $V_0 = V_0(\tau)$ and $T_0 = T_0(\tau)$. The solutions of (3.53) and (3.54) are found in Appendix C, giving the outer solution

$$\begin{aligned} V \sim& V_0 + \frac{\epsilon(V_{0\tau}(1-V_0) + (1-\eta_3)T_{0\tau})}{(1-\eta_3)T_0 + (2V_0 - \eta_3)(1-V_0)} - \epsilon^\lambda A\cos(\Omega t), \\ T \sim& T_0 + \frac{\epsilon T_{0\tau}}{1-V_0} - \frac{\epsilon T_0(V_{0\tau}(1-V_0) + (1-\eta_3)T_{0\tau})}{(1-\eta_3)T_0(1-V_0) + (2V_0-\eta_3)(1-V_0)^2} - \epsilon^\lambda B\cos(\Omega t), \end{aligned} \tag{3.55}$$

where V_0 and T_0 are the same leading order solutions from the slowly varying Stommel model in section 3.1. Unfortunately, the common theme of the Stommel model is that these outer solutions are complex but it is clear the outer expansion breaks down as $V_0 \to 0$ as the scale separation between V_0 and V_1 no longer exists. Thus we derive a scaling for the inner equations which is analogous to that of section 2.4.

For simplicity, we assume that the scaling for both V and T is the same, but this isn't necessary to arrive at the same conclusion. Hence we rescale about the bifurcation point $(\eta_{2\text{ns}}, V_{\text{ns}}, T_{\text{ns}}) = (\eta_1\eta_3, 0, \eta_1)$ with

$$V = \epsilon^\alpha X, \quad T = \eta_1 + \epsilon^\alpha Y, \quad \eta_2(t) = \eta_{2\text{ns}} + \epsilon^\beta n(t), \tag{3.56}$$

where both $\alpha > 0$ and $\beta > 0$ allow for this to be a local scaling. Applying the local variables in (3.56) to the full Stommel model (3.1) gives

$$\begin{aligned}\epsilon^{\alpha}\dot{X} =& -\epsilon^{\beta}n(t) - \epsilon^{\alpha}(X + (1-\eta_3)Y) - \epsilon^{2\alpha}X|X| + A\sin\Big(\epsilon^{-\lambda}t\Big),\\ \epsilon^{\alpha}\dot{Y} =& -\epsilon^{\alpha}(\eta_1|X| + Y) + \epsilon^{2\alpha}|X|Y + B\sin\Big(\epsilon^{-\lambda}t\Big)\\ \dot{n} =& -\epsilon^{1-\beta}.\end{aligned} \tag{3.57}$$

From (3.57) it is apparent that there is still fast behavior within the oscillations. Also note that due to the scaling in (3.56), the local variable's slow behavior has been moved into the regular time t. To flesh out the particular choice in α, we then take a multiple scales approach to capture the oscillations with t and $R = \epsilon^{-\lambda}t$. This choice comes with the ambiguity in β and is discussed further below. Applying the multiple scales in (3.57) results in

$$\begin{aligned}\epsilon^{\alpha-\lambda}X_R + \epsilon^{\alpha}X_t =& -\epsilon^{\beta}n(t) - \epsilon^{\alpha}(X + (1-\eta_3)Y) - \epsilon^{2\alpha}X|X| + A\sin(R),\\ \epsilon^{\alpha-\lambda}Y_R + \epsilon^{\alpha}Y_t =& -\epsilon^{\alpha}(\eta_1|X| + Y) - \epsilon^{2\alpha}|X|Y + B\sin(R)\\ n_t =& -\epsilon^{1-\beta}.\end{aligned} \tag{3.58}$$

Next we balance the leading order terms in each equation of (3.58), $\epsilon^{\alpha-\lambda}X_R$ and $A\sin(R)$ as well as $\epsilon^{\alpha-\lambda}Y_R$ with $B\sin(R)$, which gives us that $\alpha = \lambda$ and confirms that the scales V and T are the same. The scaling for η_2 has yet to be determined and could have multiple possibilities depending on λ. Due to this choice in α we expect the oscillatory term to persist in the inner asymptotic expansion of (3.1) regardless of choice in λ.

Here we use a multiple scales approach with t and $R = \epsilon^{-\lambda}t$ on the full Stommel model (3.1) along with the general scaling (3.56) on η_2 which gives

$$\begin{aligned}V_R + \epsilon^{\lambda}V_t =& -\epsilon^{\lambda+\beta}n(t) - \epsilon^{\lambda}(\eta_1 - \eta_1\eta_3 + \eta_3(T-V) - T - V|V| + A\sin(R)),\\ T_R + \epsilon^{\lambda}T_t =& \epsilon^{\lambda}(\eta_1 - T(1+|V|) + B\sin(R)),\\ n_t =& -\epsilon^{1-\beta}.\end{aligned} \tag{3.59}$$

In section 2.4 the results depended on the relative size of the slow variation with respect to the oscillations. The distinction in that case was when $\lambda \leq 1$, where a mixture between the slow variation and oscillations influence the tipping or $\lambda > 1$, where the slow variation dominates the tipping. We find a similar distinction here and hence consider a separate asymptotic expansion for Case I: $\lambda \leq 1$ and Case II: $\lambda > 1$ to find an accurate classification of behavior for the full Stommel model.

3.3.1 Case I: $\lambda \leq 1$

We call this the 'mixed effects' case where there is significant influence from both slow variation and fast oscillations due to the size of λ. Here we cannot determine what the next term in the expansion should be and thus we choose a general expansion with

$$\begin{aligned}V(t,R) \sim& \epsilon^{\lambda}X_0(t,R) + \epsilon^{q}X_1(t,R) + \dots,\\ T(t,R) \sim& \eta_1 + \epsilon^{\lambda}Y_0(t,R) + \epsilon^{q}Y_1(t,R) + \dots,\end{aligned} \tag{3.60}$$

with $q > \lambda$ to allow for $O(\epsilon^\lambda)$ to be the leading order term which our local analysis suggested. Substituting (3.60) into (3.59) then gives the governing dynamics for this case

$$\begin{aligned} X_{0R} + \epsilon^\lambda X_{0t} + \epsilon^{q-\lambda} X_{1R} \ldots = & -\epsilon^\beta n(t) - \epsilon^\lambda(\eta_3 X_0 + (1-\eta_3)Y_0) \\ & - \epsilon^{2\lambda}(X_0 + \epsilon^{q-\lambda}X_1 + \ldots)|X_0 + \epsilon^{q-\lambda}X_1 + \ldots| \\ & - \epsilon^q(\eta_3 X_1 + (1-\eta_3)Y_1) + A\sin(R) + \ldots, \\ Y_{0R} + \epsilon^\lambda Y_{0t} + \epsilon^{q-\lambda} Y_{1R} + \ldots = & -\epsilon^\lambda(\eta_1|X_0 + \epsilon^{q-\lambda}X_1 + \ldots| + Y_0 + \epsilon^{q-\lambda}Y_1 + \ldots) \\ & + \epsilon^{2\lambda}|X_0 + \epsilon^{q-\lambda}X_1 + \ldots|(Y_0 + \epsilon^{q-\lambda}Y_1 + \ldots) \\ & + B\sin(R) + \ldots. \end{aligned}$$

Separating by the distinct orders of ϵ gives the following equations at each order

$$O(1): \begin{cases} X_{0R} = & A\sin(R), \\ Y_{0R} = & B\sin(R), \end{cases} \tag{3.61}$$

$$O(\epsilon^\lambda): \begin{cases} \epsilon^{q-2\lambda}X_{1R} + X_{0t} = & -\epsilon^{\beta-\lambda}n(t) - \eta_3 X_0 - (1-\eta_3)X_0, \\ \epsilon^{q-2\lambda}Y_{1R} + Y_{0t} = & -\eta_1|X_0| - Y_0. \end{cases} \tag{3.62}$$

We learn from (3.62) that $q = 2\lambda$ balances the equations, which implies that $\lambda > \frac{1}{2}$ for an expansion to be found. If $\lambda \leq \frac{1}{2}$ then we would need to include the quadratic terms in $O(\epsilon^\lambda)$ and our reduced equations would be the same as the full Stommel model (3.1). This indicates that our local approximation would no longer hold and that the high frequency assumption is failing. Without this, the physical behavior of the problem is qualitatively different and we explore this further in chapter 4. On this range of λ, there are two choices for the scaling of η_2 with $\beta = 1$ or $\beta = \lambda$. The advantage to choosing $\beta = \lambda$ is that the equation (3.62) is simple, but the slow variation equation has the form $n_t = -\epsilon^{1-\lambda}$ and implies a slower time scale. On the other hand, $\beta = 1$ keeps a small coefficient on n in (3.62) but gives the slow variation equation as $n_t = -1$, which allows the time scale t to be used. Both of these choices result in the same approximation of the tipping point in original variables. Here we choose $\beta = 1$ for convenience. From (3.61) we find the appropriate forms of the leading order terms, $X_0 = P_0(t) - A\cos(R)$ and $Y_0 = Q_0(t) - B\cos(R)$. Using these forms for the leading order term and applying the Fredholm alternative (2.24) to (3.62) we find

$$\begin{aligned} P_{0t} = & -\epsilon^{1-\lambda}n(t) - \eta_3 P_0 - (1-\eta_3)Q_0, \\ Q_{0t} = & -\frac{\eta_1}{2\pi}\int_0^{2\pi} |P_0(t) - A\cos(R)|\, dR - Q_0, \\ n_t = & -1. \end{aligned} \tag{3.63}$$

Analogously to section 3.2 we must approach this integration with the relative size of $P_0(t)$ to the amplitude of oscillation A in mind. This is due to the sizes determining the contributions of the integral in (3.63). We consider these sizes of $P_0(t)$ as Sub-case I: $P_0(t) \leq -|A|$ and Sub-case II: $|P_0(t)| < |A|$ similar to section 3.2. These cases separate $X_0 = P_0 - A\cos(R)$ from either staying entirely below $V = 0$ or changing signs respectively and allows for the integration to have two distinct forms.

Sub-Case I: $P_0(t) \leq -|A|$

We call this the 'below-axis' sub-case, where the solution $P_0(t)$ is entirely below the axis $V = 0$ and this means the full solution X_0 has oscillations far from crossing. Under these conditions we don't expect any tipping behavior as the solution is far from $V = 0$, but we may use this size of $P_0(t)$ to find the range of η_2 that distinguishes these cases. With $P_0(t) \leq -|A|$, we find (3.63) simplifies to

$$\begin{aligned} P_{0t} =& -\epsilon^{1-\lambda} n(t) - \eta_3 P_0 - (1-\eta_3) Q_0, \\ Q_{0t} =& \eta_1 P_0 - Q_0. \end{aligned} \tag{3.64}$$

Although we have the means available to solve (3.64) as it takes the form of an equation we have seen in section 3.1, instead we search for when the pseudo-equilibrium fails the assumption of this sub-case. This results in the parameter range between these sub-cases and taking this approach is more convenient than solving the system. Here the form of the pseudo-equilibria is simple to find as $Q_0(P_0) = \eta_1 P_0$ and thus

$$P_0(t) = -\epsilon^{1-\lambda} \frac{n(t)}{\eta_3 + \eta_1(1-\eta_3)}.$$

We recall that for this sub-case $P_0(t) \leq -|A|$, which gives the range for n and we rewrite this in the original variables of η_2 with

$$\begin{aligned} \epsilon n \geq& \epsilon^{\lambda}(\eta_3 + \eta_1(1-\eta_3))|A|, \\ \eta_2 \geq& \eta_{2_{\text{ns}}} + \frac{(\eta_3 + \eta_1(1-\eta_3))|A|}{\Omega}. \end{aligned} \tag{3.65}$$

With the parameter range (3.65), we now have an effective region for sub-case I and have the range for sub-case II in terms of the parameter η_2.

Sub-Case II: $|P_0(t)| \leq |A|$

We call this the 'crossing' sub-case and under these conditions we see the integral in (3.63) is more complex. As this contribution changes, there is an increasing effect on the system and it is here that we anticipate the tipping point to occur. In section 2.4, we found a similar integral to (3.63) that we could evaluate with the assumption that $A \sim O(1)$. Note that the assumptions that allowed for evaluation of the integral in (2.59) from section 2.4 still hold here with a fast time R that is sufficiently large due to the high frequency. Thus we follow the approach from section 2.4 by integrating with $R_1 = \arccos(P_0/A)$ and $R_2 = 2\pi - \arccos(P_0/A)$ which is analogous to T_1 and T_2 from section 2.4 and then use a quadratic Taylor approximation about $P_0 = 0$ as in (2.63) to give

$$\begin{aligned} P_{0t} =& -\epsilon^{1-\lambda} n(t) - \eta_3 P_0(s) - (1-\eta_3) Q_0, \\ Q_{0t} =& -\frac{2\eta_1|A|}{\pi} - \frac{\eta_1}{\pi|A|} P_0^2 - Q_0. \end{aligned} \tag{3.66}$$

The form in (3.66) is known as a quadratic two component Riccati-type equation. We recall the assumption that the solution to the equation for T being in terms of V was realistic to the THC, so the behavior we are interested in lies within the dynamics for V.

For this reason, we choose to approximate by reducing (3.66) to a one component model by assuming our equation for Q_0 is in pseudo-equilibrium with

$$Q_0(P_0) = -\frac{2\eta_1|A|}{\pi} - \frac{\eta_1}{\pi|A|}P_0^2. \tag{3.67}$$

The resulting reduced system from introducing the equilibrium (3.67) into the inner equation (3.66) is then

$$\begin{aligned} P_{0t} =& -\epsilon^{1-\lambda}n(t) + \frac{2\eta_1(1-\eta_3)|A|}{\pi} - \eta_3 P_0 + \frac{\eta_1}{\pi|A|}P_0^2, \\ n_t =& -1. \end{aligned} \tag{3.68}$$

Again for convenience, we rewrite the differentiation in (3.68) in terms of the parameter n giving

$$P_{0n} = \epsilon^{1-\lambda}n - \frac{2\eta_1(1-\eta_3)|A|}{\pi} + \eta_3 P_0 - \frac{\eta_1(1-\eta_3)}{\pi|A|}P_0^2. \tag{3.69}$$

Now (3.69) is in a form where the result from (1.2) applies. Thus we determine that (3.69) is an Airy-type equation and that the tipping point follows with (1.4). We write the solution in original variables and obtain results similar to previous sections with

$$\begin{aligned} n_{\text{tip}} =& -\epsilon^{(\lambda-1)/3}\left(\frac{\pi|A|}{\eta_1(1-\eta_3)}\right)^{1/3}(2.33810) + \epsilon^{\lambda-1}\frac{\eta_1(1-\eta_3)|A|}{\pi}\left(2 - \left(\frac{\pi\eta_3}{2\eta_1(1-\eta_3)}\right)^2\right), \\ \eta_{2\text{tip}} =& \left(\frac{\pi|A|}{\eta_1(1-\eta_3)\Omega}\right)^{1/3}\mu_{\text{smooth}} + \eta_{2\text{osc}}. \end{aligned} \tag{3.70}$$

We conclude that the tipping point in (3.70) has a similar form as the tipping point found with (2.67) in section 2.4, where we found a weighted average between the smooth tipping point μ_{smooth} from [24] and the oscillatory bifurcation $\eta_{2\text{osc}}$ for this range of λ. We also found in (3.62) that any choice for $\lambda \leq \frac{1}{2}$ gave equations that cannot be studied using the multiple scales approach in this section. This heuristically makes sense since for $\lambda \leq \frac{1}{2}$ we have low frequency oscillations with our polynomial relationship and the contributions to the dynamics from this behavior require a different approach than presented in this paper. See [24] for an example of a low-frequency method.

3.3.2 Case II: $\lambda > 1$

We call this case the 'slowly varying dominant' case. Here we expect integer powers of ϵ to appear in leading order due to the $O(\epsilon^\lambda)$ being quite small for this range of λ and thus we choose the expansion

$$\begin{aligned} V(t,R) \sim& \epsilon X_0(t,R) + \epsilon^\lambda X_1(t,R) + \epsilon^q X_2(t,R) + \dots, \\ T(t,R) \sim& \epsilon Y_0(s,R) + \epsilon^\lambda Y_1(t,R) + \epsilon^q Y_2(t,R) + \dots. \end{aligned} \tag{3.71}$$

Substituting (3.71) into (3.59) then gives

$$\begin{aligned}\epsilon X_{0R} + \epsilon^{\lambda+1} X_{0t} + \epsilon^{\lambda} X_{1R} + \ldots = & -\epsilon^{\lambda+\beta} n(t) - \epsilon^{\lambda+1}(\eta_3 X_0 + (1-\eta_3) Y_0) \\ & - \epsilon^{\lambda+2}(X_0 + \epsilon^{q-\lambda} X_1 + \ldots)|X_0 + \epsilon^{q-\lambda} X_1 + \ldots| \\ & - \epsilon^{2\lambda}(\eta_3 X_1 + (1-\eta_3) Y_1) + \epsilon^{\lambda} A \sin(R),\end{aligned}$$

$$\begin{aligned}\epsilon Y_{0R} + \epsilon^{\lambda+1} Y_{0t} + \epsilon^{\lambda} Y_{1R} + \ldots = & -\epsilon^{\lambda+1}(\eta_1 |X_0 + \epsilon^{\lambda-1} X_1 + \epsilon^{q-1} X_2 + \ldots| - Y_0 - \epsilon^{\lambda-1} Y_1 + \ldots) \\ & + \epsilon^2 |X_0 + \epsilon^{\lambda-1} X_1 + \epsilon^{q-1} X_2 + \ldots|(Y_0 + \epsilon^{\lambda-1} Y_1 + \ldots) \\ & + \epsilon^{\lambda} B \sin(R).\end{aligned}$$

We separate by each distinct order of ϵ to find the equations

$$O(\epsilon): \begin{cases} X_{0R} = & 0, \\ Y_{0R} = & 0, \end{cases} \tag{3.72}$$

$$O(\epsilon^{\lambda}): \begin{cases} X_{1R} = & A\sin(R), \\ Y_{1R} = & B\sin(R), \end{cases} \tag{3.73}$$

$$O(\epsilon^{\lambda+1}): \begin{cases} \epsilon^{q-\lambda-1} X_{2R} + X_{0t} = & -\epsilon^{\beta-1} n(t) - \eta_3 X_0 - (1-\eta_3) Y_0, \\ \epsilon^{q-\lambda-1} Y_{2R} + Y_{0t} = & -\eta_1 |\epsilon^{\lambda}| X_0 + \epsilon^{\lambda-1} X_1| - Y_0. \end{cases} \tag{3.74}$$

We learn in (3.74) that $q = \lambda + 1$ balances terms in the expansion. We also find that $\beta = 1$ gives both simple expressions in (3.74) but also $n_t = -1$. Here a single β is found as opposed to case I where we chose the value of β for convenience. In (3.72) we find that the leading order behavior for this case depends only on slow time, $X_0 = X_0(t)$ and $Y_0 = Y_0(t)$, thus giving dominant behavior in this case. With (3.73) we find the correction terms are given by $X_1 = P_1(t) - A\cos(R)$ and $Y_1 = Q_1(t) - B\cos(R)$ and since the slow behavior in X_1 and Y_1 is just next order corrections to the purely slow X_0 and Y_0, without loss of generality we set $P_1 \equiv Q_1 \equiv 0$. This gives purely oscillatory corrections, $X_1 = -A\cos(R)$ and $Y_1 = -B\cos(R)$. Applying Fredholm (2.24) to (3.74) then gives

$$\begin{aligned} X_{0t} = & -n(t) - \eta_3 X_0 - (1-\eta_3) Y_0, \\ Y_{0t} = & -\frac{\eta_1}{2\pi} \int_0^{2\pi} |X_0(t) - \epsilon^{\lambda-1} A\cos(R)|\, dR - Y_0, \\ n_t = & -1. \end{aligned} \tag{3.75}$$

In case I, we used the pseudo-equilibrium of Q_0 regardless of the size of the oscillations to find a solvable equation. Here we expect (3.75) to have a quadratic form like case I, so we choose a priori to use a similar reduction by assuming the equation for Y_0 is in it's pseudo-equilibrium with

$$Y_0(X_0) = -\frac{\eta_1}{2\pi} \int_0^{2\pi} |X_0 - \epsilon^{\lambda-1} A\cos(R)|\, dR. \tag{3.76}$$

We find the resulting reduced one component equation by introducing (3.76) into the inner equation (3.75) with

$$X_{0t} = -n(t) - \eta_3 X_0 + \frac{\eta_1(1-\eta_3)}{2\pi}\int_0^{2\pi} |X_0(t) - \epsilon^{\lambda-1} A\cos(R)|\, dR. \tag{3.77}$$

The behavior in (3.77) is similar to case I as long as the amplitude of oscillation inside the integral are consistent with the assumptions of case I, $\epsilon^{\lambda-1}A \sim O(1)$. Under this assumption, we find that $\lambda \approx 1$ to see mixed behavior of case I and thus we once more follow the method of section 2.4. Our assumption on the size of the oscillations allow us to integrate (3.77) with $R_1 = \arccos\big(X_0/\epsilon^{\lambda-1}A\big)$ and $R_2 = 2\pi - \arccos\big(X_0/\epsilon^{\lambda-1}A\big)$ which again are analogous to T_1 and T_2 from section 2.4. Another application of a quadratic Taylor approximation about $X_0 = 0$ as in (2.74) then yields

$$X_{0t} = -n(t) + \epsilon^{\lambda-1}\frac{2\eta_1(1-\eta_3)|A|}{\pi} - \eta_3 X_0 + \epsilon^{1-\lambda}\frac{\eta_1(1-\eta_3)}{\pi|A|}X_0^2. \tag{3.78}$$

Once more, we find a form to which we apply the result from (1.2). Thus we find the tipping point for the local parameter n with (1.4) and then transform back into the original variables to find the tipping point in η_2 with

$$\begin{aligned} n_{\text{mixed}} =& -\epsilon^{(\lambda-1)/3}\left(\frac{\pi|A|}{\eta_1(1-\eta_3)}\right)^{1/3}(2.33810) + \epsilon^{\lambda-1}\frac{\eta_1(1-\eta_3)|A|}{\pi}\left(2 - \left(\frac{\pi\eta_3}{2\eta_1(1-\eta_3)}\right)^2\right), \\ \eta_{2\text{mixed}} =& \left(\frac{\pi|A|}{\eta_1(1-\eta_3)\Omega}\right)^{1/3}\mu_{\text{smooth}} + \eta_{2\text{osc}}. \end{aligned} \tag{3.79}$$

Our result for $\eta_{2\text{mixed}}$ is not surprising as we had similar forms and assumptions to the ones of case I. For $\lambda > 1$ and away from 1, the amplitude of the oscillations is smaller, and inside the integral in (3.58) the contribution from the oscillations is reduced. Although no exact cut-off exists and, depending on the choice in other model parameters η_1 and η_3, we find this is typically for $\lambda \geq 1.5$, the system (3.75) is approximated by

$$\begin{aligned} X_{0t} =& -n(t) - \eta_3 X_0 - (1-\eta_3)Y_0, \\ Y_{0t} =& -\eta_3|X_0| - Y_0, \\ n_t =& -1. \end{aligned} \tag{3.80}$$

Here (3.80) is the same system as the slowly varying model in section 3.1. With the same inner equation and slowly varying n, we are able to use the approximation found in section 3.1 for the tipping point $\eta_{2\text{slow}}$ from (3.17) here as well. This indicates that the amplitude of the oscillations are small for larger λ, so that only the slow variation affects the tipping of the Stommel model.

With both case I and case II, we have described the tipping behavior for any choice in λ. For $\lambda \leq 1$, we found a similar combination of contributions from the oscillatory bifurcation $\eta_{2\text{osc}}$ and the smooth tipping point μ_{smooth} in the Airy equation as in section 2.4. The weighted averaging is reminiscent of the smooth tipping point analysis in [24] where here the weight depends on the frequency Ω. With this frequency dependency, we have further

evidence to see mixed behavior for medium sized frequency (which corresponds to smaller λ). This behavior is observed for both $\lambda \leq 1$ and $\lambda > 1$ but the oscillatory behavior contributes less to the advance of the tipping point for larger λ. For λ sufficiently large, the oscillations have a negligible contribution and we recover the tipping point $\eta_{2\text{slow}}$ from the slowly varying model. The results for the tipping point in the Stommel model with slowly varying parameter η_2 and oscillatory forcing are summarized in the following table.

Two Component Tipping Points	
$\epsilon > 0$ and $A = 0$:	$\eta_{2\text{slow}} = \min(\eta_1\eta_3 - \epsilon\log(\epsilon)/\lambda_i)$ for $i \in \{1, 2\}$
$\epsilon = 0$ and $A \neq 0$ with $\Omega \gg 1$:	$\eta_{2\text{osc}} = \eta_1\eta_3 + \frac{\eta_1(1-\eta_3)\lvert A\rvert}{\pi\Omega}\left(2 - \left(\frac{\pi\eta_3}{2\eta_1(1-\eta_3)}\right)^2\right)$
$\epsilon > 0$, $A \neq 0$ and $\frac{1}{2} < \lambda \leq 1$:	$\eta_{2\text{mixed}} = \left(\frac{\pi\lvert A\rvert}{\eta_1(1-\eta_3)\Omega}\right)^{1/3}\mu_{\text{smooth}} + \eta_{2\text{osc}}$
$\epsilon > 0$, $A \neq 0$ and $\lambda > 1$ with $\lambda \approx 1$:	$\eta_{2\text{mixed}} = \left(\frac{\pi\lvert A\rvert}{\eta_1(1-\eta_3)\Omega}\right)^{1/3}\mu_{\text{smooth}} + \eta_{2\text{osc}}$
$\epsilon > 0$, $A \neq 0$ and $\lambda > 1$:	$\eta_{2\text{slow}} = \min(\eta_1\eta_3 - \epsilon\log(\epsilon)/\lambda_i)$ for $i \in \{1, 2\}$

Table 3.1: Overview of the tipping points in the two component model for each mechanism and case.

In figure 3.8, we see an example of the numerical solution of V to the Stommel model (3.1) with slow variation and oscillatory forcing. This example illustrates the tipping for case I with $\lambda \in (\frac{1}{2}, 1]$, so that both the slow variation and oscillatory forcing influence the tipping point. The vertical lines are the tipping, black solid for the numerical and blue dotted for the approximation for this case (3.70). Although there is a mixture of effects, the tipping point gives a value near the oscillatory bifurcation $\eta_{2\text{osc}}$. This tells us that for these choices in the model parameters the strongest effect is the oscillatory forcing. The results are shown in figure (3.9) in the $V - T$ plane. Here we see that due to the early tipping in V, the solution for T also never achieves it's maximum and there is early tipping here as well, which agrees with the assumptions we had made of considering T responding to V.

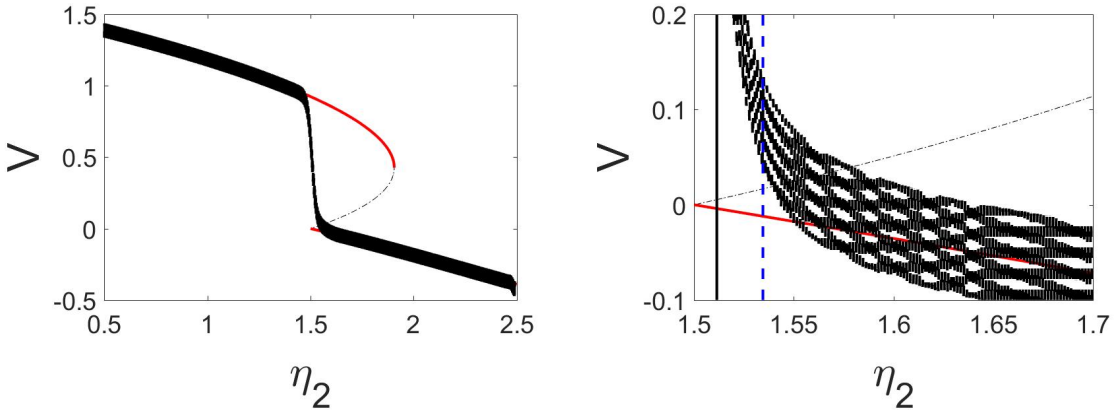

(a) (b)

Figure 3.8: The model values are $\lambda = .8$, $\epsilon = .01$ with $A = B = 2$. In (a) the numerical solution (black dotted line) to (3.1) is given with $\eta_1 = 4$, $\eta_3 = .375$. In (b) a zoom in closer to the non-smooth bifurcation region where the blue dotted vertical line is the tipping point (3.70) and the black vertical line are the tipping points with the tipping criterion $V > V_{\text{smooth}}$ on the numerical solution.

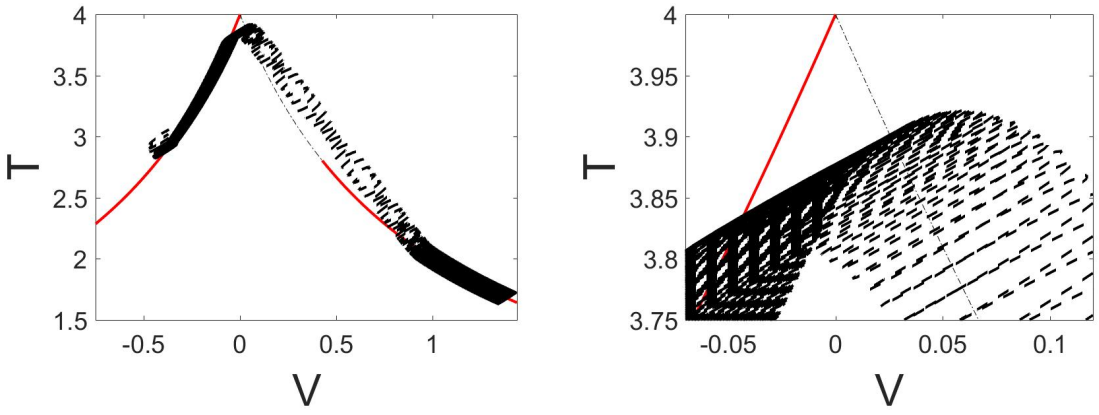

(a) (b)

Figure 3.9: The model values are $\lambda = .8$, $\epsilon = .01$ with $A = B = 2$. In (a) we have the numerical solution (black dotted) over the static equilibrium plot for V vs. T. In (b) a zoom of the bifurcation area.

In figure 3.10 we have chosen a value of λ in case II as $\lambda > 1$ but we also have that $\lambda \approx 1$. Thus we see comparable behavior to case I with the addition that the slow variation is now dominant. Upon a zoom in, it is apparent that oscillations are still present and we see a mixture of effects that cause a similar tipping to case I to take place. We've plotted the tipping point $\eta_{2\text{slow}}$ from the slowly varying model (3.17) as the green vertical dotted line for comparison. As the numerical tipping point is moving towards the slowly varying

tipping point this confirms that the slow variation is indeed dominating the tipping. In figure 3.11 we again see very similar behavior to the slowly varying model in section 3.1 but the zoom-in further reveals the oscillations are present and have minor influence by forcing the solution to cross the $V = 0$ axis near the tipping.

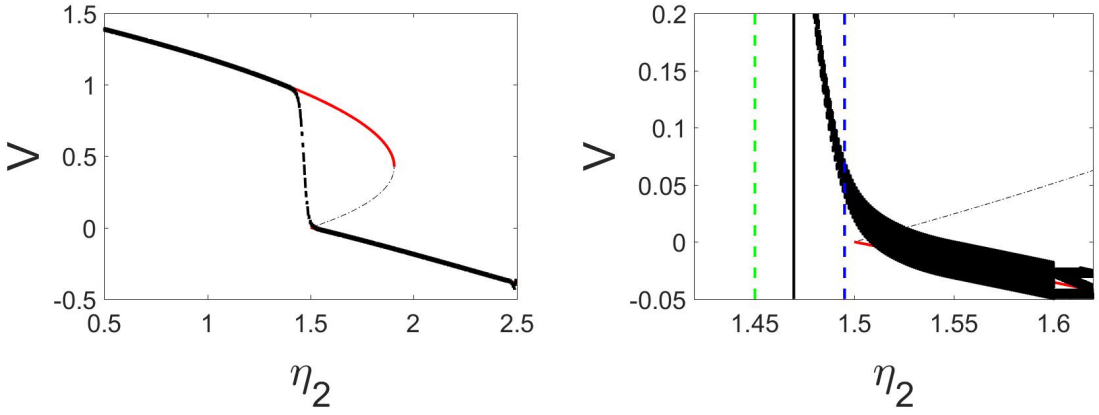

(a) (b)

Figure 3.10: The model values are $\lambda = 1.05$, $\epsilon = .01$ with $A = B = 2$. In (a) the numerical solution (black dotted line) to (3.1) is given with $\eta_1 = 4$ and $\eta_3 = .375$. In (b) a zoom in closer to the non-smooth bifurcation region where the blue dotted vertical line is the mixed tipping point (3.70), green dotted verticle line is the slow tipping point (3.17) and the black vertical line are the tipping points with the tipping criterion $V > V_{\text{smooth}}$ on the numerical solution.

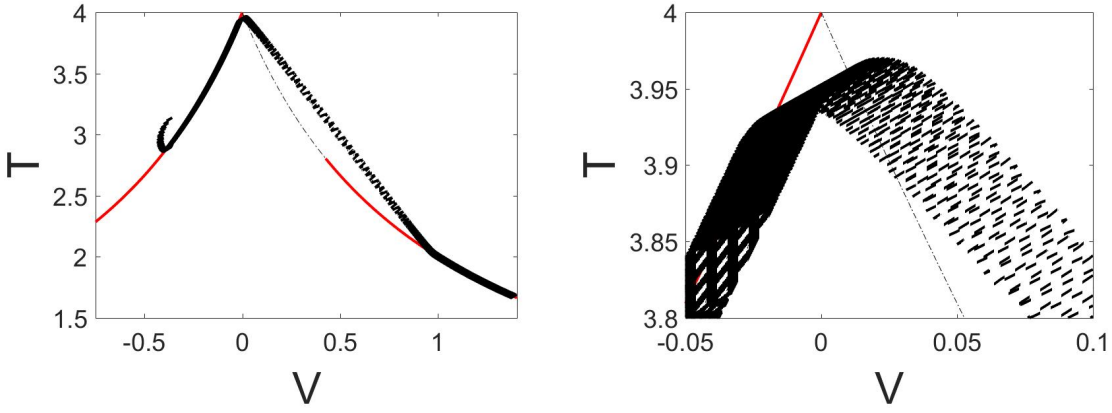

(a) (b)

Figure 3.11: The model values are $\lambda = 1.05$, $\epsilon = .01$ with $A = B = 2$. In (a) we have the numerical solution (black dotted) over the static equilibrium plot for V vs. T. In (b) a zoom of the bifurcation area is given.

In figure 3.12 we show the numerics for a λ large enough so that the oscillations are

negligible and we recover the slowly varying model in section 3.1. Even upon a zoom it is almost impossible to see oscillations in this solution. The green dotted vertical line is the slowly varying tipping estimate (3.17) where the blue dotted is the mixed approximation (3.70). Further evidence is seen in figure 3.13, where this figure resembles the slowly varying $V - T$ plot (3.2).

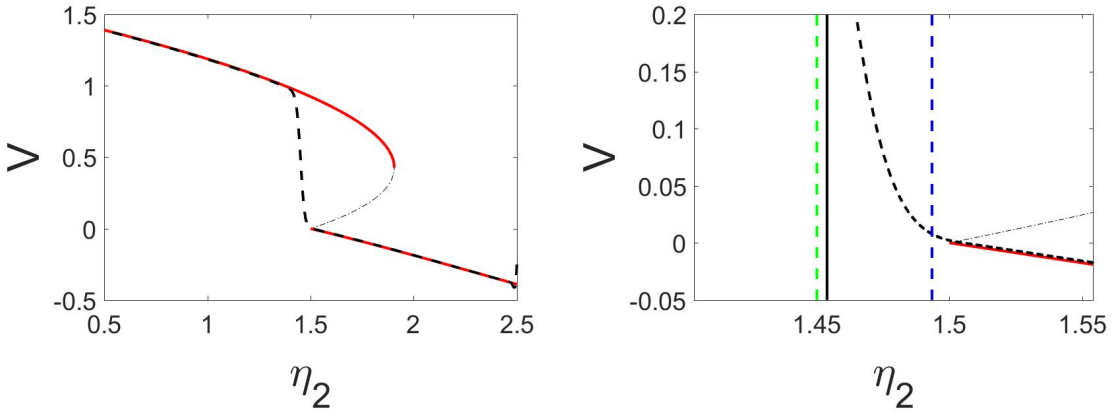

(a) (b)

Figure 3.12: The model values are $\lambda = 2$, $\epsilon = .01$ with $A = B = 2$. In (a) the numerical solution (black dotted line) to (3.1) is given with $\eta_1 = 4$ and $\eta_3 = .375$. In (b) a zoom in closer to the non-smooth bifurcation region where the blue dotted vertical line is the mixed tipping point (3.70), the green dotted vertical line is the slow tipping point (3.17) and the black vertical line are the tipping points with the tipping criterion $V > V_{\text{smooth}}$ on the numerical solution.

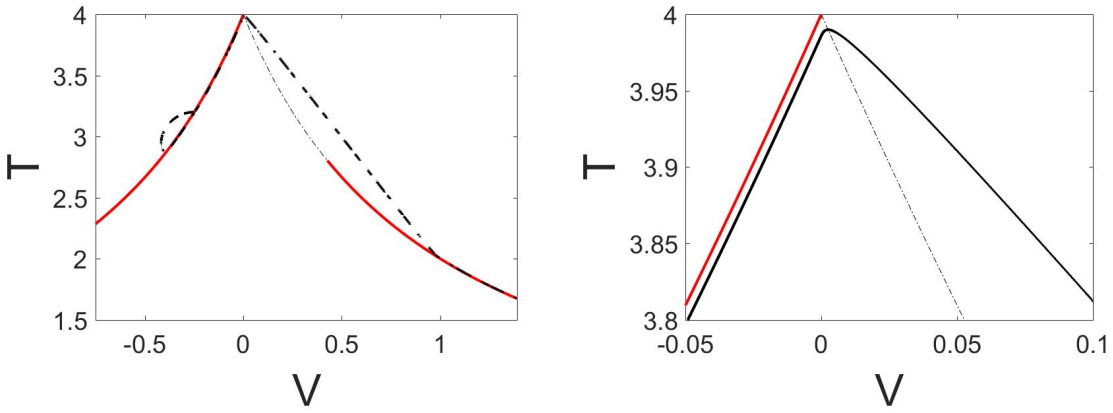

(a) (b)

Figure 3.13: The model values are $\lambda = 2$, $\epsilon = .01$ with $A = B = 2$. In (a) we have the numerical solution (black dotted) over the static equilibrium plot for V vs. T. In (b) a zoom of the bifurcation area is provided.

Although the figures above show that we have classified the behavior appropriately for the various cases in λ and relative solution sizes, performance of this approximate tipping point needs to be evaluated to compare with numerical results. In figure 3.14 we compare the tipping points between case I and case II with the numerically obtained tipping points across a range of λ with a fixed ϵ. For smaller λ, the frequency Ω is smaller and the influence of the oscillations on tipping become more predominant. Recall the assumption that $\Omega = \epsilon^{-\lambda} \gg 1$ and that for $\lambda \leq \frac{1}{2}$ we observe $\Omega \sim O(1)$. We do not consider low frequency corresponding to $\lambda < \frac{1}{2}$ in this section. For larger λ, there is a reduced influence for the oscillatory forcing until it is negligible for some $\lambda > 1$. We notice that our reduction tipping approximation for $\lambda < 1$ has some bias which can be attributed the information lost from reducing the full two component Riccati equations to a one component model. Even though we use a one component reduced equation to get these approximations, they seem to be performing quite well across all λ which confirms the approach leads to a sufficient approximation.

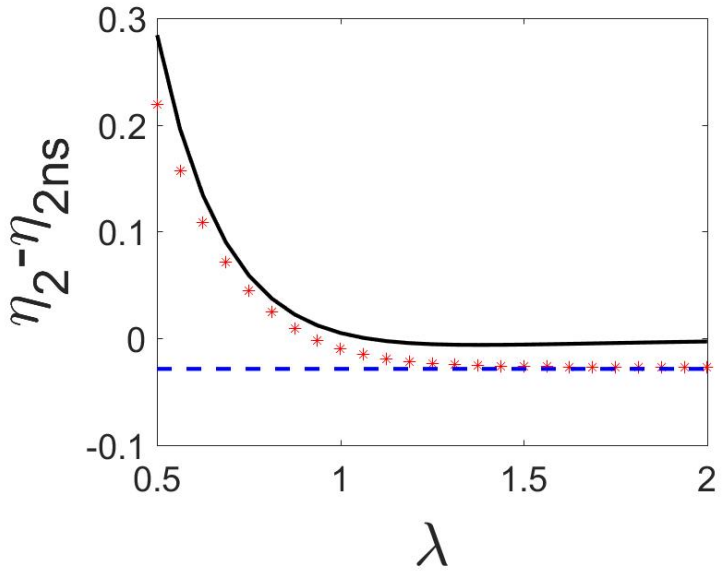

Figure 3.14: An example of numerical tipping (red stars) as the numerical solution to (3.1) passes the tipping criterion $V > V_{\text{smooth}}$. The parameter values are $\epsilon = .01$ and $A = B = 3$. The lines are the case I tipping estimate (black solid line) and the case II tipping estimate (blue dotted line).

We also are interested in the performance of the tipping approximations across values of ϵ for λ fixed, which is seen in figure 3.15. For case I tipping, the range of appropriate ϵ is highly dependent on the choice in λ. Often, the range is very small to get accurate estimates which is another artifact of using a reduced model. For case II tipping, we see that the numerical results are being approximated by the slowly varying tipping section 3.1 as the effective oscillations shrink, $\epsilon^{\lambda-1}A \to 0$ as $\lambda \to \infty$.

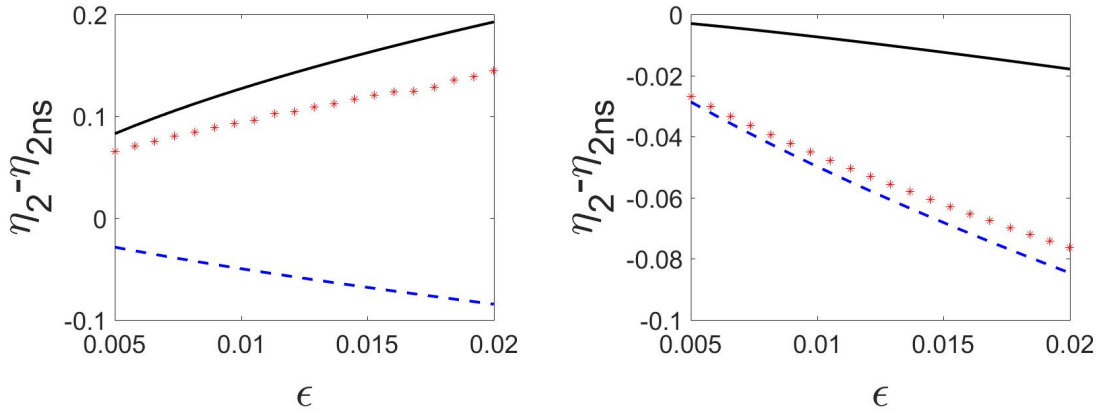

(a) $\lambda = .8$ (b) $\lambda = 1.3$

Figure 3.15: The numerical tipping (red stars) follows the appropriate case depending on λ for $\epsilon = 0.01$. The case I tipping estimate $\eta_{2\text{mixed}}$ (black solid line) and slowly varying tipping estimate $\eta_{2\text{slow}}$ (blue dotted line) are shown.

With the numerical results agreeing with our analytic results, we may finally conclude that this method is both useful for analyzing the non-smooth behavior in the Stommel model and also results in an approximation that is more accurate in the extremal cases of the model (i.e $\Omega \gg 1$ or $\epsilon \ll 1$). This gives us a very accessible means of extracting the tipping in the full two component model without needing to solve difficult Riccati equations or other complex systems that appear in the full problem. We still need to confirm that the solutions we've found are attracting until stability is lost at the tipping point.

3.3.3 Stability

Case I: $\lambda \leq 1$

From the analysis, we obtained the inner equations that govern the behavior of the solution for this range of λ are

$$\begin{aligned} P_{0t} &= -\epsilon^{1-\lambda} n(t) - \eta_3 P_0 - (1-\eta_3) Q_0, \\ Q_{0t} &= -\frac{\eta_1}{2\pi} \int_0^{2\pi} |P_0 - A\cos(R)|\, dR - Q_0. \end{aligned} \tag{3.81}$$

But we also found that the relative size of $P_0(t)$ dictates the contribution from the integral in (3.81). In the analysis we treat these as Sub-case I: $P_0(t) \leq -|A|$ and Sub-case II: $|P_0(t)| < |A|$ that each require a separate analysis.

Sub-Case I: $P_0(t) \leq -|A|$

We called this the 'below-axis' sub-case due to the solution remaining below the axis and thus we anticipate this sub-case to remain attracting to a solution near the lower branch.

The equation (3.81) simplifies for this sub-case to

$$\begin{aligned} P_{0t} =& -\epsilon^{1-\lambda} n(t) - \eta_3 P_0 - (1-\eta_3) Q_0, \\ Q_{0t} =& \eta_1 P_0 - Q_0. \end{aligned} \tag{3.82}$$

From the analysis we choose to reduce (3.82) with the pseudo-equilibria $Q_0(P_0) = \eta_1 P_0$. This gives the following reduced equation with the pseudo-equilibria $Z^0(t)$ as

$$\begin{aligned} P_{0t} =& -\epsilon^{1-\lambda} n(t) - (\eta_3 + \eta_1(1-\eta_3)) P_0 = f(t, P_0), \\ Z^0(t) =& -\epsilon^{1-\lambda} \frac{n(t)}{\eta_3 + \eta_1(1-\eta_3)}. \end{aligned} \tag{3.83}$$

We adopt a similar strategy for analyzing the stability of the one component model in section 2.4 due to (3.83) being a one-dimensional equation. Hence we perform a simple linear perturbation about the pseudo-equilibrium with $P_0(t) = Z^0(t) + U(t)$ and $\|U(t)\| \ll 1$. Taking special care to note that $Z^0(t)$ also varies in time, we find the Taylor approximation

$$\begin{aligned} P_{0t} =& f(t, Z^0) + f_{P_0}(t, Z^0)(P_0(t) - Z^0(t)) + O(\|(P_0(t) - Z^0(t))^2\|^2), \\ U_t =& -\epsilon^{1-\lambda} \frac{1}{\eta_3 + \eta_1(1-\eta_3)} - (\eta_3 + \eta_1(1-\eta_3)) U. \end{aligned} \tag{3.84}$$

From (3.84) we find that the perturbations decay exponentially to just below the pseudo-equilibrium Z^0. This indicates that the solution for this sub-case is hyperbolically attracting and that there is no tipping for this range of the parameter η_2.

Sub-Case II: $|P_0(t)| < |A|$

We called this the 'crossing' sub-case and from the analysis above we anticipate the tipping to occur here. The contributions from $V > 0$ cause the solution to grow and thus we expect to lose stability. Under the condition $|P_0(t)| < |A|$, we integrate (3.81) with $R_1 = \arccos(P_0/A)$ and $R_2 = 2\pi - \arccos(P_0/A)$ and use a Taylor approximation about $P_0 = 0$, which leads to

$$\begin{aligned} P_{0t} =& -n(t) - \eta_3 P_0 - (1-\eta_3) Q_0, \\ Q_{0t} =& -\epsilon^{\lambda-1} \frac{2\eta_1 |A|}{\pi} - \epsilon^{1-\lambda} \frac{\eta_1(1-\eta_3)}{\pi |A|} P_0^2 - Q_0. \end{aligned} \tag{3.85}$$

Once more, we assume that Q_0 has reached its pseudo-equilibrium to reduce to the following one component inner equation with pseudo-equilibrium $Z^0(t)$. Here we let $a = \frac{\eta_1(1-\eta_3)}{\pi |A|}$ for simplicity, thus the reduced equations are

$$\begin{aligned} P_{0t} =& -\epsilon^{1-\lambda} n(t) + \frac{2\eta_1(1-\eta_3)|A|}{\pi} - \eta_3 P_0 + a P_0^2 = f(t, P_0), \\ Z^0(t) =& \frac{1}{2a} \left(\eta_3 - \sqrt{4a(\epsilon^{1-\lambda} n(t) - n_{\text{osc}})} \right). \end{aligned} \tag{3.86}$$

We choose to write the argument of the square root in terms of the local oscillatory bifurcation n_{osc} found in (3.41). Next, we allow for linear perturbation about the pseudo-equilibrium $P_0(t) = Z^0(t) + U(t)$ with $\|U(t)\| \ll 1$. Taking a Taylor expansion about the

pseudo-equilibrium then allows us to find the local behavior of the perturbations, but recall that we have contributions in the derivative from the perturbation U_t as well as the pseudo-equilibrium Z_t^0. This is seen with

$$\begin{aligned} P_{0t} =& Z_t^0 + U_t, \\ Z_t^0 =& \begin{cases} \frac{\epsilon^{1-\lambda}}{\sqrt{4a(\epsilon^{1-\lambda}n(t)-n_{\text{osc}})}} & \epsilon^{1-\lambda}n(t) > n_{\text{osc}}, \\ 0 & \epsilon^{1-\lambda}n(t) = n_{\text{osc}}. \end{cases} \end{aligned} \tag{3.87}$$

Thus we find the following Taylor expansion for the perturbations

$$\begin{aligned} P_{0t} =& f(t, Z^0) + f_{P_0}(t, Z^0)(P_0 - Z^0) + O(\|P_0 - Z^0\|^2), \\ U_t =& \begin{cases} \frac{\epsilon^{1-\lambda}}{\sqrt{4a(\epsilon^{1-\lambda}n(t)-n_{\text{osc}})}} - \left(\sqrt{4a(\epsilon^{1-\lambda}n(t) - n_{\text{osc}})}\right) U & \epsilon^{1-\lambda}n(t) > n_{\text{osc}}, \\ 0 & \epsilon^{1-\lambda}n(t) = n_{\text{osc}}. \end{cases} \end{aligned} \tag{3.88}$$

From (3.88) we find exponentially decaying perturbations to just under the pseudo-equilibrium this gives asymptotic attraction to a small value for $\eta_2 > \eta_{2_{\text{osc}}}$ which is the oscillatory bifurcation from section 3.2. This corresponds to loss of the pseudo-equilibrium and so there is no longer attraction to it, yielding a tipping point for $\eta_2 < \eta_{2_{\text{osc}}}$ which agrees with the results of our analysis.

Case II: $\lambda > 1$

In the analysis we determined this to be the 'slowly varying dominant' case and we obtained the inner equations that govern the behavior of the solution for this range of λ to be

$$\begin{aligned} X_{0t} =& -n(t) - \eta_3 X_0 - (1-\eta_3)Y_0, \\ Y_{0t} =& -\frac{\eta_1}{2\pi}\int_0^{2\pi} |X_0 - \epsilon^{\lambda-1}A\cos(R)|\, dR - Y_0. \end{aligned} \tag{3.89}$$

The behavior of this case when $\lambda \approx 1$ is similar to case I, thus we anticipate the similar attraction as well. Hence we consider the behavior when $|X_0(t)| < \epsilon^{\lambda-1}|A|$ which is the sub-case where we found the tipping point to occur in the analysis. As long as we have $\epsilon^{\lambda-1}A \sim O(1)$, we are able to follow the same approach as case I where we integrate (3.89) with a $R_1 = \arccos\big(X_0/\epsilon^{\lambda-1}A\big)$ and $R_2 = 2\pi - \arccos\big(X_0/\epsilon^{\lambda-1}A\big)$ and use a Taylor approximation about $X_0 = 0$ to get

$$\begin{aligned} X_{0t} =& -n(t) - \eta_2 X_0 - (1-\eta_3)Y_0, \\ Y_{0t} =& -\epsilon^{\lambda-1}\frac{2\eta_1(1-\eta_3)|A|}{\pi} - \epsilon^{1-\lambda}\frac{\eta_1}{\pi|A|}X_0^2 - Y_0. \end{aligned}$$

As in case I, we expect to use the pseudo-equilibrium reduction for Y_0 and thus we find the inner equation with pseudo-equilibrium $Z^0(t)$, taking $a = \frac{\eta_1(1-\eta_3)}{\pi|A|}$ for simplicity,

$$\begin{aligned} X_{0t} =& -n(t) + \epsilon^{\lambda-1}\frac{2\eta_1(1-\eta_3)|A|}{\pi} - \eta_3 X_0 + \epsilon^{1-\lambda}aX_0^2, \\ Z^0(t) =& \frac{1}{2a}\left(\epsilon^{\lambda-1}\eta_3 - \sqrt{4a\epsilon^{\lambda-1}(n(t) - \epsilon^{\lambda-1}n_{\text{osc}})}\right). \end{aligned}$$

For a linear stability analysis, we consider the linear perturbation of the pseudo-equilibrium $X_0(t) = Z^0(t) + U(t)$ with $\|U(t)\| \ll 1$. We apply a Taylor expansion to find a linear equation for perturbations, but again recall that we have contributions to the derivative from both the perturbation U_t as well as the pseudo-equilibrium Z_t^0. This is seen with

$$\begin{aligned} X_{0t} =& Z_t^0 + U_t, \\ Z_t^0 =& \begin{cases} \frac{\epsilon^{\lambda-1}}{\sqrt{4a\epsilon^{\lambda-1}(n(t)-\epsilon^{\lambda-1}n_{\text{osc}})}} & n(t) > \epsilon^{\lambda-1}n_{\text{osc}}, \\ 0 & n(t) = \epsilon^{1-\lambda}n_{\text{osc}}. \end{cases} \end{aligned} \tag{3.90}$$

Thus we find the following Taylor expansion for the perturbations

$$\begin{aligned} X_{0t} &= f(t, Z^0) + f_{X_0}(t, Z^0)(X_0 - Z^0) + O(\|X_0 - Z^0\|^2), \\ U_t &= \begin{cases} -\frac{\epsilon^{\lambda-1}}{\sqrt{4a\epsilon^{\lambda-1}(n(t)-\epsilon^{\lambda-1}n_{\text{osc}})}} - \left(\sqrt{\epsilon^{\lambda-1}4a(n(t)-\epsilon^{\lambda-1}n_{\text{osc}})}\right) U & n(t) > \epsilon^{\lambda-1}n_{\text{osc}}, \\ 0 & n(t) = \epsilon^{\lambda-1}n_{\text{osc}}. \end{cases} \end{aligned} \tag{3.91}$$

Similarly to case I, (3.91) shows that the perturbations decay exponentially to just under the pseudo-equilibrium and we have hyperbolic stability for $\eta_2 > \eta_{2\text{osc}}$ which is the oscillatory bifurcation from section 3.2. After this point is reached, the system loses its pseudo-equilibrium which indicates that the tipping point occurs after the bifurcation $\eta_{2\text{osc}}$. Comparing this to case I, we see there are small nuances between these perturbations, although the overall stability remains the same. As for when λ gets large, we already established that this behaves like the slowly varying model and hence we use the stability from section 3.1 to conclude that our solution is still stable until the slow tipping point $\eta_{2\text{osc}}$.

Thus, the stability for both case I and case II agrees with the results found in the analysis. We have that the behavior of our solution is stable from the outer solution and that this stability holds before the solution begins to cross the axis $V = 0$. Once the crossing starts to happen, we lose stability at $\eta_{2\text{osc}}$. Because there is slow variation in this model, there is delayed behavior and thus the tipping point occurs after the oscillatory bifurcation $\eta_{2\text{osc}}$. In both cases we discovered that the pseudo-equilibrium has a contribution to the derivative and this in turn causes the perturbations to decay towards a small constant below the pseudo-equilibrium. This means that there is a small region around the pseudo-equilibrium that attracts the solution.

Chapter 4

Summary and Future Work

With the results found in this thesis, we have accurately described what kind of behavior is present about the non-smooth bifurcation when new mechanisms are introduced in both the one component model (2.1) and Stommel model (3.1). The novelty of this work comes from the link between delayed tipping methods to the non-smooth Stommel model which then paves the way for a more general approach to the broader class of non-smooth dynamical systems.

To describe a large class of observable behaviors, we considered the mixture of advanced bifurcation due to high oscillatory forcing with frequency $\Omega \gg 1$ and amplitude $A \sim O(1)$ as well as delayed tipping due to slow variation in the bifurcating parameter at rate $\epsilon \ll 1$. We found that addition of these mechanisms have opposite effects on the tipping point and do mix with a kind of weighted average to produce an effective tipping approximation. The main results of the paper are the relative effects for the non-smooth bifurcation as compared to the smooth bifurcation. In the case of the one component model, the strength of the non-smooth influence on the tipping point is vastly different for each component as compared to the smooth influence. All of the smooth approximations we pull directly from [24] as we delve deeper into a comparison between the two.

For the slowly varying parameter with $\epsilon > 0$ and no oscillatory forcing with $A = 0$, we compare the non-smooth tipping point, $\mu_{\text{slow}} = \epsilon \ln(\epsilon)/2$, to the smooth tipping point, $\mu_{\text{smooth}} = \epsilon^{2/3}(-2.3381)$. Immediately, we notice that these approximations have different functions as seen in figure 4.1. From the figure, it is clear that the delayed non-smooth effects are much smaller and flatten out as compared to the continuously increasing delayed smooth effects. This indicates that the response to the non-smooth bifurcation occurs sooner than the response to the smooth bifurcation. Hence we may say that the non-smooth effects are stronger than the smooth effects.

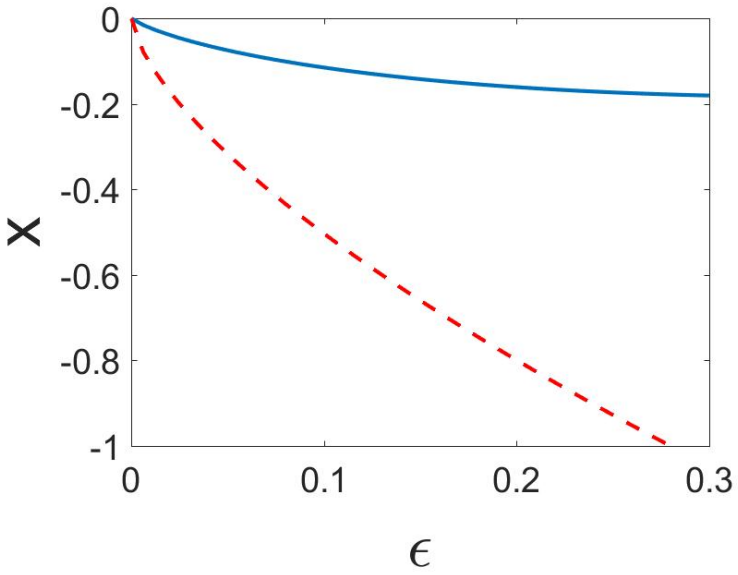

Figure 4.1: Comparison between the slow tipping points across ϵ. The blue solid line is the non-smooth tipping points where the red dotted line is the smooth tipping points.

For oscillatory forcing with $A \neq 0$ and static parameter values with $\epsilon = 0$, we compare the non-smooth bifurcation, $\mu_{\text{osc}} = \frac{4|A|}{\pi\Omega}$, to the smooth bifurcation, $\mu_{\text{sm+osc}} = \frac{A^2}{2\Omega^2}$. Here we have a sense of the strength of each case directly from the functions in terms of Ω^{-1}, the non-smooth has a linear response whereas the smooth has a quadratic response. This appears clearly in figure 4.2 where we see that the advanced bifurcation in the non-smooth case is significantly greater than that of the smooth case. This means that the non-smooth bifurcation causes the oscillations to advance the bifurcation much further away as opposed to the smooth bifurcation. Here this also indicates that the effects of the non-smooth effects are stronger than that of the smooth effects.

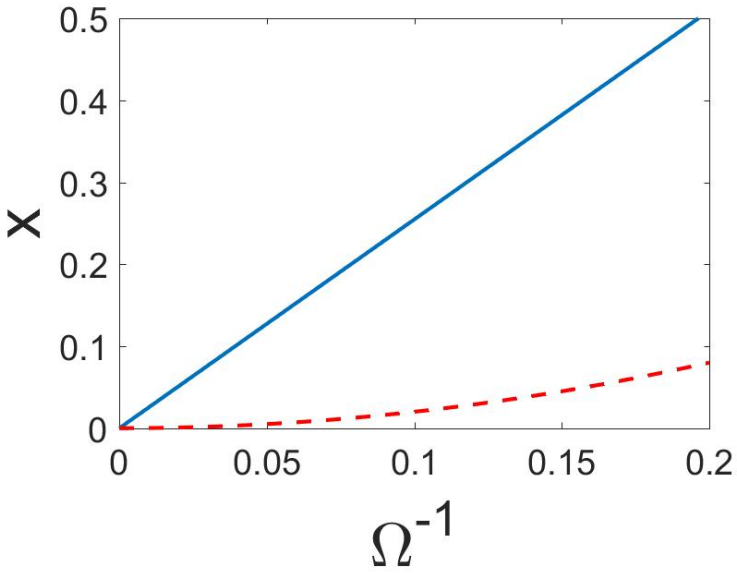

Figure 4.2: Comparison between the oscillatory bifurcation across Ω^{-1} for $A = 2$. The blue solid line is the non-smooth case where the red dotted line is the smooth case.

When we combine these mechanisms, we compare the non-smooth tipping point , $\mu_{\text{mixed}} = w(\Omega, A)\mu_{\text{smooth}} + \mu_{\text{osc}}$ with weight $w(\Omega, A) = (\frac{2|A|}{\pi\Omega})^{1/3}$, to the smooth tipping point, $\mu_{\text{smooth}} + \mu_{\text{sm+osc}}$. The case where the mixed approximation take the form of μ_{slow} for $\Omega \to \infty$ has already been discussed above so we do not consider this here. It is important to note that although we see a similar form between these two, the weight in the non-smooth tipping point is dependent on both A and Ω so it has significant influence on the value for different frequencies. This is shown in figure 4.3 for ϵ varying in (a) and Ω varying in (b). In (a), since the weight $w(\Omega, A) < 1$ for $A < O(\Omega)$, then the slope of non-smooth influence is smaller than the slope of smooth influence. We also notice the intercept for the non-smooth influence being significantly larger corresponding to the oscillatory bifurcation μ_{osc} being larger than $\mu_{\text{sm+osc}}$. Together, these indicate that the non-smooth bifurcation has a stronger advanced tipping while the curves are both positive, and a smaller delayed tipping when both curves are negative. In (b), the effect of the changing weight $w(\Omega, A)$ is most clear and we see the advanced tipping being quite strong for mid-range Ω. It is also clear the non-smoothness of the model causes the approximation μ_{mixed} to fail for $\Omega \to \infty$. This case is analogous to when $\lambda > 1$ from the one component analysis and allows us to refer back to the slowly varying problem with $\epsilon > 0$ and $A = 0$ for $\Omega \to \infty$. For both plots, we conclude the non-smooth effects are stronger than the smooth effects even under the mixed case.

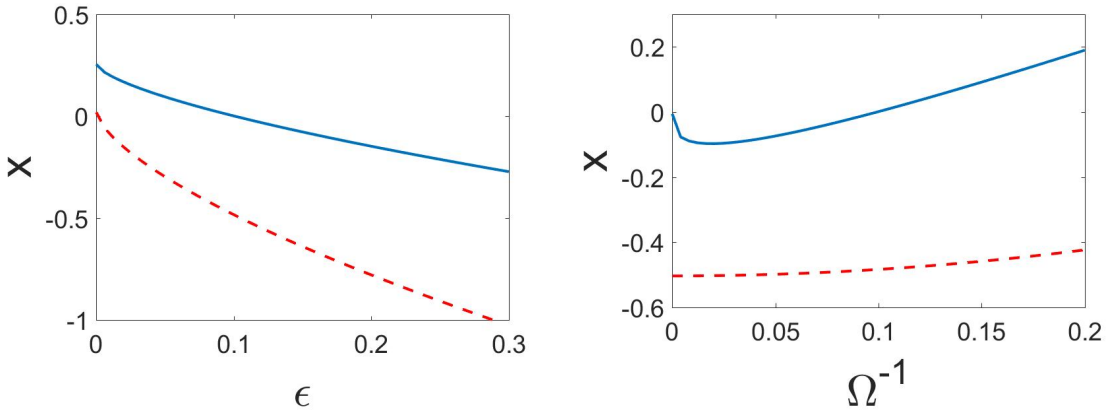

(a) (b)

Figure 4.3: Comparison between the mixed tipping in (a) with a fixed $\Omega^{-1} = .1$ and (b) with a fixed $\epsilon = .1$. The blue solid line is the non-smooth case where the red dotted line is the smooth case.

These results give insight into the hysteresis behavior of the Stommel model and the less studied realm of non-smooth dynamics. The main approach used asymptotic expansions as well as the methods of multiple scales to identify reduced equations and to find asymptotic solutions to the models. We found that with oscillatory forcing, the reduced equations have an expression dependent on the relative size of the solution to the amplitude of oscillation. In the smooth version of this problem, this type of behavior was not present and considering a case-by-case argument was not necessary. We also discovered that linking the slow variation ϵ and the frequency Ω gives important insight into how the system behaves. The methods developed for finding tipping points in the one component model (2.1) gave good approximations with the numerical results. Due to the many similarities to the two component system (3.1) we were able to modify the same analysis to find the tipping points here as well. We also anticipate the non-smooth bifurcation of the Stommel model to have a stronger influence on the solution than the smooth bifurcation.

Future work would need to be done on cases where $\Omega \sim O(1)$ or smaller. This case is qualitatively different as slow oscillations may have dramatic contributions to the dynamics. These effects are also seen from the analysis where low frequency oscillations no longer allow for asymptotic expansions in terms of Ω^{-1} and no longer fall under our assumptions to integrate with T_1 and T_2. Hence this case can influence tipping in a way we hadn't explored in this paper, we show an example of this in figure 4.4. Also, large amplitude behavior $A > O(1)$ can force an additional rescaling before any familiar approaches hold which is seen in figure 4.5. These cases were mentioned but have yet to be performed on this model, although both have been studied around the smooth case in [24]. It is possible that they could have some surprising results in the non-smooth case. Together, these could help to further classify the tipping behavior for the variety of cases in real world ocean dynamics.

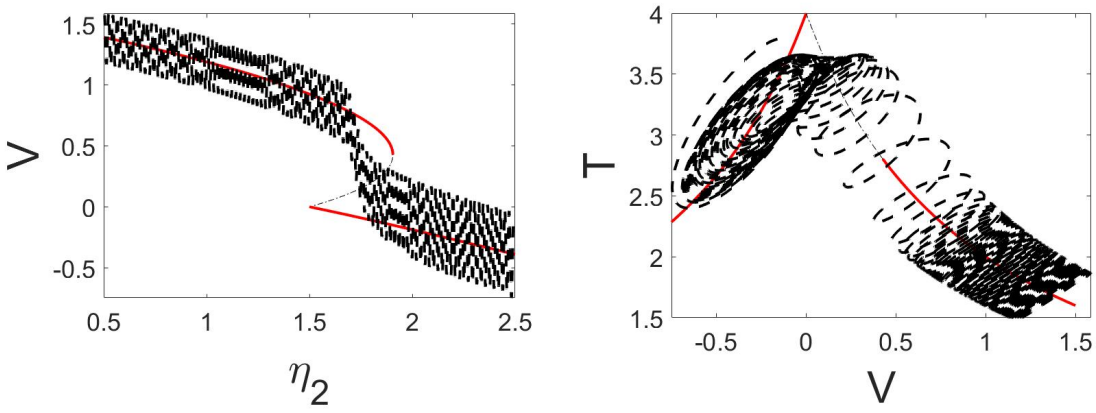

(a) (b)

Figure 4.4: Low Frequency: Model parameters are $\epsilon = .01$, $A = B = 1$ and $\Omega = 3$.

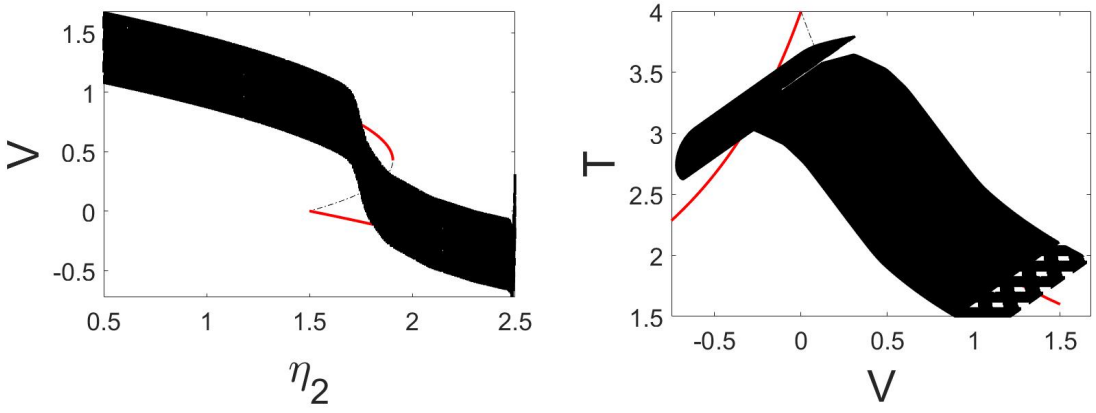

(a) (b)

Figure 4.5: Large Amplitude: Model parameters are $\epsilon = .01$, $A = B = 300$ and $\Omega = 1000$.

Lastly, we considered only deterministic behavior throughout this analysis but there are many reasons to incorporate stochastic elements into the Stommel model as well, see [13]. From [24] it is concluded that stochastic forcing has elements of both early bifurcations and delayed tipping and thus a natural follow-up to the analysis in this thesis. We could consider stochastic forcing with

$$\begin{aligned} \dot{V} &= \eta_1 - \eta_2 + \eta_3(T - V) - T - V|V| + A\xi_1(t), \\ \dot{T} &= \eta_1 - T(1 + |V|) + B\xi_2(t), \\ \dot{\eta_2} &= -\epsilon \\ V(0) = V^0, \quad T(0) &= T^0, \quad \eta_2(0) = {\eta_2}^0, \end{aligned} \tag{4.1}$$

where $\xi_i(t)$ is standard Gaussian noise with mean 0 and variance t and initial conditions

centered on the lower branch. This is shown in figure 4.6 and it is clear that a completely separate analysis is needed.

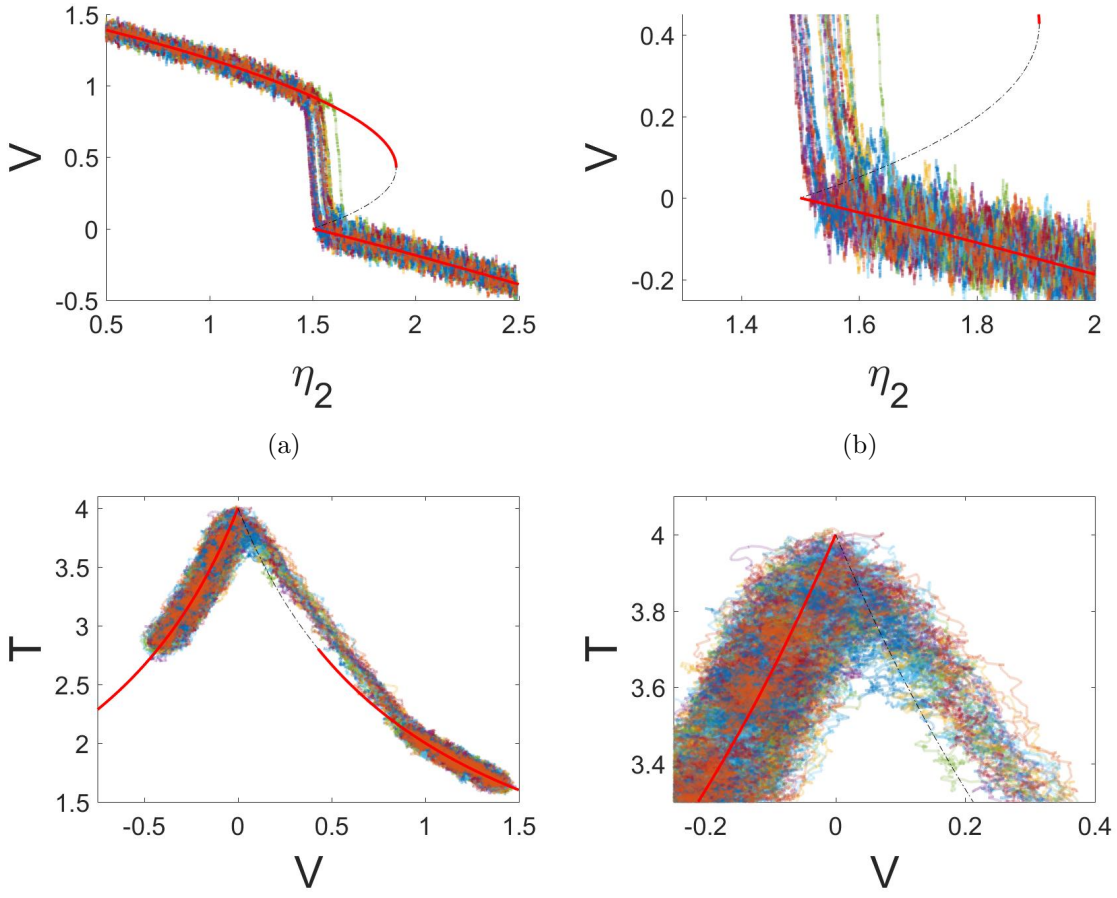

Figure 4.6: Stochastic: In (a) many realizations of the numerical solution for V in (4.1) are given with model parameters $\eta_1 = 4$, $\eta_3 = .375$, $\epsilon = .01$ and $A = B = .7$. In (b) a zoom in closer to the non-smooth bifurcation region can be seen. In (c) we have the realizations over the standard equilibrium plot for V vs. T. In (d) a zoom of the bifurcation area is shown.

Bibliography

[1] Richard B Alley, Jochem Marotzke, William D Nordhaus, Jonathan T Overpeck, Dorothy M Peteet, Roger A Pielke, RT Pierrehumbert, PB Rhines, TF Stocker, LD Talley, et al. Abrupt climate change. *science*, 299(5615):2005–2010, 2003.

[2] David Angeli, James E Ferrell, and Eduardo D Sontag. Detection of multistability, bifurcations, and hysteresis in a large class of biological positive-feedback systems. *Proceedings of the National Academy of Sciences*, 101(7):1822–1827, 2004.

[3] Alain Bensoussan, Jacques-Louis Lions, and George Papanicolaou. *Asymptotic analysis for periodic structures*, volume 374. American Mathematical Soc., 2011.

[4] Levke Caesar, Stefan Rahmstorf, Alexander Robinson, Georg Feulner, and V Saba. Observed fingerprint of a weakening atlantic ocean overturning circulation. *Nature*, 556(1):191–196, 2018.

[5] Henk A Dijkstra. *Nonlinear climate dynamics*. Cambridge University Press, 2013.

[6] T Erneux and JP Laplante. Jump transition due to a time-dependent bifurcation parameter in the bistable ioadate–arsenous acid reaction. *The Journal of Chemical Physics*, 90(11):6129–6134, 1989.

[7] Richard Haberman. Slowly varying jump and transition phenomena associated with algebraic bifurcation problems. *SIAM Journal on Applied Mathematics*, 37(1):69–106, 1979.

[8] Angela Hohl, HJC Van der Linden, Rajarshi Roy, Guillermo Goldsztein, Fernando Broner, and Steven H Strogatz. Scaling laws for dynamical hysteresis in a multidimensional laser system. *Physical review letters*, 74(12):2220, 1995.

[9] Peter Huybers and Carl Wunsch. Obliquity pacing of the late pleistocene glacial terminations. *Nature*, 434(7032):491, 2005.

[10] Amitabh Joshi, Wenge Yang, and Min Xiao. Dynamical hysteresis in a three-level atomic system. *Optics letters*, 30(8):905–907, 2005.

[11] Peter Jung, George Gray, Rajarshi Roy, and Paul Mandel. Scaling law for dynamical hysteresis. *Physical review letters*, 65(15):1873, 1990.

[12] Yuri A Kuznetsov. Saddle-node bifurcation. *Scholarpedia*, 1(10):1859, 2006.

[13] MN Lorenzo, JJ Taboada, and I Iglesias. The role of stochastic forcing in climate models: The case of thermohaline circulation. In *Climate Models*. InTech, 2012.

[14] Jochem Marotzke. Abrupt climate change and thermohaline circulation: Mechanisms and predictability. *Proceedings of the National Academy of Sciences*, 97(4):1347–1350, 2000.

[15] James Dickson Murray. *Asymptotic analysis*, volume 48. Springer Science & Business Media, 2012.

[16] W. Park and M. Latif. Atlantic meridional overturning circulation response to idealized external forcing. *Climate Dynamics*, 39(7-8):1709–1726, 10 2012.

[17] Stefan Rahmstorf. The thermohaline ocean circulation: A system with dangerous thresholds? *Climatic Change*, 46(3):247–256, 2000.

[18] Stefan Rahmstorf. Ocean circulation and climate during the past 120,000 years. *Nature*, 419(6903):207–214, 2002.

[19] Andrew Roberts and Raj Saha. Relaxation oscillations in an idealized ocean circulation model. *Climate Dynamics*, 48(7-8):2123–2134, 2017.

[20] Nestor E Sanchez. The method of multiple scales: asymptotic solutions and normal forms for nonlinear oscillatory problems. *Journal of Symbolic Computation*, 21(2):245–252, 1996.

[21] Rüdiger Seydel. *Practical bifurcation and stability analysis*, volume 5. Springer Science & Business Media, 2009.

[22] M Stastna and WR Peltier. On box models of the north atlantic thermohaline circulation: Intrinsic and extrinsic millennial timescale variability in response to deterministic and stochastic forcing. *Journal of Geophysical Research: Oceans*, 112(C10), 2007.

[23] Henry Stommel. Thermohaline convection with two stable regimes of flow. *Tellus*, 13(2):224–230, 1961.

[24] Jielin Zhu, Rachel Kuske, and Thomas Erneux. Tipping points near a delayed saddle node bifurcation with periodic forcing. *SIAM journal on applied dynamical systems*, 14(4):2030–2068, 2015.

Appendix A

The Stommel Model

The original Stommel model has the following balance equations [23]

$$\begin{aligned} B_1\frac{dT_1}{dt} =& C_1^T(T_1^s - T_1) + |V|(T_2 - T_1), \\ B_2\frac{dT_2}{dt} =& C_2^T(T_2^s - T_2) + |V|(T_1 - T_2), \\ B_1\frac{dS_1}{dt} =& C_1^S(S_1^s - S_1) + |V|(S_2 - S_1), \\ B_2\frac{dS_2}{dt} =& C_2^S(S_2^s - S_2) + |V|(S_1 - T_2), \end{aligned} \tag{A.1}$$

where B_1 and B_2 are the volumes of each box containing water of temperature and salinity (T_1, S_1) and (T_2, S_2) respectively. The surface conditions of each box are then T_i^s and S_i^s and the relaxation coefficients for the temperature and salinity are C^T and C^S. V is the flow rate between the boxes and is linearly related to the density difference. To reduce this to a two dimensional model that contains all the same information, we use the differences $T = T_1 - T_2$ and $S = S_1 - S_2$. If we also assume the relaxation coefficient is proportional to volume, then we have $\frac{C^T}{B_1} = \frac{C^T}{B_2} = R_T$ and $\frac{C^S}{B_1} = \frac{C^S}{B_2} = R_S$. This then gives (A.1) as

$$\begin{aligned} \frac{dT}{dt} =& R_T(T_1^s - T_2^s - T) - |V|T\left(\frac{1}{B_1} - \frac{1}{B_2}\right), \\ \frac{dS}{dt} =& R_S(S_1^s - S_2^s - S) - |V|T\frac{B_1 + B_2}{B_1 B_2}. \end{aligned} \tag{A.2}$$

To simplify further we scale time, temperature, salinity and the flow rate by

$$\begin{aligned} t \leftarrow& \frac{1}{C^T}t, \\ T \leftarrow& \frac{B_1 B_2 C^T}{\gamma\alpha_T(B_1 + B_2)}T, \\ S \leftarrow& \frac{B_1 B_2 C^T}{\gamma\alpha_S(B_1 + B_2)}S, \\ V \leftarrow& \frac{B_1 B_2 R_T}{B_1 + B_2}V, \end{aligned} \tag{A.3}$$

where α_T and α_S are the thermal expansion and saline contraction coefficients and γ is a

hydraulic constant. Then using (A.3) in (A.2) gives

$$\begin{aligned}\frac{dT}{dt} =&\frac{(T_1^s - T_2^s)\gamma\alpha_T(B_1+B_2)}{B_1B_2R_T} - T - |V|T,\\ \frac{dS}{dt} =&\frac{(S_1^s - S_2^s)\gamma\alpha_S(B_1+B_2)R_S}{B_1B_2R_T^2} - \frac{R_S}{R_T}S - |V|S.\end{aligned} \tag{A.4}$$

Here we define the non-dimensionalized parameters

- η_1 - the strength of thermal forcing,

$$\eta_1 = \frac{(T_1^s - T_2^s)\gamma\alpha_T(B_1+B_2)}{B_1B_2R_T}.$$

- η_2 - the strength of freshwater forcing,

$$\eta_2 = \frac{(S_1^s - S_2^s)\gamma\alpha_S(B_1+B_2)R_S}{B_1B_2R_T^2}.$$

- η_3 - the ratio of the freshwater to thermal relaxation time scales,

$$\eta_3 = \frac{R_S}{R_T}.$$

We recall that V was related to the difference in temperature and salinity, thus giving $V = T - S$. This results in the non-dimensionalized Stommel model

$$\begin{aligned}\frac{dT}{dt} =&\eta_1 - T - |T-S|T,\\ \frac{dS}{dt} =&\eta_2 - \eta_3 S - |T-S|S.\end{aligned} \tag{A.5}$$

It is more convenient to analyze ocean circulation in terms of the flow rate V which is also known as the circulation strength. Then using $V = T - S$ in (A.5) gives

$$\begin{aligned}\frac{dT}{dt} =&\eta_1 - T(1+|V|),\\ \frac{dV}{dt} =&\eta_1 - \eta_2 - \eta_3(T-V) - T - V|V|.\end{aligned} \tag{A.6}$$

Appendix B

One Component

High Frequency Oscillatory Forcing

Here we continue the analysis to explicitly find the solution of the outer equation for the purely oscillatory model. Recall that we found $x_1 = v_1(t) - A\cos(T)$, we then apply the Fredholm alternative (2.24) to the $O(\Omega^{-2})$ equation in (2.23) to get

$$\begin{aligned} 0 =& \frac{1}{2\pi}\int_0^{2\pi} -x_{1t} - 2x_1 + 2x_0x_1\, dT, \\ v_{1t} =& -2v_1 + 2(1-\sqrt{1+\mu})v_1, \\ v_{1t} =& -2\sqrt{1+\mu}v_1. \end{aligned} \tag{B.1}$$

We search for the equilibrium to find stable behavior on this order but since (B.1) has a very simple form, the equilibrium is $v_1(t) \equiv 0$ and thus we find the correction term to only have oscillatory behavior, $x_1 = -A\cos(T)$.

Slow Variation and Oscillatory Forcing

Here we continue to find the terms of the outer solution for the slowly varying and oscillatory forcing model. We have thus far found $x_0 = x_0(\tau)$ and we have equations at $O(\epsilon^{\lambda})$ and $O(\epsilon^{2\lambda})$ that give information about x_0 and x_1 respectively. We apply the Fredholm alternative (2.24) to the $O(\epsilon^{\lambda})$ equation (2.49) to find

$$\begin{aligned} 0 =& \frac{1}{2\pi}\int_0^{2\pi} -\mu(\tau) - 2x_0(\tau) + x_0(\tau)^2 + A\sin(T)\, dT, \\ 0 =& -\mu(\tau) - 2x_0(\tau) + x_0(\tau)^2, \\ x_0(\tau) =& 1 - \sqrt{1+\mu(\tau)}, \\ x_{1T} =& A\sin(T). \end{aligned} \tag{B.2}$$

From (B.2) we find that $x_1 = v_1(\tau) - A\cos(T)$, which gives us access to solving the next order equation. Thus we now do the same for the $O(\epsilon^{2\lambda})$ equation (2.50) to find

$$\begin{aligned} 0 =& \frac{1}{2\pi}\int_0^{2\pi} -\epsilon^{1-\lambda}x_{0\tau} - 2x_1 + 2x_0x_1\, dT, \\ \epsilon^{1-\lambda}x_{0\tau} =& -2v_1 + 2(1-\sqrt{1+\mu(\tau)})v_1, \\ v_1(\tau) =& -\epsilon^{1-\lambda}\frac{x_{0\tau}}{2\sqrt{1+\mu(\tau)}}. \end{aligned} \tag{B.3}$$

Recall that $\mu_\tau = -1$ and that $x_{0\tau} = -\frac{\mu_\tau}{2\sqrt{1+\mu(\tau)}} = \frac{1}{2\sqrt{1+\mu(\tau)}}$ and thus we find the form of the next order term in the expansion as

$$x_1(\tau, T) = -\epsilon^{1-\lambda}\frac{1}{4(1+\mu(\tau))} - A\cos(T). \tag{B.4}$$

Appendix C

Two Component

High Frequency Oscillatory Forcing

Here we show that the correction term of the outer solution is purely oscillatory. From the analysis, we found both leading order terms to be purely slow time dependent, i.e. $V_0 = V_0(\tau)$ and $T_0 = T_0(\tau)$. To find the explicit form for these, we apply Fredholm (2.24) to the $O(\Omega^{-1})$ equations in (3.22) to find

$$\begin{aligned}
&\begin{cases} 0 = & \frac{1}{2\pi}\int_0^{2\pi} -V_{0t} + \eta_1 - \eta_2 + \eta_3(T_0 - V_0) - T_0 + V_0^2 + A\sin(R)\,dR, \\ 0 = & \frac{1}{2\pi}\int_0^{2\pi} -T_{0t} + \eta_1 - T_0(1 - V_0) + B\sin(R)\,dR, \end{cases} \\
&\begin{cases} V_{0t} = & \eta_1 - \eta_2 + \eta_3(T_0 - V_0) - T_0 + V_0^2, \\ T_{0t} = & \eta_1 - T_0(1 - V_0), \end{cases} \\
&V_{1R} = A\sin(R), \quad T_{1R} = B\cos(R).
\end{aligned} \tag{C.1}$$

Since we have a fixed parameter η_2, we find the equilibria V_0 and T_0 as well as the form of the correction terms

$$\begin{aligned}
T_0(V_0) &= \frac{\eta_1}{1 - V_0}, \\
0 &= \eta_1 - \eta_2 + \eta_3(T_0(V_0) - V_0) - T_0(V_0) + V_0^2, \\
V_1 &= X_1(t) - A\cos(R), \quad T_1 = Y_1(t) - B\cos(R).
\end{aligned}$$

Here we note these equilibria to be the same as in the static problem with no forcing from the introduction. But with the form of the correction terms, we now solve the equation at $O(\Omega^{-2})$ (3.23) by applying Fredholm (2.24). This results in

$$\begin{aligned}
&\begin{cases} 0 = & \frac{1}{2\pi}\int_0^{2\pi} -V_{1t} + \eta_3(T_1 - V_1) - T_1 + 2V_0V_1\,dR, \\ 0 = & \frac{1}{2\pi}\int_0^{2\pi} -T_{1t} + T_1(1 - V_0) + T_0V_1\,dR, \end{cases} \\
&\begin{cases} X_{1t} = & \eta_3(Y_1 - X_1) - Y_1 + 2X_0X_1, \\ Y_{1t} = & Y_1(1 - X_0) + Y_0X_1. \end{cases}
\end{aligned} \tag{C.2}$$

We then search for the equilibria of (C.2) and find

$$\begin{aligned}
Y_1(X_1) &= -\frac{Y_0X_1}{1 - X_0}, \\
0 &= \left(\eta_3\left(\frac{Y_0}{1 - X_0} - 1\right) - \frac{Y_0}{1 - X_0} + 2X_0\right)X_1.
\end{aligned}$$

Thus we find that the correction terms are purely oscillatory since $X_1 \equiv 0$ and $Y_1 \equiv 0$. This gives $V_1 = -A\cos(R)$ and $T_1 = -B\cos(R)$.

Slow Variation and Oscillatory Forcing

Here we continue to find terms of the outer solution by working through the equations (3.53)-(3.54). In the analysis, we had already determined that the leading order terms are purely slow time dependent, $V_0 = V_0(\tau)$ and $T_0 = T_0(\tau)$. To find their exact form, we apply Fredholm (2.24) to the $O(\epsilon^\lambda)$ equation (3.53) to find

$$\begin{aligned}
&\begin{cases} 0 = & \frac{1}{2\pi}\int_0^{2\pi} \eta_1 - \eta_2(\tau) + \eta_3(T_0 - V_0) - T_0 + V_0^2 + A\sin(R)\,dR, \\ 0 = & \frac{1}{2\pi}\int_0^{2\pi} \eta_1 - T_0(1 - V_0) + B\sin(R)\,dR, \end{cases} \\
&\begin{cases} 0 = & \eta_1 - \eta_2(\tau) + \eta_3(T_0 - V_0) - T_0 + V_0^2, \\ 0 = & \eta_1 - T_0(1 - V_0), \end{cases} \\
&V_{1R} = A\sin(R), \quad T_{1R} = B\cos(R).
\end{aligned} \tag{C.3}$$

The leading order solution to (C.3) is the same as the slowly varying problem from section 3.1 with

$$\begin{aligned}
T_0(V_0) =& \frac{\eta_3}{1 - V_0}, \\
0 =& \eta_1 - \eta_2(\tau) + \eta_3(T_0(V_0) - V_0) - T_0(V_0) + V_0^2.
\end{aligned}$$

We also find the form of the correction terms, $V_1 = X_1(\tau) - A\cos(R)$ and $T_1 = Y_1(\tau) - B\cos(R)$, which allow us to solve the $O(\epsilon^{2\lambda})$ equation (3.54). Applying Fredholm (2.24) here results in

$$\begin{aligned}
&\begin{cases} 0 = & \frac{1}{2\pi}\int_0^{2\pi} \left(-\epsilon^{1-\lambda}V_{0\tau} + \eta_3(T_1 - V_1) - T_1 + 2V_0V_1 + A\sin(R)\right)\,dR, \\ 0 = & \frac{1}{2\pi}\int_0^{2\pi} \left(\epsilon^{1-\lambda}T_{0\tau} - T_1(1 - V_0) + T_0V_1\right)\,dR, \end{cases} \\
&\begin{cases} \epsilon^{1-\lambda}V_{0\tau} = & \eta_3(Y_1 - X_1) - Y_1 + 2V_0X_1, \\ \epsilon^{1-\lambda}T_{0\tau} = & Y_1(1 - V_0) + T_0X_1. \end{cases}
\end{aligned} \tag{C.4}$$

Recalling that $\eta_{2\tau} = -1$ and solving (C.4) requires the derivatives of V_0 and T_0 which are solvable explicitly as

$$\begin{aligned}
T_{0\tau}(V_{0\tau}) =& -\frac{\eta_1 V_{0\tau}}{1 - V_0}, \\
V_{0\tau} =& \frac{(1 - V_0)}{\eta_1 + \eta_3(\eta_1 + 1 - V_0) - 2V_0(1 - V_0)}.
\end{aligned}$$

With everything put together, we find the solution to (C.4) as

$$\begin{aligned}
Y_1(X_1) =& \frac{\epsilon^{1-\lambda}T_{0\tau} - T_0X_1}{1 - V_0}, \\
X_1 =& \frac{\epsilon^{1-\lambda}(V_{0\tau}(1 - V_0) + (1 - \eta_3)T_{0\tau})}{(1 - \eta_3)T_0 + (2V_0 - \eta_3)(1 - V_0)}.
\end{aligned}$$

Here we now have the first correction term as

$$V_1(\tau, R) = \frac{\epsilon^{1-\lambda}(V_{0\tau}(1-V_0) + (1-\eta_3)T_{0\tau})}{(1-\eta_3)T_0 + ((2V_0 - \eta_3)(1-V_0)} - A\cos(R),$$
$$T_1(\tau, R) = \frac{\epsilon^{1-\lambda}T_{0\tau}}{1-V_0} - \frac{\epsilon^{1-\lambda}T_0(V_{0\tau}(1-V_0) + (1-\eta_3)T_{0\tau})}{(1-\eta_3)T_0(1-V_0) + (2V_0 - \eta_3)(1-V_0)^2} - B\cos(R).$$